UNIVERSITA' DEGLI STUDI DI PADOVA

Sede Amministrativa: Università degli Studi di Padova

Dipartimento Territorio e Sistemi Agro-Forestali

DOTTORATO DI RICERCA IN: IDRONOMIA AMBIENTALE

CICLO XX

REGIONAL ANALYSIS OF FLOODING AND FLASH FLOODING

Coordinatore: Ch.mo Prof. Mario Aristide Lenzi

Supervisore: Ch.mo Prof. Marco Borga

Dottorando: Ing. Daniele Norbiato

31 gennaio 2008

Riassunto

La stima dei deflussi in bacini non strumentati è un argomento sul quale la comunità scientifica internazionale da sempre esprime interesse, e su cui recentemente è stata avviata un'iniziativa di rilievo internazionale: il progetto PUB (Prediction in Ungauged Basins) promosso dall'International Association of Hydrological Sciences (IAHS). L'importante variabilità spazio-temporale delle caratteristiche climatiche e dell'uso del suolo rende difficile e incerta l'estrapolazione delle informazioni da bacini strumentati a quelli non-strumentati e questo vale per qualsiasi approccio modellistico utilizzato. Tale problematica è ulteriormente accentuata dall'ancora incompleta comprensione della dinamica dei processi idrologici alla scala di versante e di bacino.

Questo concetto è il filo conduttore del presente lavoro di tesi nel quale vengono proposte metodologie di analisi, modellazione e previsione della risposta idrologica sviluppate secondo un approccio di tipo regionale.

La prima parte del lavoro (Cap. 2, 3 e 4) è dedicata allo studio e alla previsione dei fenomeni di piena improvvisa che, per le loro caratteristiche, colpiscono prevalentemente bacini non-strumentati. Tali eventi, infatti, sono caratterizzati da scale spazio-temporali tali da rendere le convenzionali reti di monitoraggio idrometeorologico poco idonee a coglierne le caratteristiche essenziali. La scarsa conoscenza di questi fenomeni si traduce nell'incapacità di sviluppare affidabili metodologie per la loro previsione. Al fine di migliorare l'osservabilità di tali eventi è necessario sviluppare una metodologia di monitoraggio idrologico a scala regionale utilizzando tecniche di osservazione da radar meteorologico per la valutazione degli apporti meteorici, unitamente a osservazioni post-evento per la stima dei deflussi.

Un approccio di tipo regionale è, inoltre, indispensabile nella messa a punto di metodologie volte alla mitigazione del rischio da piena improvvisa. Data l'estrema localizzazione di tali eventi è, infatti, necessario sviluppare sitemi di allerta che possano fornire indicazioni circa il pericolo di inondazione in modo distribuito nel territorio. Tali sistemi dovrebbero inglobare modelli idrologici capaci di stimare lo stato iniziale di saturazione dei suoli, fattore determinante nella risposta idrologica nel caso di eventi estremi. In questo senso, è di particolare importanza lo sviluppo di tecniche che siano in grado di trasferire le condizioni iniziali di saturazione del suolo da bacini strumentati a bacini non strumentati.

La seconda parte del lavoro (Cap. 5 e 6) è dedicata all'analisi e allo sviluppo di tecniche in grado di classificare e predire la risposta idrologica di un bacino qualsiasi in base alle informazioni relative ai fattori principali di controllo della risposta idrologica, quali per esempio la climatologia e la geomorfologia, disponibili alla scala regionale.

Questi differenti aspetti sono trattati nella tesi con l'obiettivo di fornire un contributo al miglioramento della predizione in bacini non strumentati.

Nello specifico il lavoro è articolato come segue:

Capitolo 1 *Introduction*. Introduzione generale alle tematiche affrontate.

Capitolo 2 *Development of a new observation strategy to advance understanding of flash flood hydrometeorological processes.*Al fine di migliorare l'osservabilità dei fenomeni di piena improvvisa viene proposta un'innovativa metodologia di osservazione che accoppia stime di precipitazione ottenute da radar meteorologico e analisi post-evento. Tale metodologia fornisce l'opportunità di derivare osservazioni importantissime relative alla dinamica dei processi di trasformazione afflussi-deflussi durante tali eventi. Vengono riportati alcuni risultati dell'applicazione di tale metodologia all'evento di piena improvvisa del 29 agosto 2003 che ha colpito il bacino del Fella (alto Tagliamento). L'analisi è focalizzata sullo studio dell'impatto della variabilità spazio-temporale delle precipitazioni, e delle condizioni iniziali pre-evento, nella risposta idrologica di un evento di piena improvvisa. I risultati dimostrano, principalmente, che la combinazione di alte capacità di saturazione e bassi valori di umidità pre-evento costituisce un fattore determinante nella risposta idrologica nel caso di eventi estremi.

Capitolo 3 *Regional frequency analysis of extreme precipitation in the eastern Italian Alps and the August 29, 2003 flash flood*. Vengono riportati i risultati dell'analisi di frequenza regionale delle precipitazioni estreme nel territorio del Friuli Venezia Giulia allo scopo di investigare le caratteristiche di frequenza dell'evento di pioggia del 29 agosto 2003 che ha scaturito un evento di piena improvvisa di particolare importanza. Nel lavoro viene presentato il metodo della piena indice, la tecnica di stima dei parametri mediante procedura regionale e i modelli probabilistici *GEV* (Generalized Extreme Value), *GLO* (Generalized Logistic) e *Kappa*. Viene descritta l'applicazione del metodo della piena indice al territorio friulano. L'analisi svolta ha permesso di individuare tre regioni apprezzabilmente omogenee, congruenti con la caratterizzazione orografica del territorio. L'analisi dimostra che le curve di crescita regionali basate sull'impiego della distribuzione *Kappa* si adattano particolarmente bene alla regione studiata. La metodologia è stata applicata per lo studio dell'evento estremo di pioggia del 29 agosto 2003 che ha colpito il bacino del Fella, alto Tagliamento. Stime radar di precipitazione, opportunamente corrette, sono state utilizzate per caratterizzare in modo spazialmente distribuito il tempo di ritorno dell'evento per differenti durate di precipitazione. L'analisi mostra che le stime di precipitazione ottenute da radar possono essere affette da importanti incertezze che si amplificano nella valutazione del tempo di ritorno. L'analisi mostra anche che i) l'attribuzione di un singolo tempo di ritorno per l'evento considerato non è realistica, e che ii) l'utilizzo dei dati provenienti dalla convenzionale rete di pluviometri non permette di ricostruire adeguatamente la severità dell'evento considerato. I risultati dimostrano, infine, che l'utilizzo accurato di stime radar di precipitazione opportunamente corrette è utile per valutare la severità di eventi in bacini non strumentati e per valutarne la dimensione spaziale delle caratteristiche di frequenza.

Capitolo 4 *Flash flood warning based on rainfall depth-duration thresholds and soil moisture conditions*. Vengono descritti i risultati relativi all'implementazione di un sistema di previsione delle piene improvvise basato sull'individuazione di soglie pluviometriche di allerta. Tali soglie pluviometriche che sono computate sulla base di un modello idrologico concettuale e a parametri concentrati possono essere confrontate con i valori di precipitazione misurati in tempo reale o previsti della stessa durata e nello stesso bacino. Se la precipitazione osservata o prevista è maggiore della soglia pluviometrica il pericolo di inondazione nel bacino viene considerato probabile. Tale metodologia è stata testata considerando un ampio range di condizioni climatiche e fisiografiche e focalizzando l'analisi in bacini non strumentati. Sono stati analizzati 11 bacini (6 macrobacini e 5 sottobacini) localizzati in due regioni europee: Nord Est Italia e Francia centrale. Le performance del modello sono state valutate per mezzo di opportuni statistici tra i quali il CSI (Critical Success Index). Gli esperimenti numerici descritti hanno lo scopo di capire le potenzialità e le limitazioni di questo sistema di previsione sotto diversi scenari climatici in modo da fungere da guida per sviluppi futuri. Vengono analizzati in particolare i) l'accuratezza della previsione nei macrobacini calibrati, ii) l'accuratezza della previsione in sottobacini non strumentati nel caso di semplice traslazione dei parametri a partire dai macrobacini che li contengono, iii) le performance di previsione negli stessi sottobacini nel caso di trasferimento combinato dei parametri e delle condizioni iniziali, iv) la perdita in accuratezza delle previsioni associata all'ipotesi di una condizione di umidità del suolo mantenuta costante se confrontata con le stime di umidità ottenute da modello idrologico continuo. I risultati mostrano che il CSI globale (pari a 1 in caso di previsione eccellente) è uguale a 0.43 per i macrobacini, dove il modello idrologico è calibrato, si riduce a 0.28 per i bacini interni quando i parametri sono trasferiti a partire dai macrobacini e a 0.21 quando vengono trasferiti sia i parametri sia le condizioni iniziali. Le performance del modello decrescono nel caso di utilizzo di utilizzo di soglie costanti di precipitazione corrispondenti a un valore prefissato di umidità del suolo. Tale perdita di efficienza è particolarmente importante nel caso dei macrobacini calibrati.

Capitolo 5 *Controls on event runoff coefficients in the eastern Italian Alps*. Viene riportata un'analisi del coefficiente di deflusso a scala regionale. Tale parametro è un parametro chiave in idrologia e può essere utilizzato per predire la risposta idrologica in bacini non strumentati; capirne i fattori principali di controllo è quindi di estrema importanza. Nel capitolo vengono analizzati gli effetti relativi al clima, alla geologia, all'uso del suolo, al tipo di piena e alle condizioni iniziali di umidità del suolo nelle funzioni di distribuzione cumulata del coefficiente di deflusso per 14 bacini localizzati nelle Alpi orientali italiane. I coefficienti di deflusso sono stati computati in modo automatico a partire dalle serie orarie misurate di precipitazione, portata e scioglimento nivale misurato. 535 eventi sono stati estratti nel periodo compreso tra il 1989 e il 2004. Ogni bacino è stato classificato dal punto di vista geologico tramite un indice di permeabilità dedotto dall'analisi delle mappe geologiche e variabile tra condizioni di

bassa a condizioni di alta permeabilità. Un modello idrologico di tipo continuo (il medesimo utilizzato nel Capitolo 4) è stato utilizzato al fine di classificare le condizioni precedenti alla piena in umide o secche. I risultati mostrano che la distribuzione spaziale del coefficiente di deflusso è fortemente correlata con la precipitazione media annua e il coefficiente di deflusso medio di bacino aumenta con la stessa. La geologia è un altro fattore di controllo importante per bacini caratterizzati da precipitazioni medie annue minori di 1200 mm. L'uso del suolo caratterizzato dal SCS Curve Number influenza le funzioni di distribuzione cumulata in maniera minore. E' stato trovato, inoltre, che il coefficiente di deflusso aumenta all'aumentare dello scioglimento nivale. I risultati mostrano, infine, che l'effetto della variazione delle condizioni iniziali è ininfluente per bacini impermeabili così come per bacini caratterizzati da importante permeabilità secondaria (dovuta a effetti carsici). In bacini dalle caratteristiche geologiche intermedie la risposta idrologica può essere notevolmente diversificata in funzione dello stato iniziale di umidità del suolo.

Capitolo 6 *Analytical solutions to a hyllslope-storage kinematic wave model for subsurface flow and analysis of its hysteretic behaviour*. Viene proposto un modello integrato di versante, cioè un modello a struttura parsimoniosa che risulta formulato in modo tale da preservare la descrizione dei processi fisici dominanti alla scala di interesse (nel caso in esame: il deflusso sottosuperficiale) ed in grado di integrare in modo innovativo l'unica informazione ubiquamente disponibile: quella relativa alla struttura morfologica. Il modello si basa sulla risoluzione del sistema costituito dall'equazione di continuità e da una forma cinematica dell'equazione di Darcy. La struttura morfologica tri-dimensionale di un versante è stata sintetizzata tramite un profilo bi-dimensionale, utilizzando una relazione quadratica per la descrizione del profilo longitudinale, e una descrizione della distribuzione della forma planare, ottenuta mediante un modello esponenziale. I risultati dimostrano come sia possibile partendo dalle ipotesi citate individuare modalità di applicazione e di sintesi dell'informazione morfologica che muovono da considerazioni di similarità. Si mostra, infatti, come sia possibile sintetizzare il controllo morfologico sulla risposta di versante tramite due parametri morfologici adimensionali di similarità (α e ψ) il primo utilizzato per descrivere la forma del profilo ed il secondo inteso a rappresentare l'influenza della forma lungo le linee di livello. E' stato analizzato inoltre il comportamento isteretico nella relazione portata-volume di tale semplice modello. E' stato dimostrato che l'isteresi cresce al crescere della convergenza (per la planimetria) e della concavità (per il profilo longitudinale) e viceversa. La metodologia è stata applicata a tre diversi versanti presso il bacino sperimentale di Vizza, situato nelle alpi orientali. L'applicazione rappresenta un'opportunità di esaminare come un versante naturale possa essere rappresentato dai due parametri morfologici di similarità. La qualità delle predizioni fornite dal modello integrato di risposta di versante proposto necessitano di una verifica su base sperimentale.

Capitolo 7 *General conclusions*. Vengono riportate un riassunto di tutte le conclusioni dei capitoli precedenti e raccomandazioni per possibili sviluppi della ricerca.

Abstract

Improving the capacity to make predictions in ungauged basins is one of most difficult challenge for the scientific community (see for example the current initiative Prediction Ungaged Basins (PUB) launched by the International Association of Hydrological Sciences, IAHS). Whatever hydrological models are used, in view of the tremendous spatio-temporal heterogeneity of climatic and landscape properties, extrapolation of information, or knowledge, from gauged to ungauged basins remains fraught with considerable difficulties and uncertainties, especially in the light of the generally poor understanding of where water goes when it rains, what flow path it takes to the stream, and the age of the water that emerges in the channel.

The PUB problem is the key concept of this thesis and it is analysed from several point of view. Methodologies able to observe, model and predict the hydrological response at the regional scale are proposed.

The first part of the work (Chapters 2, 3 and 4) is dedicated to develop and test methodologies for the observation, analysis and forecasting of flash flood events, that frequently affect ungaged basins. Since flash-floods develop at space and time scales that conventional observation systems are not able to monitor, these events are generally characterised by a lack of experimental data and consequently the atmospheric and hydrological generating mechanisms of flash-floods are poorly understood , leading to highly uncertain forecasts of these events. To improve the observability of these phenomena, a regional monitoring strategy is needed. The methodology couples the analysis of radar rainfall estimates with post-flood surveys, and offers the opportunity to derive unique observations concerning rainfall-runoff dynamics during flash flood events.

In addition, a regional approach should be followed also in order to develop instruments able to mitigate flash flood risk. In fact, given the small spatial scale that characterises flash floods, every section of the drainage network should be considered as a potential target for hydrological warnings. Consequently, to devise appropriate mitigation strategies, the investigated region should be considered as a whole. Since initials soil moisture conditions represent an important factor determining land surface response to extreme rainfall, operational flood forecasting systems should be based on continuous hydrological models which are capable to provide continuous estimates of soil moisture at the subbasin scale. Moreover, in order to obtain these estimates at the spatial scales closer to the need of flash flood forecasting, it is very important to develop techniques able to transfer the soil moisture estimates from gauged to ungauged basins

The second part of the work (Chapters 5 and 6) is dedicated to the analysis and the development of methodologies based on “Basin inter-comparison and classification” in order to improve understanding of regional characteristic hydrological cycle response and prediction in ungaged basins using inter-comparisons, and reanalysis of observations from single basin studies. Such methods aim at predicting basin and hillslope hydrological

responses starting from informations concerning the most important contols on runoff response, such as climate and geomorphology, available at regional scale.

These different aspects are examined in this thesis, with the aim of improving predictions in ungaged basins.

In detail, the work includes the following chapters:

Chapter 1. *Introduction.*

Chapter 2. *Development of an observation strategy to advance understanding of flash flood in hydrometeorological processes.* The management of flash flood hazards and risks is a critical component of public safety and quality of life. Flash-floods develop at space and time scales that conventional observation systems are not able to monitor for rainfall and river discharge. Consequently, the atmospheric and hydrological generating mechanisms of flash-floods are poorly documented and understood. Lack of knowledge may translate into poor design and implementation of flash flood risk management, including both flash flood real-time warning procedures and the design and planning of flood defence measures. This study describes an innovative flash flood observation methodology. The methodology couples analysis of radar rainfall estimates and post-flood surveys, and affords the opportunity to derive unique observations concerning rainfall-runoff dynamics during flash flood events. Observations related to the case study of the August 29, 2003 flash flood on Fella river basin (North-eastern Italy) are examined in this study. A description of the post event survey is reported. Results are presented concerning the impact of space-time precipitation variability and antecedent soil moisture conditions on flood response. The analysis of this flash flood event suggests that the combination of high soil moisture storage capacity and low antecedent soil moisture conditions is an important factor determining land surface response to extreme rainfall.

Chapter 3. *Regional frequency analysis of extreme precipitation in the eastern Italian Alps and the August 29, 2003 flash flood.* The main objective of the study is to analyse the spatial distribution of precipitation return times for the flash flood-generating storm occurred on 29 August 2003 on the upper Tagliamento river basin, in the eastern Italian Alps. This storm was characterised by extraordinary rainfall amounts and large spatial variability. Regional frequency analysis based on the flood index method and L-moments is utilized to analyse short duration annual maximum precipitation for the Friuli-Venezia Giulia region, in north-eastern Italy, which includes the storm location. It is shown that the regional growth curves based on the Kappa distribution may be useful for the subregions specified. This analysis provides a framework to investigate the frequency characteristics of the 29 August 2003 flash-flood-generating storm for various rainfall durations. Radar rainfall estimates, adjusted by using a physically-based methodology and data from a raingauge network, are used to characterise the return period of the storm rainfall amounts, highlighting the importance of considering its spatial dimension. Severity graphs are developed to visualise the return periods and their variability for different rainfall durations

within the storm. It is shown that adjusted radar rainfall estimates may suffer for considerable uncertainty and that the uncertainty magnifies in the evaluation of the relevant return periods. The analysis shows also that i) attributing a single return period to a storm event is not realistic, and ii) the severity of flash flood generating storms is poorly captured by using conventional raingauge networks. The reported results show that estimates obtained by using careful adjustment of radar observations may be useful to evaluate the severity of the storm for ungauged basins and to evaluate the spatial dimension of the frequency characterisation.

Chapter 4. *Flash flood warning based on rainfall depth-duration thresholds and soil moisture conditions*. The main objective of this study is to evaluate a threshold-based flash flood warning approach, by considering a wide range of climatic and physiographic European conditions, and by focusing on ungauged basins. The system is derived from the Flash Flood Guidance (FFG, hereafter) approach. The FFG is the depth of rain of a given duration, taken as uniform in space and time on a certain basin, necessary to cause minor flooding at the outlet of the considered basin. This rainfall depth, which is computed based on a lumped hydrological model, is compared to either real time-observed or forecasted rainfall of the same duration and on the same basin. If the nowcasted or forecasted rainfall depth is greater than the FFG, then flooding in the basin is considered likely.
The study provides an assessment of this technique based on operational quality data from eleven basins (six nested included in five larger parent basins) located in two European regions: north-eastern Italy and central France. The model used in this study is a semi-distributed conceptual rainfall-runoff model, following the structure of the PDM (Probability Distributed Moisture) model. System performances are evaluated by means of categorical statistics, such as the Critical Success Index (CSI).
The simulation experiments described in this study are designed to understand the potential benefits and limitations of the flash flood warning approach under different scenarios of data availability for model calibration and use, and to guide further development. The study explores three major questions: How technique accuracy at ungauged interior points, simulated by using transposed parameters from parent basins, compares with results obtained for parent basins where calibration has been carried out? Which are the technique performances when soil moisture status is transposed from the larger scale parent basins? Which is the decrease in accuracy associated to use of time-constant soil moisture status, compared to results obtained by using estimates of soil moisture status provided by the hydrological model?
Results show that overall CSI is equal to 0.43 for the parent basins, where the hydrological model has been calibrated. CSI reduces to 0.28 for the interior basins, when model parameters are transposed from parent basins, and to 0.21, when both model parameters and soil moisture status is transposed from parent basins. Performance differences between FFG and use of time-constant soil moisture status are very high for the parent basins and decrease with decreasing the system accuracy. The percent difference amounts to 53% for

the parent basins, to 25% for interior basins with parameter transposition, and to 19% for interior basins with parameter and soil moisture status transposition.
These results improve our understanding of the applicability and reliability of this technique at various scales and under various scenarios of data availability.

Chapter 5. *Controls on event runoff coefficients in the eastern Italian Alps.* This chapter shows an analysis of event runoff coefficients at regional scale. Analysis of event runoff coefficients provides essential insight on catchment response, particularly if a range of catchments and a range of events are to be compared by a single indicator. This study examines the effect of climate, geology, land use, flood types and initial soil moisture conditions on the distribution functions of the event runoff coefficients for a set of 14 small-to-medium size mountainous catchments located in the eastern Italian Alps. Runoff coefficients were computed from hourly precipitation and runoff data and estimates of snowmelt. A total of 535 events were analysed over the period 1989-2004. We classified each basin using a "permeability index" which was inferred from a geologic map and ranges from "low" to "high permeability". A continuous soil moisture accounting model was applied to each basin to trace the soil moisture conditions of catchments in a continuous way and to classify 'wet' and 'dry' initial soil moisture conditions. The results indicate that the spatial distribution of runoff coefficients is highly correlated with mean annual precipitation, with mean runoff coefficient increasing with mean annual precipitation. Geology, through the 'permeability index', is another important control on runoff coefficient for catchments with mean annual precipitation less than 1200 mm. Land use, as indexed by the SCS curve number, influences runoff coefficient distribution to a lesser degree. An analysis of the runoff coefficients by flood type indicates that runoff coefficients increase with event snowmelt. Results show that it exists an optimum region of soil moisture capacity, as indexed by a flow duration curve-based index, which maximises the impact of initial soil moisture conditions on runoff coefficient. This means that the difference between runoff coefficients characterised by wet and dry initial conditions is negligible for basins with very larger groundwater capacity (given by largely karstified aquifer) and for basins with reduced groundwater capacity. For basins characterised by intermediate conditions, the difference (and hence the impact of the initial soil moisture conditions) may be relatively large.

Chapter 6. *Analytical solutions to a hillslope-storage kinematic wave model for subsurface flow and analysis of its hysteretic behaviour*. The subsurface flow dynamics is analysed by means of a model based on the kinematic wave assumptions and by using a width weighting/depth averaging scheme which allows to map the three-dimensional soil mantle into a one-dimensional profile. Continuity and a kinematic form of Darcy's law lead to a hillslope-storage kinematic wave equation for subsurface flow, solvable with the method of characteristics. Adopting a second order polynomial function to describe the bedrock slope and an exponential function to describe the variation of the width of the hillslope with hillslope distance, we derive general solutions to the hillslope-storage

kinematic wave equations, applicable to a wide range of hillslopes. These solutions provide a physical basis for deriving two geometric parameters α and ψ which define the hydrological similarity between hillslopes with respect to their characteristic response. Results of the application of this simplified model for subsurface flow processes show the existence of a hysteretic behaviour in the saturated storage - flux relationships at the hillslope scale. The influence of topographic factors on the hysteretic behaviour has been widely explored on the study. The hysteresis η, quantified by the area of the hysteretic dimensionless loop, has been computed for a range of values of parameters α and ψ. Slopes exhibit generally clockwise hysteretic loop in the flux-storage plot, with higher groundwater mean volume for given discharge on rising limb than at same discharge on falling limb. It has been found that hysteresis increases with decreasing α and ψ, i.e. with increasing convergence (for the shape) and concavity (for the profile), and viceversa. For relatively large values of α and ψ the hysteresis may take a complex pattern, with combination of clock-wise to anticlock-wise loop cycles. Application of the theory to three hillslopes in the Eastern Italian Alps provides an opportunity to examine how natural topographies are represented by the two hillslope hydrological similarity parameters.

Chapter 7. *General conclusions.*

This work is dedicated to my parents
and to my dear sister Margherita

Acknowledgement

First and foremost I would like to express my gratitude to my advisor, Prof. Marco Borga, for essential guidance and insight throughout my studies. His support, genius, and inspiration for scientific research has contributed to give me energy and enthusiasm during my researches.

Additionally, I thank everyone at the TESAF Department for the unique and stimulating environment they have provided, and most notably: Francesco Zanon, Paolo Tarolli, Daniele Penna, Marco Sangati, Alberto De Luca, Silvia Degli Esposti, Fabrizio Tonelli, Paolo Boscolo and Jacopo Selleroni. Their friendship was essential for me particularly during some difficulties happend during my PhD; I will not forget this.

The Regional Meteorological Observatory of Friuli-Venezia- Giulia and the Hydrological Office of Carinzia (Autria) is thanked for making the radar and the raingauge dataset available. Data for the Adige and Brenta river systems were kindly provided by Provincia Autonoma di Bolzano - Ufficio Idrografico and by Provincia Autonoma di Trento – Servizio Bacini Montani, respectively. ARPA – Regione Veneto kindly provided the data for the Bacchiglione and Piave river systems. The Direction Régionale de l'Environnement de la Région Centre and the Etablissement Public Loire kindly provided the data for the Loire river basin.

Needless to say, my family deserves a great deal of credit for my development. I thank my parents and my sister for all their love and support. Finally, I thanks Chiara, whose love carries me through life.

Daniele Norbiato

Index

Riassunto i
Acknowledgement xv
Index xvii
Index of figures xix
Index of tables xxii
1 Introduction 1
1.1 References 5
2 Development of an observation strategy to advance understanding of flash flood hydrometeorological processes 7
2.1 Introduction 7
2.2 The Fella 2003 flash flood 9
2.3 Post event field campaign 12
2.4 Influence of spatial temporal rainfall variability and of antecedent soil moisture conditions 13
2.5 Analysis of flood severity 14
2.6 Conclusions 15
2.7 References 15
3 Regional frequency analysis of extreme precipitation in the eastern Italian Alps and the August 29, 2003 flash flood 17
3.1 Introduction 17
3.2 Regional frequency analysis methodology 18
3.2.1 The four steps of the HW regional frequency analysis methodology 20
3.3 Data Analysis and Results 22
3.3.1 Spatial mapping of at-sites means 23
3.3.2 Partitioning the region and estimation of regional growth curves 24
3.3.3 Severity analysis of the 29 August 2003 flash-flood generating storm 30
3.3.3.1 Analysis of storm severity 31
3.4 Summary and conclusions 36
3.5 References 38
4 Flash flood warning based on rainfall depth-duration thresholds and soil moisture conditions 43
4.1 Introducion 43
4.2 Study Areas and Data 45
4.2.1 Rationale for basins selection 49
4.3 The threshold-base technique 50
4.3.1 Description of the hydrological model 50
4.4 Assessment methodology 52
4.4.1 Model application 52
4.4.2 FFG assessment 55

4.4.3 Threshold flooding conditions 57
4.5 Results 58
4.5.1 Model application 58
4.5.2 FFG assessment 59
4.6 Conclusions and future works 65
4.7 References 67
5 Controls on event runoff coefficients in the eastern Italian Alps 71
5.1 Introduction 71
5.2 Study basins: morphology, climate, land use and geology 72
5.3 Computation of event runoff coefficients 77
5.3.1 The baseflow separation method 77
5.3.2 The event separation method 78
5.3.3 Estimation of the runoff coefficient 79
5.3.4 The continuous soil-moisture accounting hydrological model 80
5.4 Results 82
5.4.1 The role of climate 85
5.4.2 The role of geology 86
5.4.3 The role of land use 87
5.4.4 The role of initial soil moisture conditions 88
5.5 Conclusions 93
5.6 References 94
6 Analytical solutions to a hillslope-storage kinematic wave model for subsurface flow and analysis of its hysteretic behaviour 97
6.1 Introduction 97
6.2 The hillslope-storage kinematic wave model 100
6.2.1 Analytical solution using the method of characteristics 101
6.2.2 Determination of subsurface discharge at the hillslope outlet 105
6.2.3 Determination of the hillslope saturated moisture content 107
6.2.4 Dimensional inspection 108
6.3 Analysis of the hysteretic behaviour for basic hillslope types 110
6.4 Determination of the hillslope similarity parameters for three natural hillslopes. 114
6.5 Concluding remarks 118
6.6 References 120
7 General conclusions 123
Curriculum Vitae 131

Index of figures

Figure 2-1. Location of the North-Eastern Italy Hydrometeorological Observatory with weather radar converge. 9
Figure 2-2. The Tagliamento river basin with DTM of North-Eastern Italy. The location of the OSMER radar and location of the 15 raingauges used in the study is also reported. (PB: Pontebba; PP: Pramollo). 10
Figure 2-3. Basin map of the upper Tagliamento river basin, with subbasins of the Fella river basin. (1): Uqua at Ugovizza; (2) Fella at Pontebba; (3) Fella at Dogna; (4) Raccolana at Raccolana; (5) Resia at Borgo Povici; (6) Fella at Moggio Udinese; (7) Tagliamento at Venzone; (8) Rio del Lago at Cave del Predil; (9) Slizza at Tarvisio....11
Figure 2-4. Storm total rainfall (mm) for the August 29, 2003 storm. 11
Figure 3-1. Location of the study area with DTM of North-Eastern Italy. The locations of the raingauge stations used in the study are also reported. 22
Figure 3-2a-c. Maps of point average of maximum yearly rainfall for durations of (a) 1 hours, (b) 6 hours, and (c) 24 hours, for the Friuli region....24
Figure 3-3. Subdivision of the raingauge stations into three subregions. 25
Figure 3-4a-c. Identification of subregional frequency distribution using regional L-skewness L-kurtosis diagram: a) Subregion A; b) Subregion B; c) Subregion C. Notation: GEV: generalised extreme value; GLO: generalised logistic; PE3: Pearson type III; LN3: lognormal-3; G: Gumbel....26
Figure 3-5a-e. Subregion C growth curves for Kappa, GLO and GEV distributions compared with regional normalised sample for five durations: a) 1h, b) 3h, c) 6h, d) 12h and e) 24h. Normalised data marked in bold result from the storms of August 29, 2003, June 22, 1996 and September 11, 1983....28
Figure 3-6a-b. Severity graph obtained from raingauge data and from radar rainfall estimates for the stations located in a) Pontebba and b) Pramollo. 33
Figure 3-7a-d. Return time patterns for rainfall maxima corresponding to a) 1h, b) 3h, c) 6h and d) 12h. The bold triangle represent the position of the Pontebba raingauge station.34
Figure 3-8a,b. Severity graph for two basins in the upper Fella basin: a) Uqua; b) Aupa. ...35
Figure 3-9a-d. Ratio of point to areal rainfall maxima for rainfall duration of a) 1h, b) 3h, c) 6h and d) 12h....37
Figure 4-1. Study basins and their location in France and Italy 46
Figure 4-2. Plot of mass balance data from the study basins on the Budyko curve. 49
Figure 4-3a-e. One year (01.01.1993-31.12.1993) of hourly results at the outlet for the Cordevole river at Vizza (a) simulation results with model parameter transposition from Cordevole at Saviner; (b) simulation residuals, (c) simulation results with model parameter and soil moisture transposition from Cordevole at Saviner; (d) simulation residuals (e) relative soil moisture content of the PDM storage obtained from model parameter transposition at Vizza and from model simulation at Saviner. 55

Figure 4-4a-c. Evaluation of the threshold-based technique for: a) parent basin with model calibration; b) interior basins with model parameter transposition; c) interior basins with both model parameter ans soil moisture status transposition. POD and FAR scores are plotted. 61
Figure 4-5a-c. Evaluation of the threshold-based technique for: a) parent basin with model calibration; b) interior basins with model parameter transposition; c) interior basins with both model parameter ans soil moisture status transposition. CSI scores are plotted. 62
Figure 4-6a-c. Overall assessment of the threshold-based technique for: a) parent basin with model calibration; b) interior basins with model parameter transposition; c) interior basins with both model parameter and soil moisture status transposition. POD and FAR scores are plotted. 64
Figure 4-7a-c. Overall assessment of the threshold-based technique for: a) parent basin with model calibration; b) interior basins with model parameter transposition; c) interior basins with both model parameter and soil moisture status transposition. CSI scores are plotted. 64
Figure 5-1. Study basins and their location in Italy 72
Figure 5-2. Plot of mass balance data from the study basins on the Budyko curve 74
Figure 5-3. a) mean monthly rainfall over MAP; b) mean monthly snowfall over MAP; c) mean monthly runoff over mean annual runoff..... 75
Figure 5-4. Separation of baseflow and runoff events. a) Basin 5 (San Vigilio at Longega), b) Basin 13 (Cordevole at Saviner), c) Basin 12 (Posina at Stancari)..... 78
Figure 5-5. Distribution function of the event runoff coefficients for the study basins 82
Figure 5-6a-b. Mean runoff coefficients plotted versus: a)coefficients of variation of runoff coefficient distributions; b) skewness of runoff coefficient distributions. 83
Figure 5-7a-c. Event runoff depth vs. event rainfall depth; event runoff depth vs. runoff coefficient; flood peak vs. runoff depth (with indication of the mean runoff coefficient, the mean maximum annual flood and the mean flood), for three representative basins: a) Basin 5 (San Vigilio at Longega), b) Basin 13 (Cordevole at Saviner), c) Basin 12 (Posina at Stancari). Note the change of scale for the three basins. 84
Figure 5-8. Relationship between mean event rainfall and MAP for the study basins..... 85
Figure 5-9. Mean runoff coefficients versus MAP for the study basins 86
Figure 5-10. Mean runoff coefficients versus MAP for the study basins stratified by permeability index. 87
Figure 5-11. Quantiles of runoff coefficient distributions versus the SCS Curve Number. 88
Figure 5-12. The influence of geology on the gradient of the standardised flow duration curve. 89
Figure 5-13. Distribution function of the event runoff coefficients for different percentages of snow melt over event rainfall depth 91
Figure 5-14a-c. Distribution functions of initial relative soil moisture, runoff coefficients and event rainfall depths for dry and wet periods. a) Basin 5 (San Vigilio at Longega), b) Basin 13 (Cordevole at Saviner, c) Basin 3 (Riva at Seghe). 92

Figure 5-15. Optimum region of groundwater capacity, as indexed by the parameter Q90/Q50. 93
Figure 6-1. Three-dimensional view of a convergent hillslope 100
Figure 6-2. (x,t) plane with characteristic curves and domain definition 102
Figure 6-3. Three-dimensional view of the nine hillslopes considered in this study. 111
Figure 6-4. Time series of subsurface flow rates and hillslope saturated moisture content for the nine hillslopes 111
Figure 6-5. Storage-flux relationships for the nine hillslopes 112
Figure 6-6. Normalised storage ($\sigma(t)=V(t)/V_{max}$) versus flux ($\varphi(t)=Q(L,t)/Q_{max}$) relationships for the hillslopes 1, 3, 7 and 9. 113
Figure 6-7. The α - ψ plot, with hysteresis η as function of the hillslope similarity parameters α and ψ. 114
Figure 6-8. Rio Vauz basin and localization of the three natural hillslopes 115
Figure 6-9. Topography of the three natural hillslopes 115
Figure 6-10. The centroid profiles (a,b,c) and the width of hillsopes (d,e,f) and their representation by means of the second order polynomial function (for profile) and the exponential function(for width). 117
Figure 6-11. The hillslope similarity parameters α and ψ for the three natural hillsplopes.118

Index of tables

Table 2-1. Characteristics of the surveyed river sections and of the corresponding drainage basins 13
Table 2-2. Rainfall and runoff for the surveyed basins (NA: not available) 14
Table 3-1. Heterogeneity measures (H(1) and H(2)) for the three subregions and for the five rainfall durations. 25
Table 3-2. Values at the normalised rainfall maxima exceeding a threshold value of 3.0 for Subregion C 29
Table 3-3. Z statistic reported for GEV and GLO distribution for the three Subregions and the five durations 29
Table 3-4. Normalised quantiles obtaine based on Kappa distribution for various rainfall durations and return periods for Subregion C 29
Table 3-5. Maximum rainfall depths obtained for various durations from raingauge measurements and from adjusted radar estimates for the stations located in Pontebba and Pramollo 32
Table 4-1. Basins characteristics 47
Table 4-2. Periods with data considered: parent basins 47
Table 4-3. Periods with data available: interior points 48
Table 4-4. Relationship among parent and nested basins 48
Table 4-5. Four-cell contingency table used in the study 56
Table 4-6. Model validation and calibration results. Parent basins 58
Table 4-7. Model validation results. Interior Points 59
Table 5-1. Basins characteristics 73
Table 5-2. Land use for the study basins 76
Table 5-3. Permeability index 76
Table 5-4. Periods with data available 81
Table 5-5. Continuous soil moisture accounting model validation and calibration results 81
Table 5-6. Statistical characteristics of the event runoff coefficient distribution functions 82
Table 5-7. The soil moisture capacity index (Q_{90}/Q_{50}). The table reports also the permeability index. 90
Table 6-1. Geometrical parameters for the nine slopes 110
Table 6-2. Geometrical parameters for the three natural slopes 117
Table 6-3. Hillslope similarity parameters for the three natural hillsplopes 117

1 Introduction

Over the years, hydrologists have developed numerous predictive tools (e.g. empirical models, lumped models, distributed models, statistical regionalizations) that allow objective and quantitative decision-making with respect to water resources and water quality management, as well as natural hazard assessments. The most widely used tools, such as unit hydrographs, flood frequency curves, flow duration curves, etc., are essentially data driven, and are estimated from hydrometric (gauged) data at drainage basin scales. Application of these tools for prediction in other basins is based on the premise that: (a) the past is a reasonable guide to the future, and (b) that data from any one basin, and models derived there from, are useful guides to estimate hydrological responses at another basin (Sivapalan et. al 2003 [12]). Whatever models are used, in view of the tremendous spatio-temporal heterogeneity of climatic and landscape properties, extrapolation of information, or knowledge, from gauged to ungauged basins remains fraught with considerable difficulties and uncertainties, especially in the light of the generally poor understanding of where water goes when it rains, what flow path it takes to the stream, and the age of the water that emerges in the channel. Meanwhile, new knowledge and new technological advances are becoming available to the hydrological community, in the form of increased process understanding, more advanced theories (e.g. scaling theories), new measurement technologies such as satellites and environmental tracers, and advanced data processing, data archiving and visualization technologies. Improving the capacity to make predictions in ungauged basins is one of most difficult challenge for the scientific community (see for example the current initiative PUB launched by the International Association of Hydrological Sciences, IAHS).

The PUB problem is the key concept of this thesis and it is analysed under several point of view. The first part of the work (Chapters 2, 3 and 4) is dedicated to develop and test methodologies for the observation, analysis and forecasting of flash flood events, that frequently affect ungaged basins. The second part of the work (Chapters 5 and 6) is dedicated to the analysis and the development of methodologies based on “Basin inter-comparison and classification” in order to improve understanding of regional characteristic hydrological cycle response and prediction in ungaged basins using inter-comparisons, and reanalysis of observations from single basin studies. Such methods aim at predicting basin and hillslope hydrological responses starting from informations concerning the most important controls on runoff response, such as climate and geomorphology, available at regional scale.

In the following the different aspect examined in this thesis are introduced..

A type of flood common in watersheds of few hundred kilometres or less (hence probably ungaged) is known as a flash flood and it is frequently associated with convective storms of short duration and high intensity. Flash floods are localized phenomena that occur in watersheds with response times of a few hours or less (Creutin and Borga, 2000[6]).

Such basins respond rapidly to intense rainfall because of steep slopes and impermeable surfaces, saturated soils, or because of human- (i.e., urbanization) or fire-induced alterations to the natural drainage. These floods follow the causative storm event in a short period of time, with water levels in the drainage network reaching a crest within minutes to a few hours after the onset of the rain event, leaving extremely short time for warning (Andrieu et al., 2005 [1]). The management of flash flood hazards and risks is a critical component of public safety and quality of life. Since flash-floods develop at space and time scales that conventional observation systems are not able to monitor for rainfall and river discharge, these events are generally characterised by a lack of experimental data and consequently the atmospheric and hydrological generating mechanisms of flash-floods are poorly understood , leading to highly uncertain forecasts of these events. To improve the observability of these phenomena, a monitoring strategy structured on two levels has been developed in the last years (Borga, 2005 [2]). First level is represented by the study of hydrologic response on slope and small basin scale in a network of instrumented sites, with the aim of providing data needed for a detailed description of processes which influence flow generation and shallow landsliding. Second level is represented by monitoring on a regional scale, where radar observations are used for assessing precipitation (Borga et al., 2000 [3]; Borga et. al, 2002 [4]) and a network of crest-stage gauges and post-event field observations are exploited for the evaluation of peak discharge and slope instabilities. In this way, it is possible to implement a monitoring strategy suitable for recording, on a regional scale, a number of floods, which display a low frequency at local (single basin) scale. Collected data can be used to characterise the 'global' basin response to rainstorms and recognise the influence of rainfall time-space variability on flood formation and shallow landsliding.

Results of a first application of this monitoring strategy are described in Chapters 2 and 3. The methodology, which couples analysis of radar rainfall estimates and post-flood surveys, has been applied to an alpine environments represented by the upper Tagliamento basin (North-eastern Italy). Particularly the analysis is focuses on the case study of the August 29, 2003 flash flood on Fella river basin which was characterised by extraordinary rainfall amounts and large spatial variability.

Chapter 2 reports a description of the post event survey and results concerning the impact of space-time precipitation variability and antecedent soil moisture conditions on flood response, and on the analysis of the flood peak discharge severity.

Chapter 3 is focuses on the use of both regional frequency analysis and radar rainfall observations to asses return periods for the above mentioned extreme flash flood-producing storm, for various rainfall durations. Regional frequency analysis based on the flood index method and L-moments is utilized to analyse short duration annual maximum precipitation for the Friuli-Venezia Giulia region, in north-eastern Italy, which includes the storm location. Radar rainfall estimates, adjusted by using a physically-based methodology and data from a raingauge network, are used to characterise the return period of the storm rainfall amounts, highlighting the importance of considering its spatial dimension.

In the case of flash-flood hazard, it is generally accepted that the most effective way (and in many instances the only affordable in a sustainable perspective) to mitigate the risk is by reducing the vulnerability of the involved communities, in particular by implementing flood warning systems and community self-help programs. However, both the inherent characteristics of the atmospheric and hydrologic processes involved in flash-flooding and the changing societal needs provide a tremendous challenge to traditional flood forecasting and warning concepts. In fact, the targets of these systems are traditionally localised like urbanised sectors or hydraulic structures. Given the small spatial scale that characterises flash floods and the development of dispersed urbanisation, transportation, green tourism and water sports, human lives and property are exposed to flash flood risk in a scattered manner (Creutin and Borga 2003 [6]). This must be taken into consideration in flash flood warning strategies and the investigated region should be considered as a whole and every section of the drainage network as a potential target for hydrological warnings. Operational flood forecasting systems are implemented and used in several European basins. These are often based on continuous hydrological models which are: i)capable to provide continuous estimates of soil moisture at the subbasin scale; ii) operate at spatial and temporal scales which are not commensurate with the requirements of flash flood detection and forecasting. Under certain conditions, the basin-scale soil moisture estimates provided by these models can be used to evaluate the antecedent moisture conditions at spatial scales closer to the need of flash flood forecasting (Carpenter et al., 1999 [5]; Georgakakos, 2006 [9]). Based on these soil moisture estimates, it may be possible to provide an estimate of the rainfall depth of a given duration which can bring the basin to flooding. This is the basis of Flash Flood Guidance (FFG), a methodology pioneered in the United States (Carpenter et al., 1999 [5]; Georgakakos, 2006 [9]) which provides flash flood forecasting and warning without explicitly modelling the event dynamics. At the ground of FFG is the computation of threshold runoff values, or the amount of effective rainfall of a given duration, taken as uniform in space and time, that is necessary to cause flooding at the outlet of the considered basin. This rainfall depth, which is computed based on a lumped hydrological model, is compared to either real time-observed or forecasted rainfall of the same duration and on the same basin. If the nowcasted or forecasted rainfall depth is greater than the FFG, then flooding in the basin is considered likely. The relationship between FFG and threshold runoff is a function of the current soil moisture conditions, which are estimated in real time by operational soil moisture accounting models.

Chapter 4 shows results concerning the evaluation of a threshold-based flash flood warning approach based on the FFG concept by considering a wide range of climatic and physiographic European conditions, and by focusing on ungauged basins. A semi-distributed conceptual rainfall-runoff model was used to estimate antecedent soil moisture conditions. The simulation experiments reported in this chapter are designed to understand the potential benefits and limitations of the flash flood warning approach under different scenarios of data availability for model calibration and use, and to guide further development. The study explores three major questions: How technique accuracy at

ungauged interior points, simulated by using transposed parameters from parent basins, compares with results obtained for parent basins where calibration has been carried out? Which are the technique performances when soil moisture status is transposed from the larger scale parent basins? Which is the decrease in accuracy associated to use of time-constant soil moisture status, compared to results obtained by using estimates of soil moisture status provided by the hydrological model?

Solving the PUB (prediction in ungaged basins) problem calls for new approaches in basin analysis and modelling. Methodologies based on "Basin inter-comparison and classification" can improve understanding of regional characteristic hydrological cycle response and prediction in ungaged basins using inter-comparisons, and reanalysis of observations from single basin studies. Following this direction, Chapter 5 shows an analysis of event runoff coefficients at regional scale. The analysis provides essential insights on basin response, particularly if a range of basins and a range of events are to be compared by a single indicator. The study analysis the process controls on event runoff coefficients using data from 14 basins, located in the eastern Italian Alps, with area ranging from 7 to 600 km^2. Following the methodology described in Merz et al. (2006 [11]), a total of 535 events have been back calculated from hourly runoff data, hourly precipitation data and model-based estimates of snowmelt over the period 1989-2004. A continuous soil moisture accounting model was applied to each basin to derive initial soil moisture conditions prior to each event. Basins were classified according to the permeability characteristics of the lithological units, as inferred from geological surveys, and according to the soil moisture capacity, inferred from analysis of the flow duration curve. The statistical characteristics of the distribution functions of the runoff coefficients as well as the effect of event rainfall characteristics, climate, geology, land use and antecedent soil moisture conditions on the runoff coefficients are examined.

PUB advancement can be obtained through the development of a new generation of models able to integrate in an innovative way the information concerning the basin's morphological structure, which is the only one everywhere available, particularly in the case of ungaged basins. The availability of high resolution topography offers new opportunities for objectively extracting the channels directly from a Digital Elevation Model (DEM) using local topographic information, instead of inferring them indirectly based on global criteria, such as area or area-slope threshold relationships. There are, however, alternative ways of applying geomorphic data in a more implicit way, that, by doing so, do respect these larger scale geomorphic structures. Thus far, Fan and Bras (1998 [8]) and the Hydrology and Quantitative Water Management (HWM) group of Wageningen University (The Netherlands) and then at the Arizona University have developed methods that account for the three-dimensional hillslope form while still using simple flow equations. Recently, Troch et al. (2002 [13], 2004 [14]) developed storage-based equations able to capture the flow processes of all elementary hillslopes by simple scaling laws pertaining to hillslope length, slope and form. Such a description can give rise

to a new generation of distributed rainfall-runoff models because it captures the essential behaviour of the natural system while being low-dimensional and computationally efficient. Hillslope response has traditionally been studied by means of the hydraulic groundwater theory. Solving the three-dimensional Richards equation for different hillslopes within a basin is a complex task. Fan and Bras (1998 [8]) presented a way to transfer the three-dimensional soil mantle into a one-dimensional profile. Continuity and a kinematic form of Darcy 's law lead to quasi-linear wave equations for subsurface flow, solvable with the method of characteristics. Adopting a power function of the form proposed by Di Stefano et al. (2000 [7]) to describe the bedrock slope, Troch et al. (2002 [13]) derive more general solutions to the hillslope-storage kinematic wave equation for subsurface flow, applicable to a wide range of complex hillslopes. Chapter 6 describes a theoretical framework which can be used to define the hydrological similarity between hillslopes with respect to their characteristic response. The study is a development of the approach proposed by Troch et al. (2002 [13]). The subsurface flow dynamics is analysed by means of a simplified model based on the kinematic wave assumptions and using a method first proposed by Horton (1936 [10]) and then further developed by Fan and Bras (1998 [8]) to transfer the three-dimensional soil mantle into a one-dimensional profile. The hillslope-storage subsurface flow equation considered in this study takes into account the topographic controls exerted on the flow processes by the plan shape and profile curvature. A second order polynomial function was used to describe the bedrock slop whereas an exponential function is used to describe the variation of the width of the hillslope with hillslope distance. Under these assumptions general solutions to the hillslope-storage kinematic wave equations, applicable to a wide range of hillslopes, have been found. These analytical solutions affords a broad and clear view of the essential features of the problem and allows to derive two geometric parameters α and ψ which define the hydrological similarity between hillslopes with respect to their characteristic response. Therefore, each hillslope may be represented in a α - ψ plot which allows deriving essential information on its response. Results of the application of this simplified model for subsurface flow processes show the existence of a hysteretic behaviour in the saturated storage - flux relationships at the hillslope scale. The influence of topographic factors on the hysteretic behaviour has been widely explored on the study. Application of the theory to three hillslopes in the Eastern Italian Alps provides an opportunity to examine how natural topographies are represented by the two hillslope hydrological similarity parameters.

1.1 References

[1] Andrieu et al., 2005. A Blueprint On Storm Driven Floods In The Mediterranean: Observation, predictability and Social Vulnerability. INPG, Grenoble, France, 63 pp.

[2] Borga, M., Degli Esposti, S., Dalla Fontana, G., 2005. Analisi e sintesi del regime delle precipitazioni intense in Friuli Venezia Giulia. In: "La prevenzione del rischio idrogeologico nei piccoli bacini montani della regione: Esperienze e conoscenze

acquisite con il progetto CATCHRISK". Convegno finale del Progetto CATCHRISK, Udine, 28 - 29 Giugno 2005, 75-93.

[3] Borga M., Anagnostou, E.N., Frank, E., 2000. On the use of real-time radar rainfall estimates for flood prediction in mountainous basins. Journal of Geophysical Research, 105, D2, 2269-2280.

[4] Borga M., Tonelli F., Moore, R.J., Andrieu, H., 2002. Long-term assessment of bias adjustment in radar rainfall estimation. Water Resources Research, 38(11), 1226, doi:10.1029/2001WR000555.

[5] Carpenter, T.M., Sperfslage, J.A., Georgakakos, K.P., Sweeney, T., Fread, D.L., 1999. National threshold runoff estimation utilizing GIS in support of operational flash flood warning systems. Journal of Hydrology, 224, 21–44.

[6] Creutin, J.D., Borga, M., 2003. Radar hydrology modifies the monitoring of flash flood hazard. Invited commentary. 10.10002/hyp.5122, Hydrological Processes, 17, 7, 1453-1456.

[7] Di Stefano, C., Ferro, V., Porto, P., Tusa,. G., 2000. Slope curvature influence on soil erosion and deposition. Water Resoir.Res., 36, 607-617.

[8] Fan, Y., Bras, R.L, 1998. Analytical solutions to hillslope subsurface storm flow and saturation overland flow. Water Resour. Res., 34(4):921-927.

[9] Georgakakos, K. P., 2006. Analytical results for operational flash flood guidance. Journal of Hydrology, 317 (1-2), 81-103, doi:10.1016/j.jhydrol.2005.05.009.

[10] Horton, R. E., 1936. Maximum groundwater levels. Trans. Am. Geophys. Union. 17(2), 344–357.

[11] Merz, R., Bloeschl, G., Parajka, J., 2006. Spatio-temporal variability of event runoff coefficients. Journal of Hydrology, 331, 591-604.

[12] Sivapalan, M., Takeuchi, K., Franks, S.W., Gupta, V.K., Karambiri, H., Lakshmi, V., Liang, X., McDonnell, J.J., Mendiondo, E.M., O'Connell, P.E., Oki, T., Pomeroy, J.W., Schertzer, D., Uhlenbrook, S., Zehe, E., 2003. IAHS decade on Predictions in Ungauged Basins (PUB), 2003-2012: shaping an exciting future for the hydrological sciences. Hydrological Sciences Journal, 48, 857-880.

[13] Troch P., van Loon, E., Hilberts, A., 2002. Analytical solutions to a hillslope-storage kinematic wave equations for subsurface flow. Advances in Water Resources, 25:637–49.

[14] Troch, P. A., van Loon, A. H., Hilberts, A. G. J., 2004. Analytical solution of the linearized hillslope-storage Boussinesq equation for exponential hillslope width functions. Water Resour. Res., 40, W08601, doi:10.1029/2003WR002850.

2 Development of an observation strategy to advance understanding of flash flood hydrometeorological processes[1]

2.1 Introduction

Europe experienced several catastrophic flash floods in the last decades. Data concerning a number of these floods occurred during the last 15 years have been reported by Borga (2006 [1]). Examination of these data shows that:

- flash floods occur in any of the hydroclimatic regions of Europe, even though three regions appear to be characterized by high flash flood potential: Mediterranean, Alpine Mediterranean, and Inland Continental Europe;
- heavy rainfall accumulation is a necessary but not sufficient condition for flash floods, since hydrology critically controls flash-flood-triggering. Without hydrological analysis, it is impossible to evaluate the flood potential of storms, particularly in the fringe of the flood/no flood threshold;
- flash flood hazard is related to both stream response (flood) and landscape response (landslide and erosion). The intense erosion and solid transport associated with these extreme events add to the hazard and strongly influence the quality of soils, waters and ecosystems.

Large research efforts have been made on the analysis and modelling of the meteorological aspects of the flash-flood triggering storms (see for instance the proceedings of the European Geophysical Union Plinius conferences on Mediterranean storms). In comparison, the analysis of the dynamics of the runoff processes during flash-floods is still at its infancy. Lack of observations concerning rainfall and discharge is probably the main limiting factor to advance the understanding of the hydrological processes at work during flash floods. This form of process understanding is required for flash flood forecasting, due to the fact that the small basins prone to flash-floods are rarely gauged and must be modelled without prior calibration. Furthermore, the dominant processes of runoff generation may change with the increase of storm severity, and therefore the understanding based on analysis of moderate flood events may be questioned when applied to forecast the response to extreme storms.

Observational limitations mainly stem from the fact that flash floods develop at space and time scales that conventional observation systems of rain and river discharges are not able to monitor (Cretin and Borga, 2003 [6]). As these events are locally rare, they are also difficult to capture during classical field-based experimentation, designed to last a

[1] The study described in this chapter has been proposed in Norbiato et al. (2007a [12]).

few months over a given region (e.g., Mesoscale Alpine Programme, MAP) or on experimental basins, with drainage area of a few km squares.

There is a strong need, therefore, to develop an innovative flash flood-focused observational strategy in order to improve our knowledge about flash flood generating processes. This strategy has been advocated by Creutin and Borga (2003 [6]) and more recently by Carpenter et al. (2007 [5]), and it is based on the concept of the Hydrometeorological Observatory (HO). This is a cooperative structure, linking together operational forecasting centres and research centres, capable to maintain a long term hydrometeorological monitoring over geographical areas large about 10 000–30 000 km^2. These areas are large enough to have a good probability of observing flash-flood events within a period of reasonable duration (three to five years).

The common objective of the HO is to observe flash flood wherever they occur by combining:

- conventional hydrometeorological monitoring;
- weather radar observations;
- complementary information acquired from field surveys executed during the days following the event.

On one hand, data provided by state of the art radar networks (such as those currently used in several European countries), together with rain gauge network data, have the potential to increase substantially the resolution and accuracy of precipitation measurement for flash flood-generating storms (Borga et al., 2000 [2], 2006 [3]). On the other hand, operational discharge measurements and post-event surveys, including indirect flood discharge estimates based on high water marks and peak time estimates based on interviews, can provide a spatially-detailed account of the stream response (Gaume, 2006 [8]).

This observations strategy has been implemented within a network of Hydrometeorological Observatories developed in the frame of the EU R&TD Projects FLOODsite and HYDRATE (Figure 2-1 shows the location of the North-Eastern Italy Hydrometeorological Observatory). These HOs are characterised by a good density of hydrometeorological stations and by a reliable weather radar coverage. All these observatories are already operational, and incorporate considerable detailed information about flash floods observed in the last decade.

Observations related to the case study of the August 29, 2003 flash flood on Fella river basin (North-eastern Italy) are examined in the following sections where a description of the post event survey is reported. Results are presented concerning the impact of space-time precipitation variability and antecedent soil moisture conditions on flood response, and on the analysis of the flood peak discharge severity.

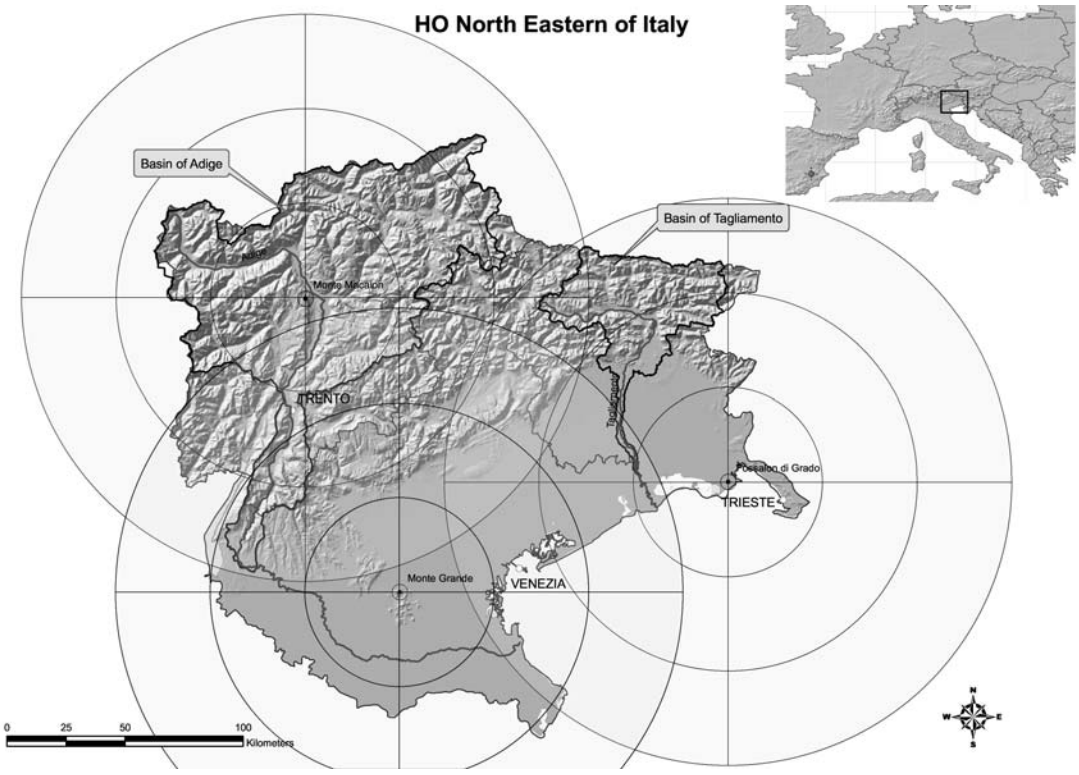

Figure 2-1. Location of the North-Eastern Italy Hydrometeorological Observatory with weather radar converge.

2.2 The Fella 2003 flash flood

On August 29, 2003, at the end of a prolonged drought, a Mesoscale Convective System affected the Fella basin, which is a major left-hand tributary of the Tagliamento river system (Figure 2-2). This event is one of the most devastating flash flood events in North-eastern Italy. The storm affected a 1500 km^2 wide area, and caused loss of lives and substantial disruption of a local economy, with damages close to 1 billion Euro (Tropeano et al., 2004 [15]). The rainfall event started at 10:00 (Local Standard Time) and lasted for 10 hours, mainly focused on the 705 km^2-wide Fella basin (Figure 2-3). The Fella basin has a mean altitude of 1140 m a.s.l., with an average annual precipitation of 1920 mm. Major subbasins of the Fella river are Pontebbana (70 km^2) and Aupa (50 km^2) (right-hand tributaries) and Dogna (47 km^2), Raccolana (63 km^2) and Resia (107 km^2) (left-hand tributaries).

Radar and raingauge observations were used to derive rainfall fields: 5-minute raingauge data were collected at 15 raingauges (Figure 2-2), whereas storm total rainfall was available at further six daily raingauges. Volume scan reflectivity data from the Doppler, dual-polarised C-band OSMER radar station, located at Fossalon di Grado (Figure 2-2) (time resolution of 5 min and spatial resolution of 250 m in range by 0.9 degree in azimuth), were used to derive radar rainfall rates.

The storm total precipitation (Figure 2-4) exhibits three local peaks of rainfall accumulations exceeding 320 mm. The most extended accumulation is over the upper Aupa basin and the mid-Pontebbana basin; the second peak is close to the Uqua basin and near the Italian Austrian border; the third one (and also the less extended) is located over

the extreme eastern portion of the study area. The storm total rainfall distribution reflects south west - north east motion of the storm elements and west-east shift of the tracks of the storms. Rainfall intensity up to 100 mm hr^{-1} was recorded during the explosive growth phase of the storm (between 15:00 and 18:00 LST). Extreme rainfall from the August 2003 storm was produced by quasi-stationary convective banded structures. Some of the bands persisted in the same locations for the duration of the event. The steadiness of these rainbands led to highly variable precipitation accumulations and runoff. Rainfall produced by the August 2003 storm resulted in severe flooding throughout the Fella river basin.

The storm produced catastrophic flooding at drainage areas up to 80-90 km^2, with dominance of debris floods (Slaymaker, 1988 [13]) at basin scale up to some tens of km^2. These debris floods were essentially extreme streamflows with large quantities of muds, rocks and debris, including woody debris. It was also a case of extreme rainfall with point values of up to 400 mm recorded within a 10 hour period over an area of 600 km^2.

River stage data from ultrasound sensor were available at nine stations. These data were reviewed during the post-event analysis and allowed to derive flood discharge estimates. Antecedent soil moisture distribution appears to have played an important role in flood response. Measured peak discharges were large and devastating, but not as exceptional as implied by the measured rainfall. The exceptionally dry summer season of 2003, combined with the high soil moisture storage capacity which characterises the basins in the upper Tagliamento watershed, resulted in low runoff ratios and emphasised the non-linearity of the flood response.

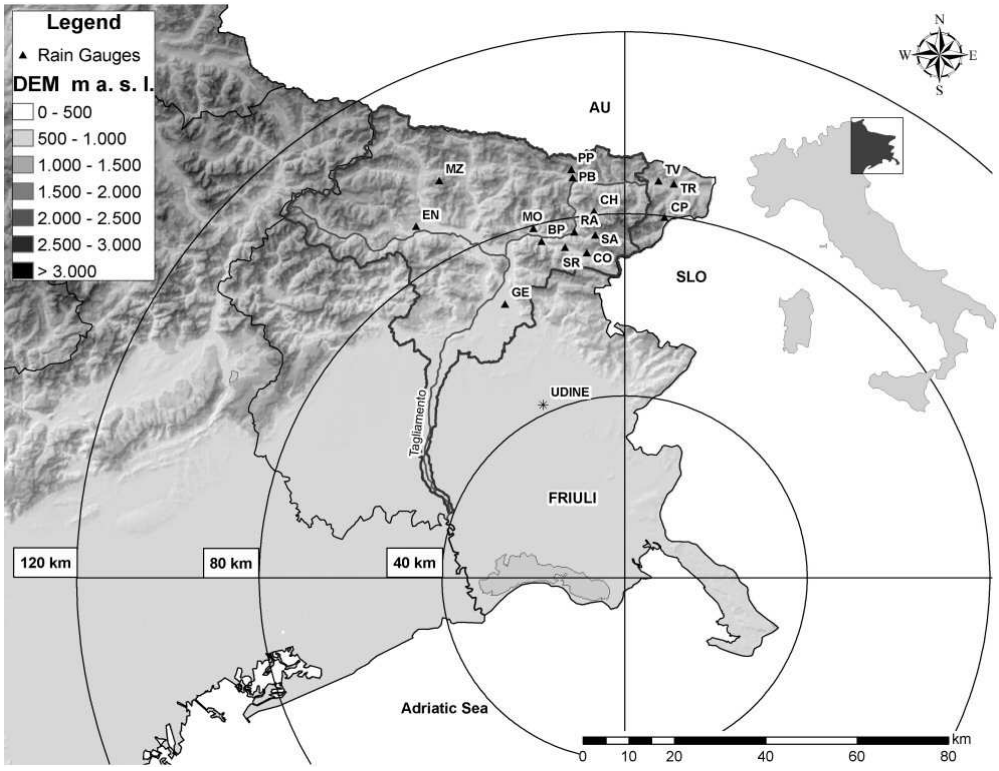

Figure 2-2. The Tagliamento river basin with DTM of North-Eastern Italy. The location of the OSMER radar and location of the 15 raingauges used in the study is also reported. (PB: Pontebba; PP: Pramollo).

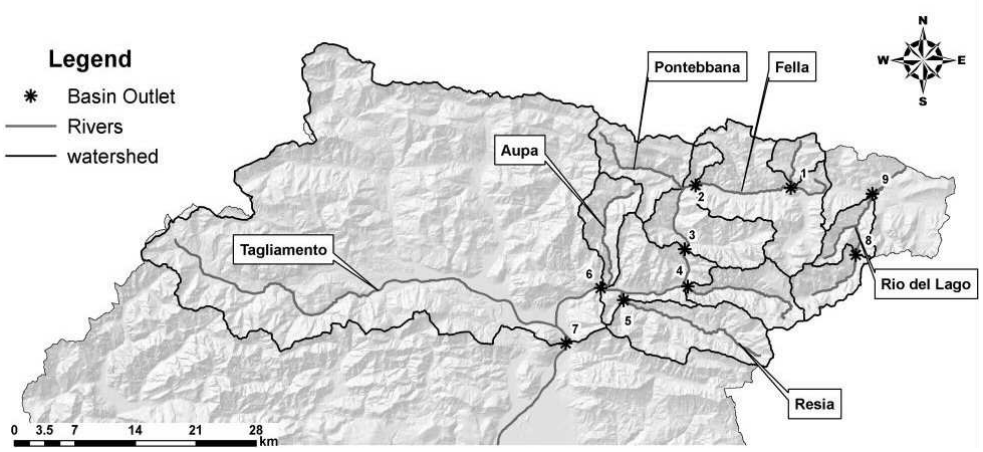

Figure 2-3. Basin map of the upper Tagliamento river basin, with subbasins of the Fella river basin. (1): Uqua at Ugovizza; (2) Fella at Pontebba; (3) Fella at Dogna; (4) Raccolana at Raccolana; (5) Resia at Borgo Povici; (6) Fella at Moggio Udinese; (7) Tagliamento at Venzone; (8) Rio del Lago at Cave del Predil; (9) Slizza at Tarvisio.

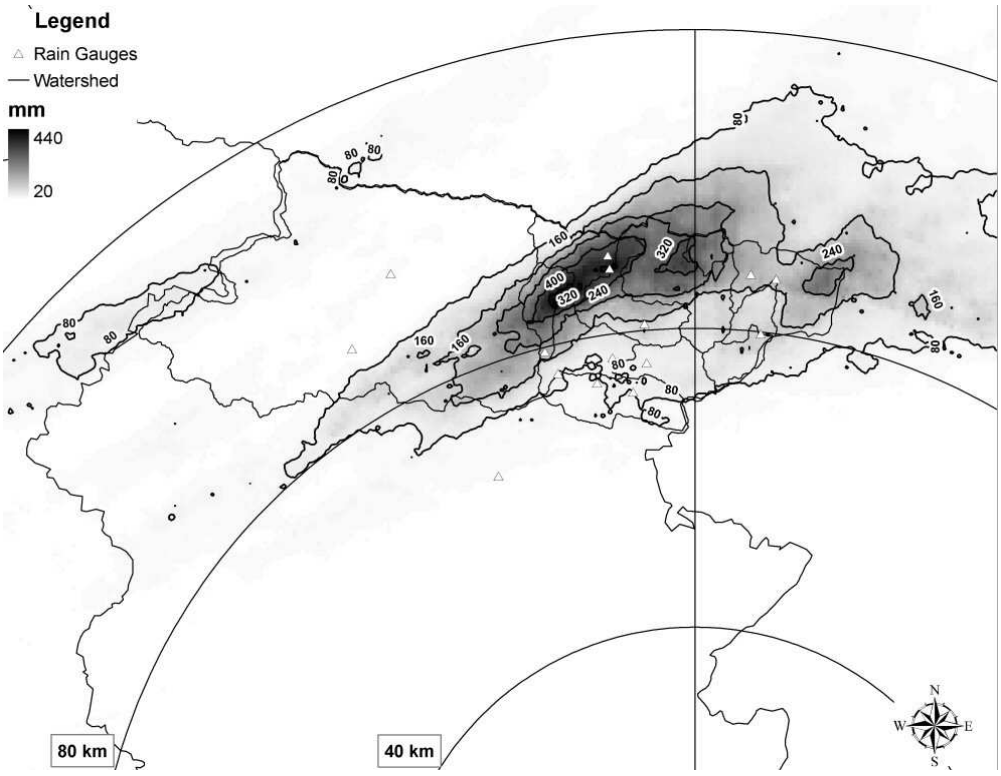

Figure 2-4. Storm total rainfall (mm) for the August 29, 2003 storm.

2.3 Post event field campaign

Following the August 2003 event, post flood surveys were planned. Surveys were concentrated in the upper Fella basin and included: (i) collection of rainfall data, (ii) collection of streamgauge data and execution of indirect peak flood estimation, (iii) mapping of geomorphic effects, (iv) collection of hydraulic saturated conductivity values in a number of sites, and (v) post-flood interviews. A remarkable contribution to the understanding of the flash flood was provided by post-event surveys operated by the local Regional Administration and by the "Amt der Kärntner Landesregierung" in the Carinthia Region of Austria.

The event was analysed by using spatially detailed radar rainfall estimates adjusted by accounting for the physics of the radar observations and incorporating accumulated values of the available raingauge stations. A detailed analysis concerning the use of radar data to estimate the return time of the storm is reported in Chapter 3.

Streamgauge data and observations from post-event surveys, combined with hydraulic modelling, were used to examine hydrologic response to the storm. Stream gauge data were available at eight sites (Figure 2-3 and Table 2-1). Almost all these gauges are located either close or at bridge crossing sites, where measurements are taken by means of ultrasound sensors. Hydraulic modelling, combined with surveys of the post-flood river section geometry and data about pre- and post-flood geometry, was used to derive stage-discharge relationships at these river sections. Furthermore, hydraulic modelling was used to estimate peak discharges based on surveyed high watermarks and postflood channel geometry at another three sites (including the site at the outlet of Uqua basin Table 2-1) and to confirm the estimates at the gauged sections. Information on runoff volumes and flood peak concerning the Vorderberg river (located in Austria, bordering the Uqua basin, on the northern side of the mountain range) were obtained from Moser (2003 [10]). It was not feasible to extend indirect flood peak estimation to basins with drainage area less than 20 km2, due to the difficulties in establishing the actual flood channel geometry in river reaches subject to substantial erosion and/or deposition. Furthermore, the character of the flow process places essential limitations to traditional procedures for indirect peak estimation, which are likely to be flawed in case of debris flows. Twenty-two local residents, mostly located close to the Uqua river basin and its fan, were interviewed about the severity of the storm, occurrences of surface flow, timing of rainfall and stage peaks and timing of debris flows. Information on shallow landslides and debris flows triggered by the storm constitute another type of data collected during the field survey. This survey was focused on a number of basins with drainage area less than 10 km^2. Information on starting points, paths, deposition areas and sediment volumes were collected. A spatially distributed rainfall-runoff model, based on SCS - Curve Number procedure (US SCS, 168 1986 [14], Borga et al. 2007 [4]) was used to simulate the flash flood dynamics at a number of river sections. First, the model was used to identify possible inconsistencies in the available data, both in terms of rainfall and runoff volumes, and in terms of timing of the runoff response with respect to the space-time rainfields. Then, model results were used to gain insights into the effect of initial soil moisture and the runoff dynamics.

Table 2-1. Characteristics of the surveyed river sections and of the corresponding drainage basins

Basin	River System	Basin area (km^2)	Type of information available
Uqua at Ugovizza	Fella (Tagliamento)	23.9	Peak estimate (post-event survey)
Fella at Pontebba	Fella (Tagliamento)	164.5	River stage time series; Stage-discharge relationship (post-event survey)
Fella at Dogna	Fella (Tagliamento)	329.5	River stage time series; Stage-discharge relationship (post-event survey)
Raccolana at Raccolana	Fella (Tagliamento)	61.6	River stage time series; Stage-discharge relationship (post-event survey)
Resia at Borgo Povici	Fella (Tagliamento)	102.1	River stage time series; Stage-discharge relationship (post-event survey)
Fella at Moggio Udinese	Fella (Tagliamento)	623.1	River stage time series; Stage-discharge relationship (post-event survey)
Tagliamento at Tenzone	Tagliamento	1843.4	River stage time series
R. del Lago at Cave Predil	Slizza (Drava)	40.6	River stage time series; Stage-discharge relationship (post-event survey)
Slizza at Tarvisio	Slizza (Drava)	73.1	River stage time series; Stage-discharge relationship (post-event survey)
Vorderbergbach	Slizza (Drava)	26.9	Peak estimates and estimation of runoff volumes (post-event survey, Moser (2003))

2.4 Influence of spatial temporal rainfall variability and of antecedent soil moisture conditions

For the Fella 2003 event, a summary of the data available is reported in Table 2-2 to permit water balance and response time analysis. Data reported in Table 2-2 shows that there are systematic differences among the surveyed basins. Maximum rainfall accumulations were recorded along the Fella main stream down to Dogna and on the Vordergergbach. These four basins are all located under the central convective rainband. Much lower accumulations were received by Resia and Raccolana, which were only partially located under a rainband. The runoff ratio ranges between 0.25 for 260 mm total rainfall to less than 0.1 for the smallest rainfall totals. The low values of runoff ratios point out the impact of the dry antecedent soil moisture conditions. The strong influence of the initial conditions is confirmed by results obtained from the water balance analysis of the June 22, 1996 flood. This flood, for which only raingauge data were available for rainfall estimation, was characterised by two very intense consecutive storm episodes and a total duration of 54 hours. Initial conditions were much wetter than for the August 2003 flood. These two characteristics translate into much more uniform rainfall totals over the various subbasins (with totals ranging from 220 to almost 300 mm) and larger runoff ratios, ranging from 0,34 to 0,52. The large influence of the initial soil moisture condition on the

August 2003 flash flood is not unexpected, due to the combination of the exceptionally dry summer 2003 and high soil moisture capacity characterising the study area. In this region, soil moisture storage capacity is closely linked to the presence of densely fractured bedrock and of relatively thick superficial deposits, developed from colluvium and underlained by carbonate rocks (Mosetti, 1983 [11]). The ratio of daily discharge which is exceeded 90% of the time to the mean daily flownranges between 0.31 to 0.46 in the upper Tagliamento basin, with values ranging between 0.33 to 0.36 for the Fella basin. These are relatively high values and correspond to large groundwater storage. Large soil storage capacity is reflected also by the high value of the Curve-Number based water retention capacity of the soils and subsoils (S), which is equal, on average, to 350 mm for the considered area. The flood response in the Fella basin suggests that the combination of high soil moisture storage capacity and low antecedent soil moisture conditions is an important factor determining landsurface response to extreme rainfall. In addition to nonlinearities in the storm event water balance, there are also pronounced heterogeneities in the hydraulics of basin response. Lag time, obtained as the time difference between the discharge peak and the rainfall mass centre, is comparatively very short for the basins with large rainfall accumulations, irrespective of basin area, whereas it is relatively large for the watersheds characterised by low storm totals. This pattern reflects the systematic decrease of basin response with increasing the rainfall accumulation. Two major factors controlling this process are the expansion of stream network to unchanneled topographic elements during the flood and the increase of flow velocity with discharge.

Table 2-2. Rainfall and runoff for the surveyed basins (NA: not available)

BASIN	TOTAL RAIN (mm)	TOTAL RUNOFF (mm)	PEAK DISCHARGE ($m^3 s^{-1}$)	UNIT PEAK DISCHARGE ($m^3 s^{-1} km^{-2}$)	RUNOFF RATIO (-)	LAG TIME (hr)
Uqua at Ugovizza	287	NA	200	8.36	NA	2.0
Fella at Pontebba	247	49.4	680	4.13	0.18	2.0
Fella at Dogna	237	-	805	2.44	-	2.0
Raccolana at Raccolana	96	3.8	27	0.43	0.04	4.0
Resia at Borgo Povici	71	6.4	54	0.53	0.09	3.0
Fella at Moggio Udinese	189	28.3	1290	2.1	0.15	3.5
Tagliamento at Venzone	110	NA	NA	NA	NA	3.5
R. del Lago at Cave Predil	122	7.3	15	0.37	0.06	1.5
Slizza at Tarvisio	132	9.2	38	0.52	0.07	2.0
Vorderbergbach	260	65.0	125	4.65	0.25	NA

2.5 Analysis of flood severity

The evaluation of the extreme flood events is an important basis for learning processes during ex-post evaluation of interventions in support of future development of strategies and strategic options in flood risk management. The severity of the August 2003 flash flood-generating storm is analysed in detail in Chapter 3. Rainfall maxima from the storm were characterised by return periods in the range 200-500 years for 1-h and 24-h durations, and in the range 500-1000 years for 3-h, 6-h and 12-h durations. The analysis of

the water balance and response time analysis reported above have shown that estimated peak discharges (based on field surveys) were large, but not as exceptional as implied by the measured rainfall. In spite of these observations, analysis of peak discharges return periods based on the regional frequency analysis available for the region (Villi and Bacchi, 2001 [16]) provides estimates exceeding that of the rainfall maxima, and exceeding 10.000 years for drainage areas less than 200 km^2. Whether this outcome is due to the sparse gauge stations and possible undersampling is not clear. However, it may be observed that the sample data used for the flood peak regional analysis does not include the other two extreme flash flood events recorded in the region and occurred on September 11, 1983 and June 22, 1996. Data were not available for these events because river gauge sections were heavily damaged by the flood. Precipitation data from these events, together with the August 2003, appear to dominate the upper tail of the precipitation frequency distribution. The same should be likely for the discharge frequency distribution. This show effectively that i) gaps historically exist in the capability of conventional hydrological networks to account for extreme flash flood event, and that ii) a flash flood focused observation strategy such as the one described here has the potential to advance our understanding of these phenomena.

2.6 Conclusions

Improved understanding of flash flooding will require provision of more detailed hydrometeorological and geomorphological data over wider areas than has traditionally been available. The present study has demonstrated that under the highly localized conditions and short duration of flash flood occurrence and development, such data can be obtained from rapid response survey teams. Additional data sources include observations from weather radar and the compilation of existing data bases from disparate meteorological and streamflow networks. Quality control of these data bases may largely benefit from the comparison with the results of high resolution simulations of weather events and landscape responses. Improved understanding of flash flood controlling hydrometeorological processes relies on the systematic collection of data from multiple flash flood events over different hydroclimatic regions. This will require a new generation of field-trained geoscientists capable of collecting the interdisciplinary observations necessary to characterize flash flood processes and responses.

2.7 References

[1] Borga, M., 2006. HYDRATE project documentation. University of Padova, 122 pp.

[2] Borga, M., Anagnostou, E.N., Frank E., 2000. On the use of real-time radar rainfall estimates for flood prediction in mountainous basins. Journal of Geophysical Research, 105, D2, 2269-2280.

[3] Borga, M., Degli Esposti, S., Norbiato, D., 2006. Influence of errors in radar rainfall estimates on hydrological modelling prediction uncertainty. Water Resources Research, 42, W08409, doi:10.1029/2005WR004559, 2006.

[4] Borga, M., Boscolo, P., Zanon, F., Sangati, M., 2007. Hydrometeorological analysis of the August 29, 2003 flash flood in the eastern Italian Alps. Journal of Hydrometeorology, 8(5), 1049-1067.

[5] Carpenter, T.M., Wang, J., Taylor, S. V., Shamir, E., Sperfslage, J. A., Georgakakos, K. P., 2007. Surveying Flash Flood Response in Mountain Streams. *EOS*, 88 (6), 69-80.

[6] Creutin, J.D., Borga, M., 2003. Radar hydrology modifies the monitoring of flash flood hazard. Invited commentary. 10.10002/hyp.5122, Hydrological Processes, 17, 7, 1453-1456.

[7] Delrieu, G., Ducrocq, V., Gaume, E., Nicol, J., Payrastre, O., Yates, E., Andrieu, H., Ayral, P-A., Bouvier, C., Creutin, J-D., Livet, M., Anquetin, S., Lang, M., Neppel, L., Obled, C, Parent-du-Châtelet, J., Saulnier, G-M., Walpersdorf, A., Wobrock, W., 2005. The catastrophic flash-flood event of 8-9 September 2002 in the Gard region, France: a first case study for the Cévennes-Vivarais Mediterranean Hydro-meteorological Observatory. Journal of Hydrometeorology, 6, 34-52.

[8] Gaume, E., 2006. Post Flash-flood Investigations - Methodological Note (Draft), ENPC. FLOODsite Report T23-06-02, Paris.

[9] Gaume, E., Livet, M., Desbordes, M., Villeneuve, J.P., 2004. Hydrological analysis of the river Aude, France, flash flood on 12 and 13 November 1999. J. Hydrol., 286, 135-154.

[10] Moser, J., 2003. Hochwasser am Vorderberger Wildbach. Amt der Kärntner Landesregierung /Abteilung 18 Wasserwirtschaft (in german).

[11] Mosetti, F., 1983. Sintesi sull`idrologia del Friuli-Venzia Giulia, Quaderni dell'Ente Tutela Pesce del Friuli-Venzia Giulia. Rivista di Limnologia, N^{o} 6, (in italian).

[12] Norbiato, D., Borga, M., Gaume, E., 2007a. Hydrological processes and flash flood generation, in Proceedings of the 32nd Congress of IAHR, July 1-6 2007, Venice, CD-ROM.

[13] Slaymaker, O., 1988. The distinctive attributes of debris torrents. Hydrological Sciences-Journal des Sciences Hydrologiques, 33 (6), 567–573.

[14] U.S. SCS, 1986. Urban hydrology for small watersheds, Technical Release 55, U.S. Department of Agriculture.

[15] Tropeano, D., L. Turconi and S. Sanna, 2004. Debris flows triggered by the 29 August 2003 cloudburst in Val Canale, Eastern Italian Alps. Proceedings of the International Symposium INTERPRAEVENT 2004, Riva del Garda (Italy), 24-27 May 2004.

[16] Villi, V., Bacchi, B, 2001. Valutazione delle piene nel Triveneto. Gruppo Nazionale delle Catastrofi Idrogeologiche. 322 pp. (in italian).

3 Regional frequency analysis of extreme precipitation in the eastern Italian Alps and the August 29, 2003 flash flood[2]

3.1 Introduction

The estimation of the rarity of events such as extreme floods or precipitation is a common problem in ex-post flood risk analysis. Design, implementation and operation of measures and instruments for effective and sustainable flood risk reduction require knowledge of the flood risk mitigation system under extreme events. The evaluation of the extreme flood events, as just explained in Chapter 2, is an important basis for learning processes during ex-post evaluation of interventions in support of future development of strategies and strategic options in flood risk management. Due to the scarcity of discharge data for flash flood events, rainfall frequency estimates are often used to describe the characteristics of a flood event. In these cases, the return period of the greatest point rainfall intensity within the storm is taken as the return period of the storm (Ramos et al., 2005 [38]). However, lack of reliable raingauge coverage frustrates the hazard characterization of flash-flood generating storms, which develop at space and time scales that conventional rain observation system are not able to monitor (Creutin and Borga, 2003 [12]). Radar observations have large potential to improve the monitoring of flash-flood generating storms. In the last decade, several studies have shown that adjusted radar rainfall estimates, corrected for the dominant observation error sources, may be used for flood and flash flood analysis (Borga et al., 2000 [6]; Borga, 2002 [4]; Gaume et al., 2004 [9]; Delrieu et al., 2005 [16]; Borga et al., 2007 [8]). It is therefore interesting to evaluate the feasibility of using adjusted radar observations for hazard characterization of flash-flood generating storms.

The study is focuses on the use of both regional frequency analysis and radar rainfall observations to asses return periods for the extreme flash flood-producing storm, just described in Chapter 2, for various rainfall durations. This storm occurred on 29 August 2003 on the upper Tagliamento river basin, in the eastern Italian Alps and was characterised by extraordinary rainfall amounts and large spatial variability. Regional frequency analysis based on the flood index method and L-moments is utilized to analyse short duration annual maximum precipitation for the Friuli-Venezia Giulia region, in north-eastern Italy, which includes the storm location. Radar rainfall estimates, adjusted by using a physically-based methodology and data from a raingauge network, are used to characterise the return period of the storm rainfall amounts, highlighting the importance of considering its spatial dimension. Severity graphs are developed to visualise the return periods and their variability for different rainfall durations within the storm. The

[2] The study described in this chapter has been published in Norbiato et al. (2007b [34])

methodology analysed in this chapter represents an important tool within the innovative flash flood-focused observational strategy described in Chapter 2.

3.2 Regional frequency analysis methodology

Frequency analysis of extreme storms usually implies extrapolations well beyond the range of the available at-site data. Regional frequency analysis is therefore used to provide a framework for hazard characterization of these extremes. The regionalization concept, introduced by Dalrymple (1960 [14]), "trades space for time" by using data from nearby or similar sites to estimate quantiles of the underlying variable at each site in the homogenous region of consideration (Stedinger et al. 1993 [42]). The concept was continuously developed since, and new approaches were regularly developed by researchers (e.g., Benson, 1962 [2]; Matalas and Gilroy, 1968 [31]; Vicens et al., 1975 [46]; National Environment Research Council (NERC), 1975 [33]; Greiss and Wood, 1981 [19]; Rossi et al., 1984 [40]; Hosking et al., 1985 [25]; Lettenmaier et al., 1987 [30]; Burn, 1990 [10]; Buishand, 1991 [9]; Stedinger and Lu, 1995 [43]; Hosking and Wallis, 1997 [26]; Reed et al., 1999 [39]; Sveinsson et al., 2001 [44]; Koutsoyiannis, 2004 [29]). A common method for pooling summary statistics from different sites is the index variable procedure, referred to also as the "index flood" from early studies (Dalrymple 1960 [14]) that used flood data when implementing the procedure. The main assumption of an index variable procedure is that the sites in a homogeneous region have an identical frequency distribution apart from a site-specific scaling factor, the *index variable*. The index variable is usually the mean of the site specific data (Hosking and Wallis 1997 [26]). Regional analysis involves the following steps: i) identification of the region, i.e., the sites that belong to the region, and testing whether the proposed region is homogeneous, ii) choice of the distribution to fit the regional data, and iii) estimation of parameters and quantiles.

Cunnane (1988 [13]) reviewed twelve different methods of regional frequency analysis and rated a regional algorithm based on probability weighted moments (PWMs) as the best one. PWMs were introduced by Greenwood et al. (1979 [18]). Hosking (1986 [21], 1990 [22]) defined L-moments as a linear combination of PWMs. L-moments are less influenced by the effects of sampling variability than conventional moments and can in some cases yield more efficient parameter estimates than other estimation methods, such as the method of maximum likelihood or the conventional product moments method. Schaefer (1990 [41]) developed a regional procedure for annual maximum rainfall of the state of Washington based on L-moments and two regression curves relating the coefficient of variation and the coefficient of skewness of the data to mean annual precipitation.

The methodology used here for deriving rainfall quantiles for the Eastern Italian Alps is an index variable regional frequency analysis approach as outlined by Hosking and Wallis (1997 [26]) (called "HW methodology" hereinafter) and based on annual maximum data. The procedure assumes that sites from a homogeneous region have an identical frequency distribution apart from a site-specific scaling factor represented by the mean of the site-specific data. Three models based on this methodology are considered: a generalized extreme value (GEV) distribution, a generalized Logistic (GLO) distribution

and a Kappa distribution. Analogously to the usual method of moments, the method of L-moments obtain parameter estimates for a *p*-parameter probability distribution by equating the first *p* sample L-moments to the corresponding population quantities. Hence, the parameters of the three-parameter distributions (GEV, GLO) and of the four-parameter distribution (Kappa) are obtained by using the first three and four sample L-moments, respectively (Hosking 1990 [22]; Hosking and Wallis 1997 [26]). The relationships for parameter estimations are reported in the following sections. In the following, τ indicates the L-CV of a frequency distribution, while λ_r and τ_r indicates the r*th* L-moment and the r*th* L-moment ratio of a frequency distribution, respectively.

Parameter Estimation for GEV Distribution

The CDF of the generalized extreme value (GEV) distribution with parameters α (location), β (scale) and κ (shape) is given by

$$F_X(x) = \exp\left\{-\left[1-\frac{\kappa}{\beta}(x-\alpha)\right]^{1/\kappa}\right\}, \text{ if } \kappa \neq 0 \tag{3.1}$$

where $\alpha+\beta/\kappa<x<\infty$ if $\kappa<0$ and $-\infty<x<\alpha+\beta/\kappa$ if $\kappa>0$.

The *q*th quantile estimate is then

$$\xi_q = \alpha + \frac{\beta}{\kappa}\left[1-(-\ln q)^{\kappa}\right], \text{ if } \kappa \neq 0 \tag{3.2}$$

The shape parameter κ is estimated numerically from the L-Skewness relation

$$\tau_3 = -3 + \frac{2\left(1-3^{-\kappa}\right)}{\left(1-2^{-\kappa}\right)} \tag{3.3}$$

with relative accuracy better than 9×10^{-4} for $-0.5\leq\tau_3\leq0.5$ using (Hosking and Wallis, 1997 [26])

$$\kappa = 7.8590C + 2.944C^2 \tag{3.4}$$

where $C=2/(\tau_3+3)-\ln2/\ln3$ and τ_3=sample L-skewness.

Given an estimate of κ, estimates of β and α are obtained from

$$\begin{aligned}\beta &= \frac{\lambda_2\kappa}{\left(1-2\beta^{-\kappa}\right)\Gamma(1+\kappa)}\\ \alpha &= \lambda_1 - \frac{\beta}{\kappa}\left[1-\Gamma(1+\kappa)\right]\end{aligned} \tag{3.5}$$

where $\Gamma(\cdot)$=gamma function.

Parameter Estimation for GLO Distribution

The CDF of the generalized logistic (GLO) distribution with parameters α (location), β (scale) and κ (shape) is given by

$$F_X(x) = \frac{1}{1+\exp\left\{\kappa^{-1}\log\left[1-\kappa(x-\alpha)/\beta\right]\right\}}, \text{ if } \kappa \neq 0 \tag{3.6}$$

where $\alpha+\beta/\kappa<x<\infty$ if $\kappa<0$ and $-\infty<x<\alpha+\beta/\kappa$ if $\kappa>0$.

The *q*th quantile estimate is then

$$\xi_q = \alpha + \frac{\beta}{\kappa}\left\{1 - \left[\frac{(1-q)}{q}\right]^{\kappa}\right\}, \text{if } \kappa \neq 0 \tag{3.7}$$

The parameters are estimated using L-moments as follows:

$$\kappa = -\tau_3$$
$$\beta = \frac{\lambda_2 \sin \kappa\pi}{\kappa\pi} \quad . \tag{3.8}$$
$$\alpha = \lambda_1 - \beta\left[\frac{1}{\kappa} - \frac{\pi}{\sin \kappa\pi}\right]$$

Parameter Estimation for Kappa Distribution

The CDF of the Kappa distribution with parameters α (location), β (scale), κ and h is given by

$$F_X(x) = \left\{1 - h\left[1 - \frac{\kappa(x-\alpha)}{\beta}\right]^{1/\kappa}\right\}^{1/h} \tag{3.9}$$

where $\alpha+\beta/\kappa<x<\infty$ if $\kappa<0$ and $h<0$. The *q*th quantile estimate is then

$$\xi_q = \alpha + \frac{\beta}{\kappa}\left\{1 - \left[\frac{(1-q^h)}{h}\right]^{\kappa}\right\}, \text{if } \kappa \neq 0 \text{ and } h \neq 0 \quad . \tag{3.10}$$

To enable the four parameters of the distribution to be estimated from the first four L-moments, the parameter space must be restricted, so that only one set of parameters corresponds to a given set of the first four L-moments. This corresponds to the following conditions on the parameters (Hosking, 1994 [23]):

$$\begin{aligned} &\text{(a) } \kappa > -1; \\ &\text{(b) if } h < 0, \text{ then } h\kappa > -1; \\ &\text{(c) } h > -1; \\ &\text{(d) } \kappa + 0.725h > -1. \end{aligned} \tag{3.11}$$

Conditions 3.11a and 3.11b ensure the existence of the L-moments; conditions 3.11c and 3.11d ensure the uniqueness of the parameters, given the four L-moments. No explicit equations are available for the determination of the parameters based on the L-moments. However, Hosking (1996 [24]) provided a Newton-Raphson algorithm for the determination of κ and h in terms of τ_3 and τ_4. This procedure is used here for parameter estimation.

3.2.1 The four steps of the HW regional frequency analysis methodology

The HW regional frequency analysis is articulated into four steps: (i) screening of the data, (ii) testing of regional homogeneity, (iii) identification of the regional distribution, and (iv) development of regional storm frequency relationships for gauged and ungauged sites. Since these procedures are presented in detail by Hosking and Wallis (1997 [26]), only a summary is reported below.

Screening of Data Using Discordancy Measure Test

The first step in the procedure is to test for gross outliers, inconsistencies, shifts, and trends. Furthermore, a discordancy measure (Hosking and Wallis, 1997 [26]) is used to identify those sites from a group of given sites that are grossly discordant with the group as a whole. The discordancy measure is a single statistic based on the difference between the *L*-moment ratios of a site and the average *L*-moment ratios of a group of similar sites. This statistic can also be used to identify erroneous data. The discordancy measure is useful only for regions with $N \geq 7$. A site is declared to be discordant if the discordancy measure is large and the definition of large depends on the number of sites in the group. Thus a site is regarded as discordant if the measure exceeds the critical value given in tabular form (Hosking and Wallis, 1997 [26]).

Identifying Homogeneous Regions

The purpose of this step is to form groups of stations that satisfy the homogeneity condition-that is, stations with frequency distributions that are identical apart from a station-specific scale factor. A heterogeneity measure called the *H*-statistic is then used to compare the between site variation in sample *L*-moments for a group of sites with what would be expected for a homogeneous region (Hosking and Wallis, 1997 [26]). To determine what would be expected, repeated Monte Carlo simulations of a homogeneous region with sites having record lengths equal to those of the observed data are performed. A large positive value of the *H*-statistic indicates that the observed L-moments ratios are more dispersed than is consistent with the hypothesis of homogeneity.

There are three measures of the H-statistic. The first, H(1), is the standard deviation, weighted according to record length, of the at-site L-CVs. The second measure, H(2), is the average distance from the site coordinates to the regional average on a plot of L-CV versus L-skewness. The third measure, H(3), is the average distance from the site coordinates to the regional average on a plot of L-skewness versus L-kurtosis. In this work, heterogeneity is tested using H(1) and H(2) because the L-CV and L-skewness are required for fitting pooled growth curves with a GEV or GLO. Note, however, that Hosking and Wallis (1997 [26]) found that H(2) is a weaker test of heterogeneity than H(1). A region is declared 'acceptably homogeneous' if $H<1$, 'possibly heterogeneous' if $1 \leq H<2$, and 'definitely heterogeneous' if $H \geq 2$ (Hosking an Wallis, 1997 [26]). The heterogeneity measure H(2) is used also by the FEH (Institute of Hydrology, 1999 [27]). According to the FEH, a region is said to be heterogeneous if $2<H(2) \leq 4$; it is described as strongly heterogeneous if $H(2)>4$.

Identifying a Robust Regional Frequency Distribution

Regional frequency analysis requires determining the underlying probability model of the variable under consideration. For this purpose, a number of goodness-of-fit techniques are available in the literature. In our study, we compare the relation of L-Kurtosis versus L-Skewness for various commonly used distributions duration with the corresponding relations obtained from the at-site and regional data. Furthermore, we use the Z-statistic

introduced by Hosking and Wallis (1997 [26]). This statistic was developed for three-parameter distributions and measures how well the theoretical *L*-kurtosis of the fitted distribution matches the regional average *L*-kurtosis of the observed data. The fit of the distribution is considered satisfactory if $|Z| \leq 1.64$, corresponding to an acceptance of the hypothesised distribution at a confidence level of approximately 90% (Hosking and Wallis, 1997 [26]).

3.3 Data Analysis and Results

The region considered in this study (Figure 3-1) includes a portion of the central chain of eastern Alps and the Alpine foreland region. The arc-shaped mountainous range of the eastern Alps constitutes the major topographic feature within the analysis domain. The most prominent valleys are aligned along the main ridge in the west-east direction for some tens of kilometers. The area is included within the Friuli-Venezia Giulia region, which borders to the north with Austria, to the east with Slovenia and to the west with Veneto. The region is characterised by three distinct pluviometric regimes: (i) the upper plain area, with mean annual precipitation (herewith called MAP) ranging from 1200 to 1500 mm; (ii) the Alpine foreland area, where MAP increases up to 3300 mm, which represents the highest mean values for the Alps; (iii) the inner Alpine area, where MAP decreases to 1600 -1800 mm, due to rain shadow effect of the southern ridges.

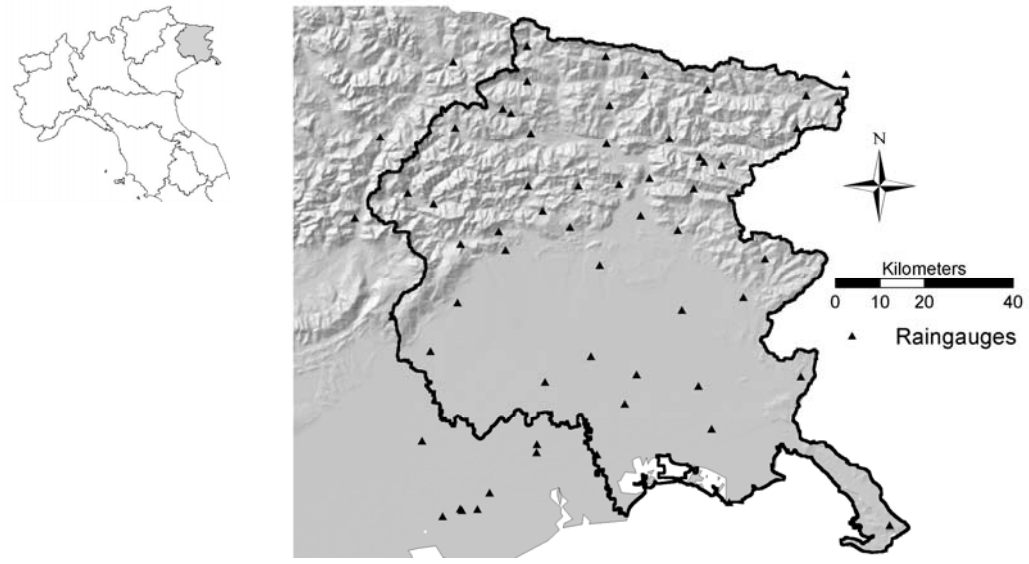

Figure 3-1. Location of the study area with DTM of North-Eastern Italy. The locations of the raingauge stations used in the study are also reported.

Daily rainfall amounts exceeding 500 mm may be locally recorded in this area in a 20 to 30 years time span (Villi et al., 1986 [47]; Ceschia et al., 1991 [11]). For instance, 617 mm and 543 mm daily precipitation were recorded in Oseacco, close to Moggio Udinese, on October 9, 1933 and on November 14, 1969, respectively. During late fall, winter and spring, heavy precipitations are normally related to synoptic circulations and to southerly humid flows. During summer and partially during fall, the contribution from

convective or mesoscale rainfall becomes significant or even prevailing. Due to the rugged topography of the region, together with its densely fractured bedrock and its high seismicity (Querini, 1984 [37]), heavy convective precipitations result often in flash floods, associated to diffused landsliding, debris flows and sediment transport.

The total number of stations used in the analysis is 63 with an average usable record length of 51 years. The screening procedure using discordancy measure was implemented to identify gauges the sample statistics of which were markedly different from the majority of gauges. The test base on discordancy measures was repeated both at the regional and at the subregional level, according to the regional subdivision reported below. Suspicious gauges and data were checked to verify the validity of records. This led to remove 6 stations, which included data clearly erroneous.

3.3.1 Spatial mapping of at-sites means

The spatial mapping of the at-site means has been carried out by using the multiquadratic surface fitting technique (Borga and Vizzaccaro, 1997 [5]). Results are reported in Figure 3-2 for duration of 1-, 6- and 24-h. The maps show clearly (i) the relatively high values of these rainfall accumulations, and (ii) the orographic control on the spatial distribution of the average values. It is interesting to note that the highest values for 6-h duration are located on the Alpine foreland area, while for 1-h duration high values are also found on the south-eastern coastal plain. The maps reveal also a marked decrease of the average annual precipitation maxima values (for all durations) in the inner Alpine region.

A quantitative measure was required to evaluate the relative accuracy of the spatial estimation procedure. This is difficult in all studies of this type because the true value of the at-site means are unknown, since sample values of the station at-site means will differ from the true population values due to sampling variability. Therefore, this problem was approached by cross-validating estimates obtained by the interpolation technique against the actual observed ones. A leave-one-out cross-validation procedure was used. This is the limiting case and probably best form of the Jacknife validation (Miller, 1974 [32]). With this procedure, the interpolation technique is used to produce an estimated value at each of the observation locations using data only from the other stations. The accuracy of the surface fitting technique has been evaluated by computing the bias and the RMSE of the standardised residuals

$$SR_i = \frac{S_i - P_i}{P_i} \tag{3.12}$$

where S_i is the cross-validated estimate and P_i is the observed value at each site i. Bias range from 0.5% at 1-h duration to 1.1% at 24-h duration; RMSE range from 9,6% at 1-h duration to 13,5% at 24-h duration. The decrease in accuracy with increasing rainfall duration is due to the higher spatial variability of the rainfall fields at longer duration.

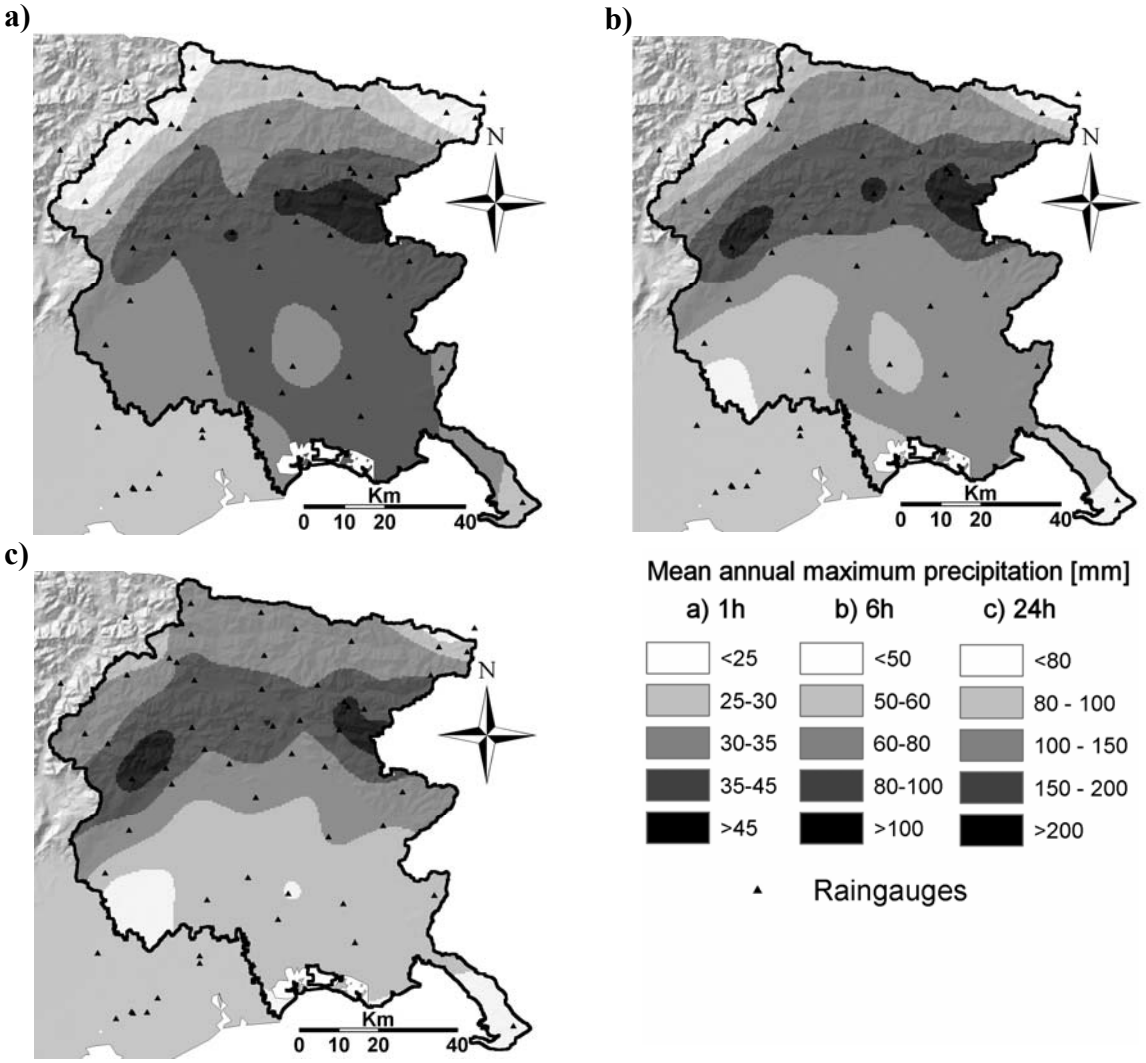

Figure 3-2a-c. Maps of point average of maximum yearly rainfall for durations of (a) 1 hours, (b) 6 hours, and (c) 24 hours, for the Friuli region.

3.3.2 Partitioning the region and estimation of regional growth curves

The whole region was initially considered as a candidate homogeneous region for the analysis. However, this selection exhibited high heterogeneity measures (H statistics) for several durations, suggesting large site-to-site variation in statistics. Thus, this selection was deemed inappropriate for a regional frequency analysis. Orographic differences between the Alpine foreland area and the upper plain area, shadow effect, establishment of orographic convective bands during Mesoscale Convective Systems over the eastern inner Alpine area are all factors influencing the frequency of extreme precipitation. Recognizing that interaction between warm moist air masses from south and south-west direction and orography are major driving force behind rainfall intensity for the considered area, three regions were identified. Hence, the southern plains and the Alpine range are considered as two subregions. In addition, to account for the effects of convective orographic bands over the north-eastern portion of the region, the Alpine range was further subdivided into two subregions depending on aspects. Thus, three subregions are considered (Figure 3-3): Subregion A, with 24 stations located in the southern plain region; Subregion B, which

includes 21 stations located in the alpine foreland area and the upper Tagliamento basin closed upstream the junction with the Fella; Subregion C, which includes 12 stations within and around the Fella basin. Heterogeneity measures H(1) and H(2) are reported for the three subregions in Table 3-1.

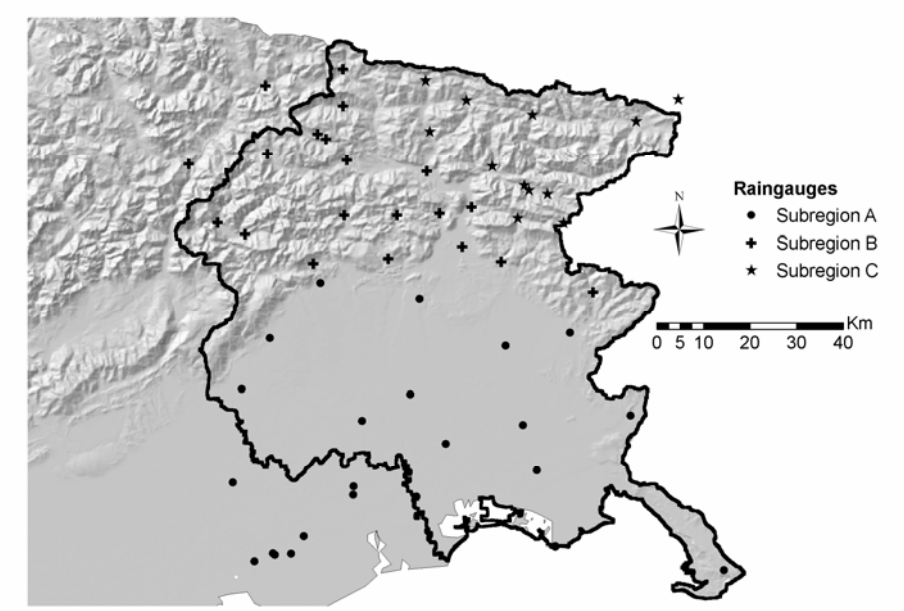

Figure 3-3. Subdivision of the raingauge stations into three subregions.

Table 3-1. Heterogeneity measures (H(1) and H(2)) for the three subregions and for the five rainfall durations.

Duration	Subregion A		Subregion B		Subregion C	
	H_1	H_2	H_1	H_2	H_1	H_2
1	0.22	0.64	1.58	0.26	0.33	-1.19
3	1.61	-0.32	1.89	-2.07	0.64	-0.19
6	**2.44**	0.53	-0.09	-2.23	1.10	1.42
12	**2.37**	1.29	0.08	-0.50	1.98	**2.33**
24	1.34	-0.52	0.20	-1.47	1.17	1.26

Values exceeding the heterogeneity threshold (H=2) are marked in bold.

Examination of results reported in Table 3-1 shows that H(2) exceeds the heterogeneity threshold only in the Subregion C for rainfall maxima of 12-h. Furthermore, H(1) exceeds the threshold in Subregion A for durations of 6h and 12h. A number of negative values are also found, particularly for H(2) and for Region B. According to Hosking and Wallis (1997 [26]), these indicate that there is less dispersion among the at-site statistics than would be expected of a homogenous region with independent at-site frequency distributions. This is usually an indication of large cross-correlation between the sites' frequency distributions. Research is ongoing to quantify these effects for the various rainfall durations.

Results from Table 3-1 lead to investigate causes for H(2) being high. For the rainfall duration of 12-h and Subregion C, the plausible cause is the rainfall maximum recorded for the event of August 29, 2003 by the station located in Pontebba. The value of

H(2) for this duration is the most sensitive to the outlier represented by the rainfall depth recorded on August 29, 2003 (as shown by a sensitivity analysis conducted by either including and excluding the 2003 maximum from the evaluation). This value has been retained into the analysis, because a representative heterogeneous region is better than one that has been made homogeneous by removing similar sites with unusual rainfall amounts (Hosking and Wallis, 1997 [26]).

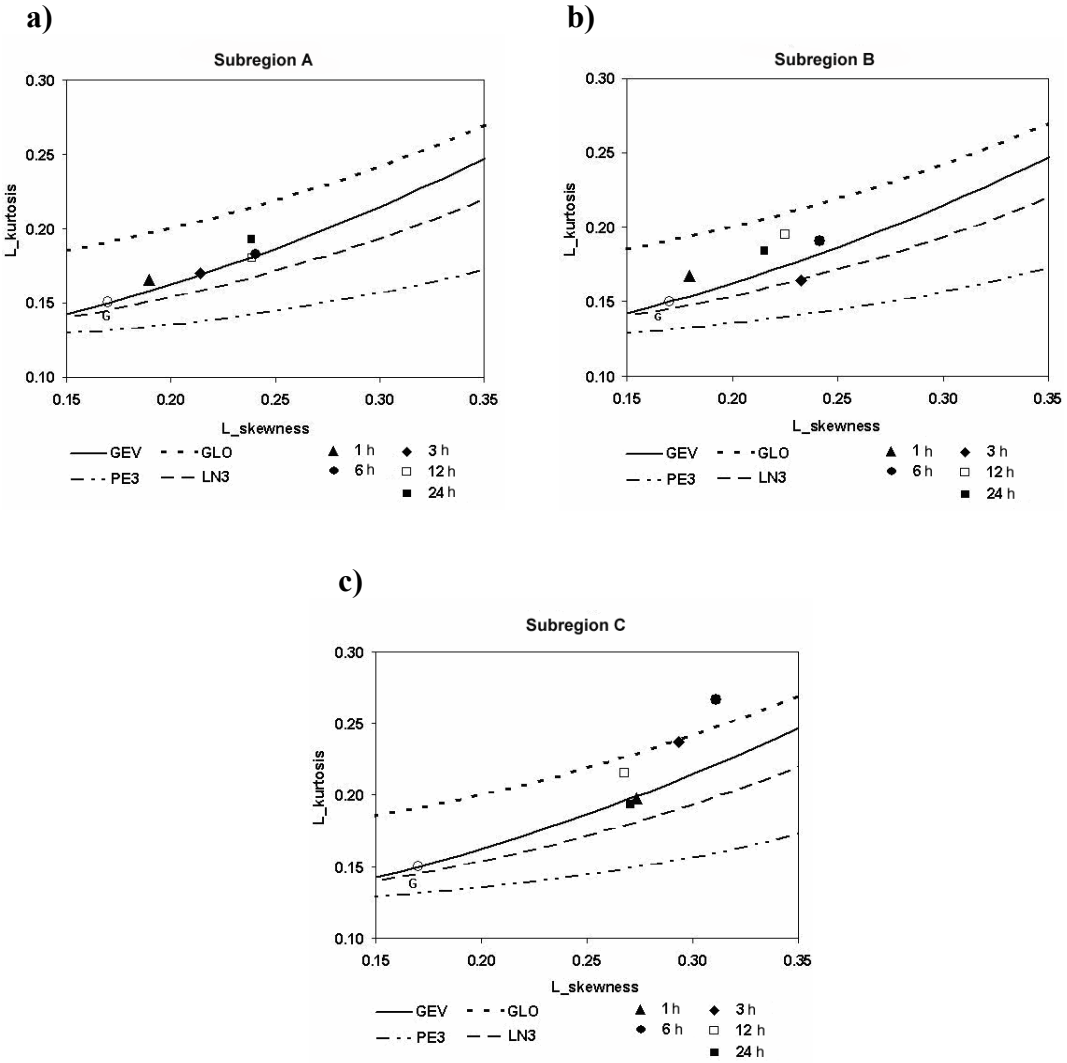

Figure 3-4a-c. Identification of subregional frequency distribution using regional L-skewness L-kurtosis diagram: a) Subregion A; b) Subregion B; c) Subregion C. Notation: GEV: generalised extreme value; GLO: generalised logistic; PE3: Pearson type III; LN3: lognormal-3; G: Gumbel.

Figure 3-4a-c shows the moment ratio diagrams, L-Skewness versus L-Kurtosis, for the three subregions, where the regional averages of the L-Skewness and L-Kurtosis for the three subregions are plotted together with the L-Skewness - L-Kurtosis relations for different distributions. The average points exhibit a shift towards larger values of L-Skewness and of L-Kurtosis when moving from the plains (Subregion A) to the inner eastern alpine area (Subregion C). This is consistent with the idea that changes in elevation, shadow effect and aspect are reflected in different climatic response, i.e.

different extreme rainfall regimes. More than half of the points for all durations lie above the GEV curve, with the Subregion C point for the 6-h lying over the GLO curve. This suggest that either GEV or GLO may provide good fit to the data, depending on rainfall duration. For instance, in the case of Subregion C the GEV model may be a good choice for 1-h and 24-h, whereas the GLO model may be a better model for the 3-h, 6-h and 12-h data.

The GEV and the GLO are suitable distribution for estimation of precipitation quantiles out to 500-year recurrence interval. If quantiles estimates are desired for more extreme events than the 500-year recurrence interval, it would be worthwhile to refine the selection of the regional probability distribution. In these cases, it may be better to use a four-parameter distribution such as the Kappa distribution, which is more robust to misspecification of the frequency distribution (Wallis et al., 2007 [48]). The Kappa distribution can mimic both the GEV and the GLO and produce a variety of regional growth curves intermediate between the GEV and the GLO. The L-moments of the Kappa distribution cover a large area of the moment ratio diagram (L-Skewness versus L-Kurtosis); in Figure 3-4a-c, the L-moments of the Kappa distribution cover the area below the curve corresponding to the GLO distribution. Therefore, the choice of the Kappa distribution is consistent with the arrangement of the empirical average moment ratio points for the various Subregions. Given these considerations, it was decided to use the four-parameter Kappa distribution for Subregion C, which includes the storm location.

Subregional C growth curves for the Kappa, GEV and GLO distributions along with the empirical growth curves based on the APL plotting position (Stedinger et al., 1993 [42]) are shown for all durations of annual maxima precipitation in Figure 3-5. In Figure 3-5, growth curves for the Kappa match closely those for the GEV in the case of 1-h and 24-h durations, and those for the GLO in the case of 6-h and of 3-h durations. For 12-h duration, the growth curve from the Kappa is intermediate between GEV and GLO.

In Figure 3-5, the normalised sample data exceeding 3.0 are marked in bold. It is interesting to note that all these extremes result from three flash flood – generating storm events, occurred on September 11, 1983, June 22, 1996 and August 29, 2003, sampled by 6 stations (Table 3-2). These events appear to dominate the upper tail of the precipitation frequency distribution. Furthermore, the data reported in show clearly an effect of intersite dependence for these extreme storms. Intersite dependence has not been explicitly addressed in this study and is the subject of on going investigation in the study region.

Values of the Z statistic are reported in Table 3-3 for GEV and GLO for the three subregions. In agreement with the observations reported above, the values show a shift from GEV to GLO when moving from Subregion A to Subregion C. Only for Subregion C and 6-h, the frequency distributions used here appear to provide a goodness-of-fit criterion larger than 1.64. This is due to the large value of both L-skewness and L-kurtosis. Results from Figure 3-5 confirm that the Kappa distribution, which is intermediate between GEV and GLO, is appropriate for quantile estimation for Subregion C. Quantiles for various return periods and rainfall durations obtained from the application of the Kappa distribution are reported in Table 3-4.

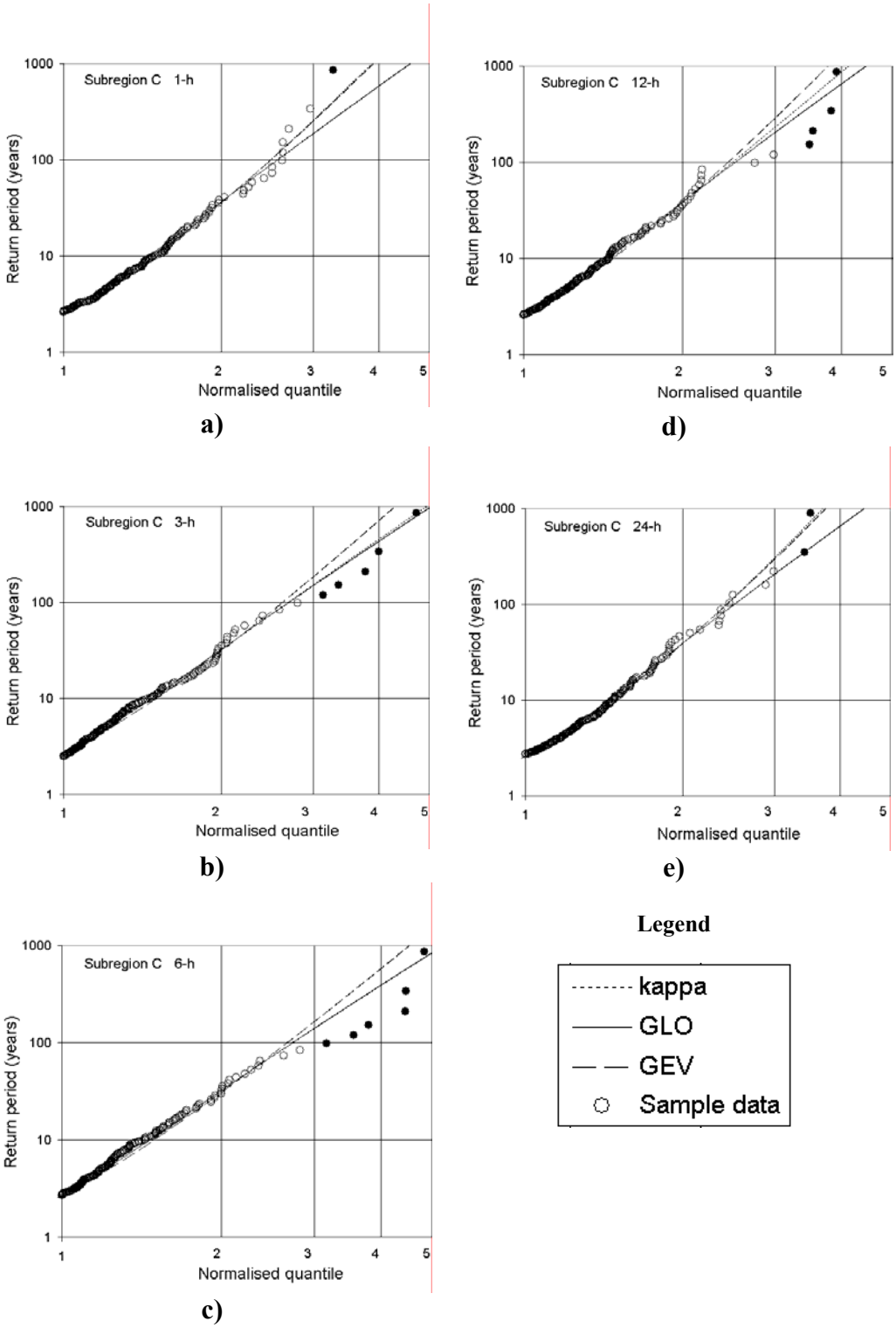

Figure 3-5a-e. Subregion C growth curves for Kappa, GLO and GEV distributions compared with regional normalised sample for five durations: a) 1h, b) 3h, c) 6h, d) 12h and e) 24h. Normalised data marked in bold result from the storms of August 29, 2003, June 22, 1996 and September 11, 1983.

Table 3-2. Values at the normalised rainfall maxima exceeding a threshold value of 3.0 for Subregion C

Station	1-h	3-h	6-h	12-h	24-h
Avosacco	-	-	4.47[1]	-	-
Moggio Udinese	-	3.78[2]	3.79[2]	3.83[2]	3.43[2]
Paularo	3.27[2]	4.0[2]	4.43[1]; 3.56[2]	3.54[1]	-
Pontebba	-	4.72[3] 3.13[2]	4.84[3]	3.93[3] 3.48[2]	3.51[2]
Timau	-	3.36[1]	-	-	-
Arnoldstein	-	-	3.17[3]	-	-

The sampling stations and the generating event are reported for each data
[1]: September, 11, 1983
[2]: June, 22, 1996
[3]:August, 29, 2003

Table 3-3. Z statistic reported for GEV and GLO distribution for the three Subregions and the five durations

Duration	Subregion A		Subregion B		Subregion C	
	GEV	GLO	GEV	GLO	GEV	GLO
1	**-0.88**	2.46	**-1.29**	1.93	**-0.20**	1.19
3	**-0.32**	2.44	**0.85**	3.49	-1.51	**-0.43**
6	**-0.39**	1.96	**-0.95**	1.42	-2.85	**-1.92**
12	**-0.24**	2.27	-1.80	**0.58**	-1.18	**0.14**
24	-1.25	**1.14**	-1.37	**1.20**	**-0.08**	1.36

For each region and duration, the lower value of goodness-of-fit criterion is marked in bold.

Table 3-4. Normalised quantiles obtaine based on Kappa distribution for various rainfall durations and return periods for Subregion C

TR (years)	1-h	3-h	6-h	12-h	24-h
5	1.234	1.217	1.207	1.220	1.229
10	1.486	1.472	1.462	1.459	1.472
20	1.756	1.766	1.760	1.724	1.731
50	2.151	2.240	2.254	2.129	2.106
100	2.486	2.684	2.727	2.489	2.422
200	2.856	3.220	3.311	2.903	2.768
500	3.407	4.106	4.302	3.550	3.278
1000	3.877	4.944	5.263	4.129	3.710

Even though the statistic H(2) in the Subregion C exceeds the heterogeneity threshold only for rainfall maxima of 12-h, we wanted to examine the effect of reducing the amount of heterogeneity on the computed quantiles. A further smaller subregion, composed by 8 stations in Subregion C chosen, based on geographical proximity, was analysed. This new subregion was tested for homogeneity. The amount of heterogeneity is less than for Subregion C, as expected. The statistics H(1) and H(2) are always less than 1.3, with the exception of H(2) for 12-h duration, which amounts to 1.9. The Kappa distribution was fitted to these data and precipitation quantiles were computed for the return periods reported in Table 3-4. The precipitation quantiles for the new smaller subregion are somewhat larger than for the Subregion C. However, the relative difference between 500-yr quantiles for the various durations is less than 8%. This suggests that the

reduction of the amount of heterogeneity obtained by redefining the region has a relatively minor effect on the computed quantiles. Taking into account that with the smaller subregion the analysis of the August 2003 storm implies extrapolations beyond the range of the cumulative record length, we decided to use Subregion C for estimation of regional growth curve Table 3-4.

3.3.3 Severity analysis of the 29 August 2003 flash-flood generating storm

Radar and raingauge observations are used to derive rainfall fields for the August 2003 storm which has been described in Chapter 2. 5-minute raingauge data were collected at 15 raingauges (Figure 2-2), whereas storm total rainfall was available at further six daily raingauges. Twelve out of the 15 raingauges are located within the Fella watershed closed at Moggio Udinese (623 km^2) and the nearby Slizza watershed (73.1 km^2), that is an average density of about one rain gauge per 50 km^2. In spite of the density of the raingauge network, only two raingauges (Pontebba and Pramollo) sampled the high intensity area of the storm.

Volume scan reflectivity data from the Doppler, dual-polarised C-band OSMER radar station, located at Fossalon di Grado (Figure 2-2) (time resolution of 5 min and spatial resolution of 250 m in range by 0.9 degree in azimuth), were used to derive radar rainfall rates. The radar measures the reflectivity in two orthogonal (horizontal and vertical) polarizations, Zh and Zv, respectively. When the two reflectivities are measured in an approximately simultaneous fashion, the differential reflectivity (in decibels) can be derived by dBZDR=10 log10(ZH/ZV). In this study, rainfall rates were estimated based on horizontal-polarised observations; ZDR values were use to discriminate ground clutter from rainfall observations. A number of procedures were applied to the reflectivity data to correct for the following error sources: (i) ground clutter; (ii) partial beam occlusion; (iii) path attenuation. Hail was not observed during the event, so no correction was implemented to remove hail contamination.

An algorithm based on a three-step decision tree, based on Doppler velocity, clear air echo statistics and Z_{DR} variance, was used to flag clutter contaminated data in the polar volumes (Bechini et al., 2002 [1]). Correction for beam occlusion is based on off-line computation of the percentage of beam power intercepted by the orography by using a model of beam propagation and a digital description of the orography (Borga et al., 2000 [6]; Pellarin et al., 2002 [36]). Path attenuation due to precipitation (which can generate large errors at C- band at high rainfall rates - Delrieu et al., 2000 [15]) is corrected by using a variational method with gauge accumulations as external constraints and the Hitschfel-Bordan (1954) equation as model (Berenguer et al., 2002[3]).

Rainfall estimation was based on reflectivity observations from the 2.06° beam elevation, which is the lowest elevation affected by minimal beam occlusion over the study area. Effects due to non uniform reflectivity along the vertical were not included in the analysis and correction procedure, due to the difficulties of separating the effects of attenuation from those generated by vertical variability of reflectivity and of beam occlusion for localised storms. After correction, the reflectivity factor Z was converted to

rainfall rate *R* through an empirical *R-Z* power function of the form $R=aZ^b$. The *R-Z* parameters used are a=0.022 and b=0.67 for *R* in mmh^{-1} and *Z* in mm^6m^{-3}. These parameter values are used in this region for estimation of convective events and are similar to those used in the so-called NEXRAD convective relationship (Ogden et al., 2000 [35]).

Comparison of hourly rainfall obtained from raingauges and radar-based estimates after adjustment shows a general good agreement; the largest rainfall accumulations are accurately portraied by radar. The squared correlation coefficient for hourly accumulation is 0.73, while for rainfall accumulaton on 12 hours it raises to 0.94. The radar estimates after adjustment show a slight positive bias, with an overestimation around 10%. The storm total precipitation (Figure 2-4) exhibits three local peaks of rainfall accumulations exceeding 320 mm. The most extended accumulation is over the upper Aupa basin; the second peak is close to the Uqua basin and near the Italian-Austrian border; the third one (and also the less extended) is located over the extreme eastern portion of the study area. The position of the Aupa and Uqua basins is shown in Figure 2-3.

A striking characteristic of the event is its organization in four well defined banded structures. Some of the bands persisted in the same locations for the duration of the event. The steadiness of these rainbands led to highly variable precipitation accumulations; the rain gauge at Pontebba recorded 389.6 mm of precipitation in 12 hours, while San Giorgio di Resia, located just 15 km to the south but not directly under a band, recorded only 68.4 mm during the same period. Extreme spatial gradients in precipitation accumulations up to 80 mm/km can be recognised in (Figure 2-4).

The size of the storm measured at the Pontebba raingauge, close to the core of the precipitation event, was 88.6, 233.4, 343.0, 389.6, and 396.2 mm for the 1-, 3-, 6-, 12- and 24- maximum, respectively. Except for the 24-h these were the largest precipitation events ever recorded at Pontebba since 1928, when precipitation monitoring started. Previous largest recorded events were 78.4, 155, 199.6, 345.6 and 465 mm, for the 1-, 3-, 6-, 12- and 24-h maximum, respectively, all recorded during the previous June 22, 1996, flash flood event. Comparing the above figures, it is evident that what made the August 29, 2003, event so extraordinary (at least in Pontebba) was the excessive precipitation for the durations in the range between 3 and 12 hours.

3.3.3.1 Analysis of storm severity

This section aims to analyse the spatial distribution of storm point return periods, for various rainfall durations, for the August 29, 2003 storm event. The analysis is based on rainfall estimates obtained by using both raingauge measurements and radar observations. As a first step, a comparison has been carried out to evaluate the quality of the point return period estimates obtained by using adjusted radar observations. To this purpose, the maximum rainfall depths for the different rainfall durations have been computed for the raingauges of Pontebba and Pramollo from both raingauge measurements and adjusted radar estimates. The classical moving-window procedure for rainfall accumulation was adopted to select the maximum rainfall depth observed for each duration. To account for

possible errors in the computation of the geographical position of the radar observations, maximum rainfall depths over different rainfall durations were computed by selecting, for each duration, the maximum rainfall depth over a 3*3 km kernel centered on the 1-km size grid cell of interest. Rainfall maxima obtained from raingauges and from radar observations are reported in Table 3-5.

Table 3-5. Maximum rainfall depths obtained for various durations from raingauge measurements and from adjusted radar estimates for the stations located in Pontebba and Pramollo.

Duration	Maximum rainfall depths (mm)			
	Pontebba		Pramollo	
	Raingauge	Radar-based estimates	Raingauge	Radar-based estimates
1-h	88.6	86.8	77.2	85.5
3-h	233.4	200.4	197.2	202.4
6-h	343.0	333.6	282.6	314.4
12-h	389.6	398.4	333.6	374.4
24-h	396.2	398.4	333.6	374.4

Inspection of these data show that adjusted radar estimates are generally in good agreement with raingauge data, with errors ranging between -14% for 3-h at Pontebba to +12% for 12-h at Pramollo. Since cumulated raingauge data were used in the adjustment procedure of the radar observations, a good correspondence is expected for 12-h maxima between the two measures; the agreement for shorter durations provides an indication of the feasibility of using radar rainfall estimates for rainfall maxima analysis of extreme storms. Return periods were computed for these data based on Kappa distribution specified for Subregion C. According to the terminology introduced by Ramos et al. (2005 [38]), the graphs obtained by associating, for a given station, the return periods of maximum rainfall intensities to the different rainfall durations have been named here severity graphs. Severity graphs obtained from adjusted radar estimates and raingauge measurements are reported in Figure 3-6a-b for Pontebba and Pramollo, respectively. These graphs show clearly that even small-to-moderate errors in rainfall estimation (as are those implied in the radar-raingauge comparison reported above) amplify strongly in the return period estimation. With a 15% under/overestimation, return periods for Pontebba may be under/overestimated by more than 50-60% (depending on rainfall durations). This shows clearly that the main outcome of a radar-based evaluation of storm hazard is an analysis of patterns of relative severity, rather than a determination of absolute values of return periods.

Maps of point return periods are reported in Figure 3-7a-d for durations of 1-h, 3-h, 6-h and 12-h. The map for 24-h is not reported because the corresponding depths are the same as those reported for 12-h. Examination of the maps reveals large differences both among various durations and in space for a given duration. First of all, it is shown that extreme rainfall is concentrated on the right-hand tributaries of the river Fella system. Return periods for 1-h are generally comprised between 100 and 300 years (the station of Pontebba recorded a rainfall depth in this range), with peaks exceeding 300 years over the

Uqua basin, on the mid Pontebbana and over the mid Aupa basin. 3-h and 6-h maps are pretty similar, showing three peaks exceeding 600 years over the eastern portion of the study area, the Uqua basin and on the area ranging between mid-Pontebbana and mid Aupa. 12-h map reveals a different pattern, with two peaks exceeding 600 years over mid Aupa and the eastern portion of the area. A synthesis of this information is reported in Figure 3-8a-b, which shows the envelope of the severity graphs for the grids covering the Uqua and Aupa basins in terms of 10%, 50% and 90% percentiles.

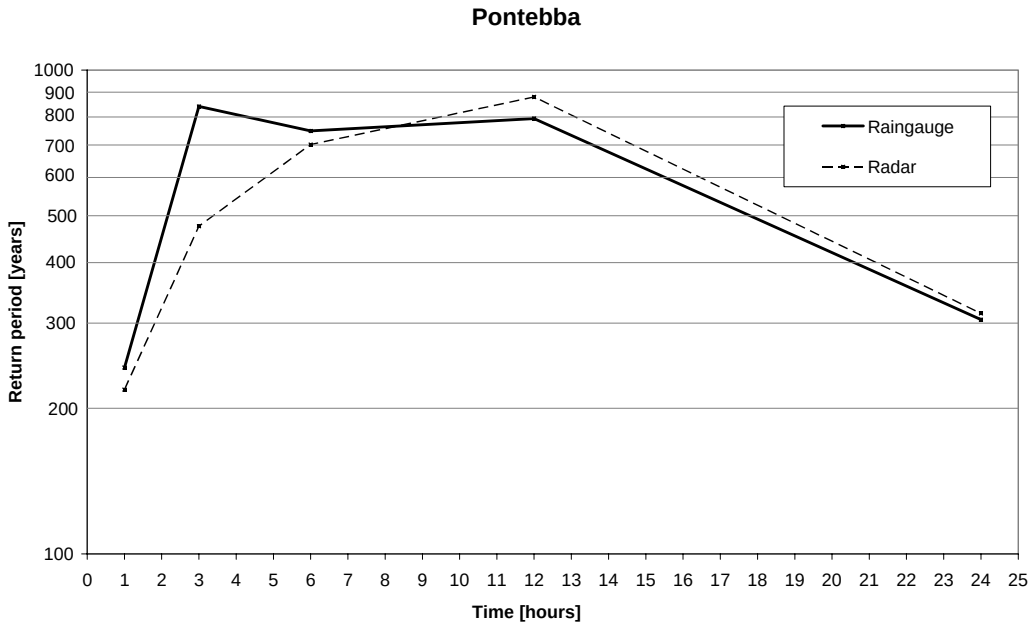

a)

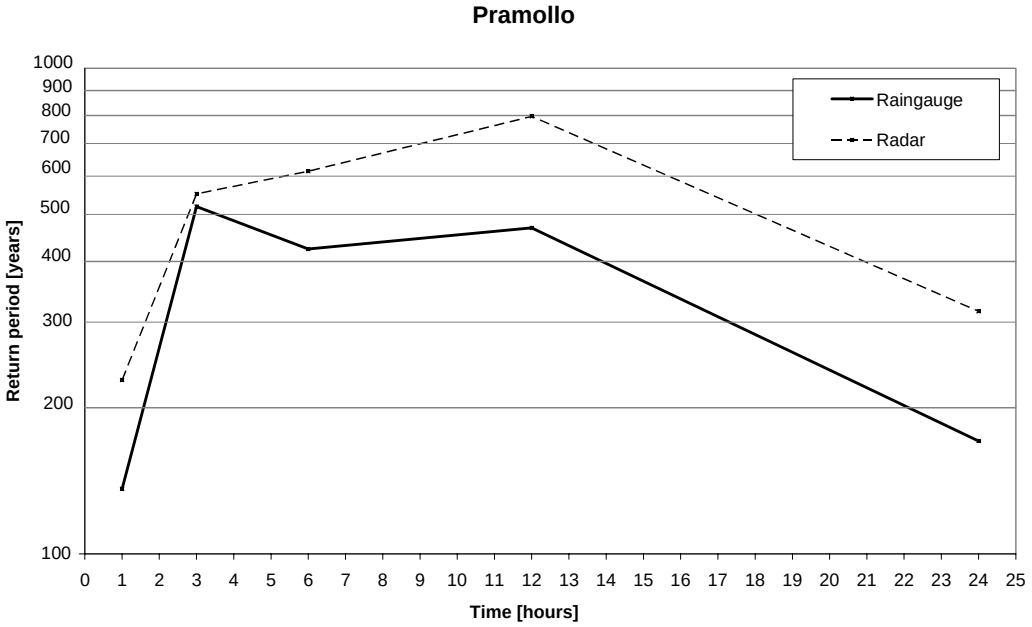

b)

Figure 3-6a-b. Severity graph obtained from raingauge data and from radar rainfall estimates for the stations located in a) Pontebba and b) Pramollo.

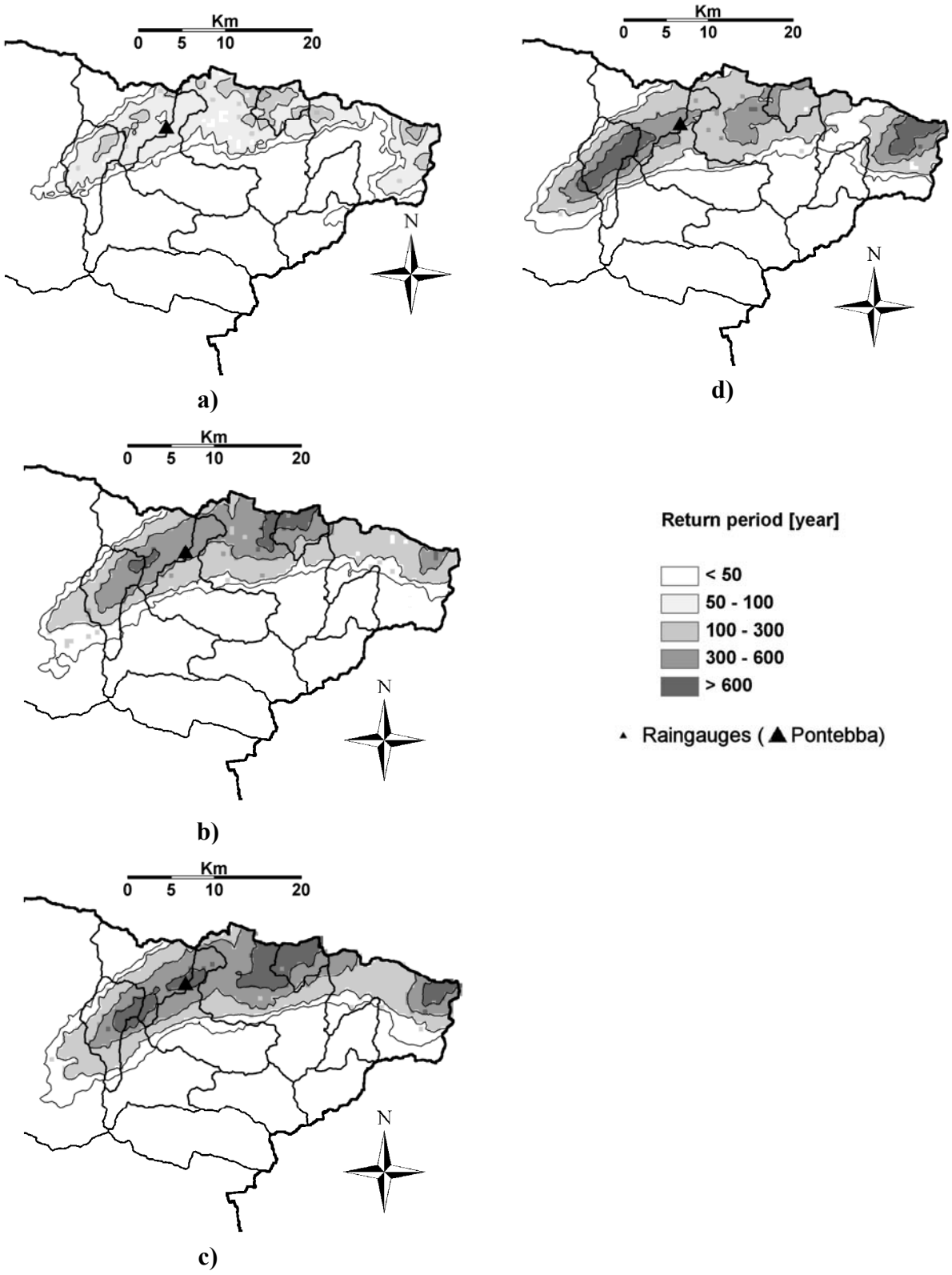

Figure 3-7a-d. Return time patterns for rainfall maxima corresponding to a) 1h, b) 3h, c) 6h and d) 12h. The bold triangle represent the position of the Pontebba raingauge station.

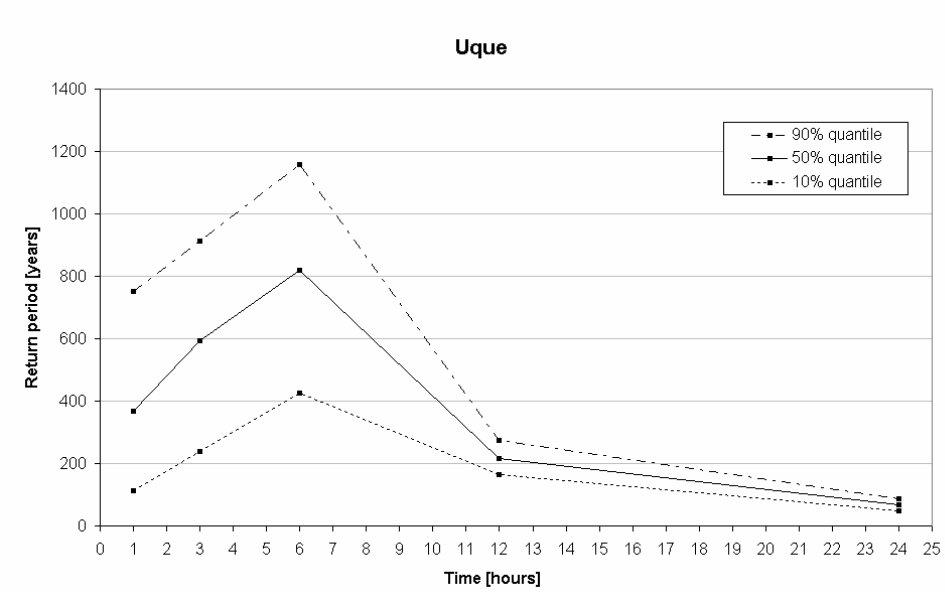

a)

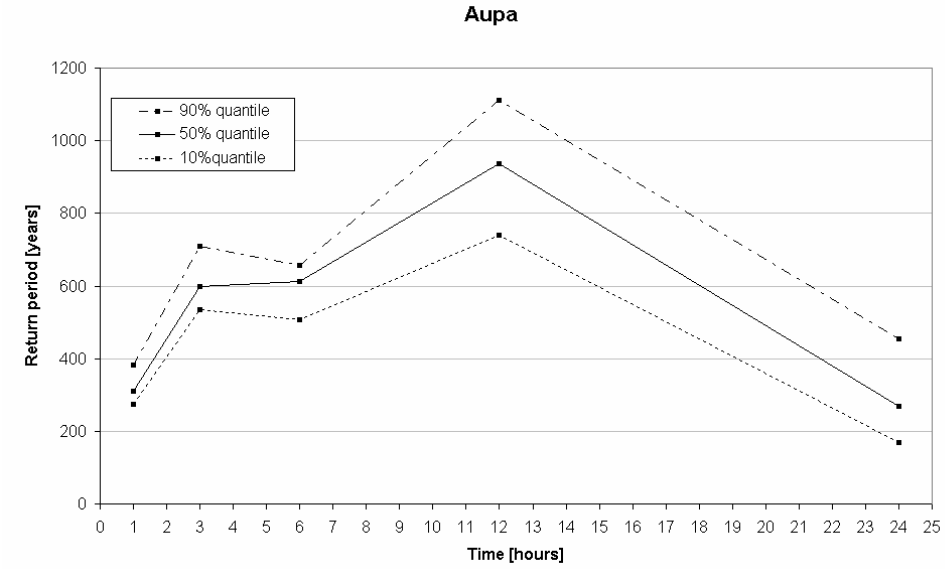

b)

Figure 3-8a,b. Severity graph for two basins in the upper Fella basin: a) Uqua; b) Aupa.

Figure 3-8a-b shows clearly that the severity peak over the Uqua is concentrated on 3-h and 6-h durations, whereas severity on the Aupa show a peak at 12-h duration.

Globally, this analysis shows that attributing a single return period to a storm event is not realistic, even for a storm developing at a relatively small spatial scale such as the one considered here. The analysis shows also that the severity of this flash flood generating storm is poorly captured by using conventional raingauge networks.

A comparison between the mapped damages and the return period patterns (Tropeano et al., 2004 [45]) shows a remarkable agreement for the Uqua basin and nearby basins. In these basins, the relatively large duration of extreme rainfall explains also why the event was associated to widespread shallow landsliding and debris flows. Rainfall

duration and infiltration amounts were evidently adequate to produce the positive pore pressures necessary to initiate large mass movements (Borga et al., 2002 [7]). However, less damages were recorded over the Aupa basin, in spite of the severity of the relevant precipitation. This prompted to analyse the spatial character of the hazard evaluation.

Actually, severity graphs provide only partial information regarding the potential for flooding, emphasising the point scale of storm rarity (Konrad, 2001 [28]). It is the timing and spatial distribution of precipitation within a basin that are the key factors in determining whether a flooding will be observed (Hirschboeck et al., 2000 [20]). In order to gain a deeper view of the spatial extent and of the simultaneity of the intensities in the storm, we analysed the ratio between point and areal precipitation. Areal precipitation were computed over a support of $11 \cdot 11$ km^2, this area being the upper threshold for basin scales which reproduce the shape of the central convective band and experienced extreme flooding during the event. For each rainfall duration, the following steps were taken:

i) for each grid characterised by a return period greater than 50 years, the maximum rainfall depth over the area of $11 \cdot 11$ km^2 centered on the grid was computed according to the moving window procedure;
ii) the ratio was computed between the point and areal rainfall depths and mapped over the region (Figure 3-9a-d).

Values of the ratio close to one imply simultaneity of the rainfall across the area investigated and for the considered duration. On the contrary, low values of the ratio imply a high degree of heterogeneity and loss of simultaneity of the rainfall depth across the area. Ratios are reported in Figure 3-9a-d for the four durations of 1-h, 3-h, 6-h and 12-h, respectively. As expected, ratios for short durations (1-h and 3-h) are generally lower than for longer durations (6-h and 12-h). Ratios for 6-h an 12-h show also a remarkable spatial pattern with values consistently higher over the Uqua basin and the upper Fella basin (with values in the 0.6-0.8 range, with peaks close to one), and lower values over the mid Pontebbana and the Aupa (with values in the range 0.4-0.6). This helps to explain the explosive character of the flooding (and corresponding damages) over the Uqua and nearby basins with respect to the Aupa basin, where the rainfall rates peaked at different times across the basin.

3.4 Summary and conclusions

Regional frequency analyses were conducted on AMP data using the index variable method. The study area was the Eastern Italian Alps. AMP data were collected at 63 stations for durations of 1, 3, 6, 12 and 24 h. The region was analyzed as composed by three smaller subregions, namely, i) the southern plains, ii) the alpine foreland area and the upper Tagliamento basin closed upstream the junction with the Fella and iii) the region within and around the Fella basin. The last region was of particular interest because it includes the area hitted by an exceptional flash flood event occurred on August 29, 2003.

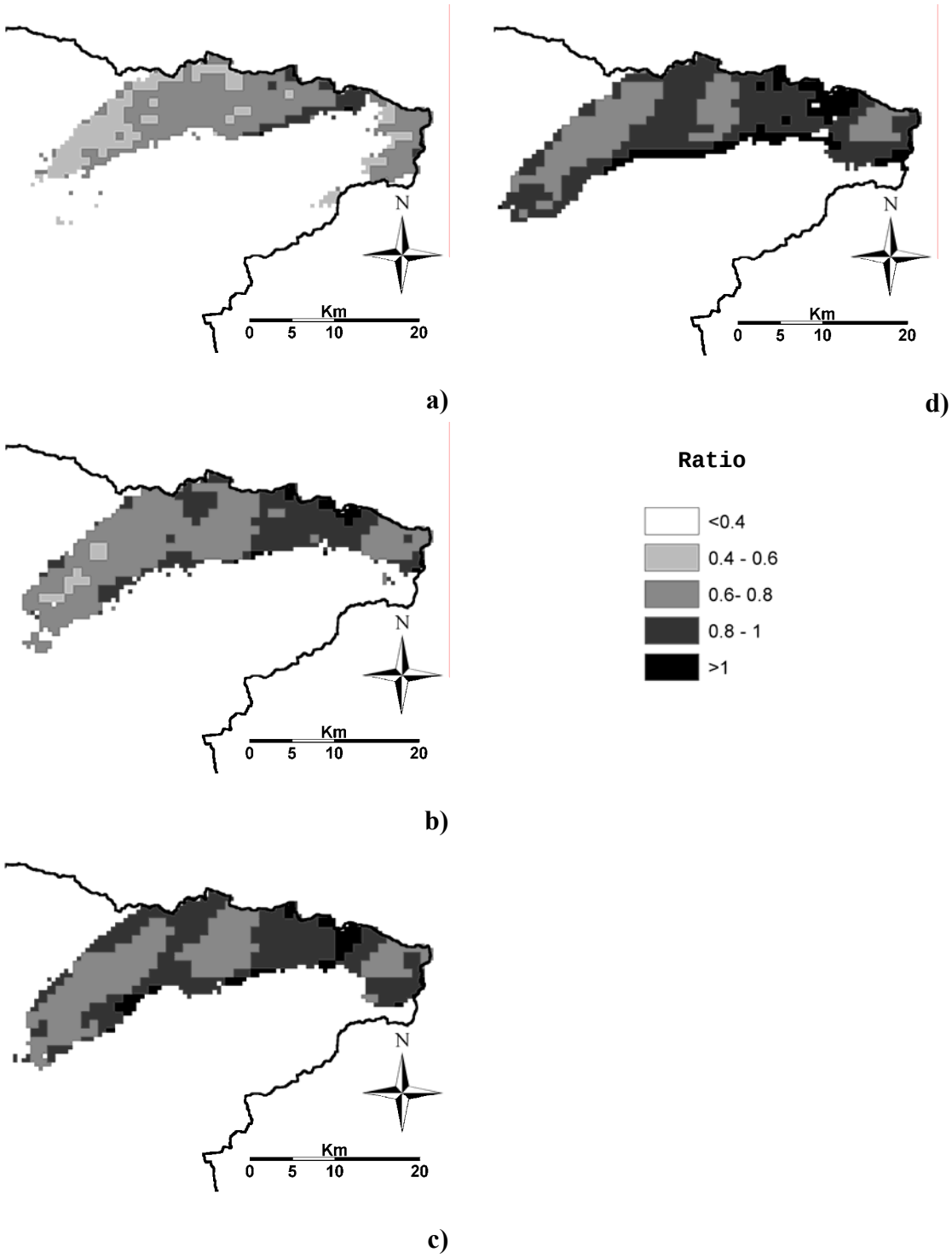

Figure 3-9a-d. Ratio of point to areal rainfall maxima for rainfall duration of a) 1h, b) 3h, c) 6h and d) 12h.

The subregions passed a regional homogeneity test and were treated as homogeneous. L-moments analysis suggests that either GEV or GLO may provide good fit to the data, depending on rainfall duration. For instance, in the case of the Fella-centered Subregion the GEV model may be a good choice for 1-h and 24-h, whereas the GLO model may be a better model for the 3-h, 6-h and 12-h data. This suggests that a distribution intermediate between GEV and GLO may be more appropriate for analysis of all rainfall durations. The four-parameter Kappa distribution is such a distribution, and it was used together with

GEV and GLO. The Kappa distribution was used to estimate growth curves for the Fella-centered region for the various rainfall durations, providing a framework to investigate the frequency characteristics of the 29 August 2003 flash-flood-generating storm for various rainfall durations. Rainfall maxima from the Pontebba station, which recorded the highest rainfall depths, were characterised by return periods in the range 200-500 years for 1-h and 24-h durations, and in the range 500-1000 years for 3-h, 6-h and 12-h durations.

Radar rainfall estimates, adjusted by using a physically-based methodology and data from a raingauge network, were used to characterise the return period of the storm rainfall amounts, highlighting the importance of considering its spatial dimension. Severity graphs were developed to visualise the return periods and their variability for different rainfall durations within the storm. The analysis shows that i) attributing a single return period to a storm event is not realistic, and ii) the severity of this flash flood generating storm is poorly captured by using a conventional raingauge network, which is too sparse to provide adequate sampling. It has been shown that adjusted radar rainfall estimates may suffer for considerable uncertainty and that the uncertainty magnifies in the evaluation of the relevant return periods. Whereas this call for development of standard procedures for evaluation of uncertainties in radar rainfall estimation, the reported results show that these estimates may be useful to evaluate the severity of the storm for ungauged basins and to evaluate the spatial dimension of the frequency characterisation. Both these features represent important basis for learning processes during ex-post evaluation of interventions in support of future development of strategies and strategic option in flood risk management in the study area.

3.5 References

[1] Bechini, R., Gorgucci, E., Scarchilli, G., Dietrich, S., 2002. The operational weather radar of Fossalon di Grado (Gorizia, Italy): accuracy of reflectivity and differential reflectivity measurements. Meteorol. Atmos. Phys., 79, 275-284.

[2] Benson, M. A., 1962. Evaluation methods for evaluating the occurrence of floods, U.S. Geol. Surv. Water Supply Pap, 1543–A., 279– 300.

[3] Berenguer, M., Lee, G. W., Sempere-Torres, D., Zawadzki, I., 2002. A variational method for attenuation correction of radar signal. Proceedings of the ERAD, 2002.

[4] Borga, M., 2002. Accuracy of radar rainfall estimates for streamflow simulation. Journal of Hydrology, 267, 26-39.

[5] Borga, M., Vizzaccaro, A., 1997. On the interpolation of hydrologic variables: formal equivalence of multiquadratic surface fitting and kriging. Journal of Hydrology 195, 160–171.

[6] Borga, M., Anagnostou, E. N., Frank, E., 2000. On the use of real-time radar rainfall estimates for flood prediction in mountainous basins. Journal of Geophysical Research, 105, D2, 2269-2280.

[7] Borga, M., Dalla Fontana, G., Cazorzi, F., 2002. Analysis of topographic and climatic control on rainfall-triggered shallow landsliding using a quasi-dynamic wetness index. Journal of Hydrology, 268(1-4), 56-71.

[8] Borga, M., Boscolo, P., Zanon, F., Sangati, M., 2007. Hydrometeorological analysis of the August 29, 2003 flash flood in the eastern Italian Alps. J. Hydrometeorology, in print.

[9] Buishand, T. A., 1991. Extreme rainfall estimation by combining data from several sites. Hydrological Sciences Journal, 36 (4), 345–365.

[10] Burn, D. H., 1990. Evaluation of regional flood frequency analysis with a region of influence approach. Water Resour. Res., 26(10), 2257– 2265.

[11] Ceschia, M., Micheletti, S., Carniel, R., 1991. Rainfall over Friuli Venezia Giulia: High Amounts and Strong Geographical Gradients. Theor. Appl. Climatol. **43**,175-180.

[12] Creutin, J. D., Borga, M., 2003. Radar hydrology modifies the monitoring of flash flood hazard. Invited commentary. 10.10002/hyp.5122, Hydrological Processes, 17, 7, 1453-1456.

[13] Cunnane, C., 1988. Methods and merits of regional flood frequency analysis. J. Hydrol., 100, 269-290.

[14] Dalrymple, T., 1960. Flood frequency analysis. Water Supply Paper 1543-A, USGS, Reston, VA, USA.

[15] Delrieu, G., Andrieu, H., Creutin, J. D., 2000. Quantification of path-integrated attenuation for X- and C-Band weather radar systems operating in Mediterranean heavy rainfall. J. Appl .Meteor., 39, 840-850.

[16] Delrieu G., Ducrocq V., Gaume E., Nicol J., Payrastre O., Yates E., Andrieu H., Ayral P-A., Bouvier C., Creutin J-D., Livet M., Anquetin S., Lang M., Neppel L., Obled C, Parent-du-Châtelet J., Saulnier G-M., Walpersdorf A., Wobrock W., 2005. The catastrophic flash-flood event of 8-9 September 2002 in the Gard region, France: a first case study for the Cévennes-Vivarais Mediterranean Hydro-meteorological Observatory. Journal of Hydrometeorology, 6, 34-52.

[17] Gaume, E., Livet, M., Desbordes, M., Villeneuve, J. P., 2004. Hydrological analysis of the river Aude, France, flash flood on 12 and 13 November 1999. Journal of Hydrology, 286(1), 135-154.

[18] Greenwood, J. A., Landwehr, J. M., Matalas, N.C., Wallis, J. R., 1979. Probability weighted moments: definition and relation to parameters of several distributions expressible in inverse form. Water Resour. Res., 15(5), 1049-1054.

[19] Greiss, N. P., Wood, E. F., 1981. Regional flood frequency analysis and network design, Water Resour. Res., 17(4), 1167– 1177.

[20] Hirschboeck, K. K., Ely, L. L., Maddox, R. A., 2000. Hydroclimatology of meteorologic floods. Inland Flood Hazards, E. E. Wohl, Ed. Cambridge University Press, 39–72.

[21] Hosking, J. R. M., 1986. The theory of probability weighted moments. Research report RC 12210, IBM Research Yorktown Heights.

[22] Hosking, J. R. M., 1990. L-moments: analysis and estimation of distributions using linear combinations of order statistics. J. R. Stat. Soc., Ser. B., 52(2), 105-124.

[23] Hosking, J. R. M., 1994. The four parameter kappa distribution. IBM J. Res. Develop., Vol. 38, 3, 1994.

[24] Hosking, J. R. M., 1996. Asymptotic distributions of the sample mean, autocovariances, and autocorrelations of long-memory time series. Journal of Econometrics, 73(1), 261-284.

[25] Hosking, J. R. M., Wallis, J. R., Wood, E. F., 1985. An appraisal of regional flood frequency procedure in the U. K. flood studies report. Hydrol. Sci. J., 30(1), 85–109.

[26] Hosking, J. R. M., Wallis, J. R., 1997. Regional frequency analysis. Cambridge University Press, 224 pp.

[27] Institute of Hydrology, 1999. Flood Estimation Handbook. 5 Volume. Natural Environment Research Council , Centre for Ecology and Hydrology, Wallingford, Oxfordshire OX10 8BB, UK, ISBN 0 948540 94 X .

[28] Konrad, C. E., 2001. The most extreme precipitation events over the Eastern United States from 1950 to 1996: Considerations of scale. J. Hydrometeorol., 2, 309-325.

[29] Koutsoyiannis, D., 2004. Statistics of extremes and estimation of extreme rainfall, 1, Theoretical investigation. Hydrological Sciences Journal, 49(4), 575– 590.

[30] Lettenmaier, D. P., Wallis, J. R., Wood, E. F., 1987. Effect of regional heterogeneity on flood frequency estimation, Water Resour. Res., 23(2), 313– 323.

[31] Matalas, N. C., Gilroy, E. J., 1968. Some comments on regionalization in hydrologic studies, Water Resour. Res., 4, 1361– 1369.

[32] Miller, R.J., 1974. The Jacknife – a review. Biometrika 61, 1–15.

[33] National Environment Research Council (NERC), 1975. UK Flood Studies Report, vol. 1, Hydrological Studies, London.

[34] Norbiato, D., Borga, M., Sangati, M., Zanon, F., 2007b. Regional Frequency Analysis of Extreme Precipitation in the eastern Italian Alps and the August 29, 2003 Flash Flood. Journal of Hydrology. 345, 149-166. doi:10.1016/j.jhydrol.2007.07.009

[35] Ogden, F. L., Sharif, H. O., Senarath, S. U. S., Smith, J. A., Baeck, M. L., Richardson, J. R., 2000. Hydrologic analysis of the Fort Collins, Colorado flash flood of 1997. Journal of Hydrology, 228, 82-100.

[36] Pellarin, T., Delrieu, G., Saulnier, G. M., Andrieu, H., Vignal, B., Creutin, J. D., 2002. Hydrologic visibility of weather radar systems operating in mountainous regions: Case study for the Ardèche basin (France). Journal of Hydrometeorology, 3, 539-555.

[37] Querini, R., 1984. Il nubifragio delle prealpi carniche orientali (11 settembre 1983) ed i conseguenti dissesti idrogeologici. Accademia Italiana di Scienze Forestali.

[38] Ramos, M. H., Creutin, J. D., Leblois, E., 2005. Visualization of storm severity. Journal of Hydrology, 315, 295-307.

[39] Reed, D. W., Jakob, D., Robson, A. J., Faulkner, D. S., Stewart, E. J., 1999. Regional frequency analysis: A new vocabulary. Publ. No. 255, Hydrological extremes:

Understanding, predicting, mitigating, Proc., IAHS Symposium, Birmingham, International Association of Hydrological Sciences, Wallingford, U.K., 237–243.

[40] Rossi, F., Fiorentino, M., Versace, P., 1984. Two-Component Extreme Value distribution for flood frequency analysis. Water Resour. Res., 20 (2), 847-856.

[41] Schaefer, M. G., 1990. Regional analyses of precipitation annual maxima in Washington state. Water Resour. Res., 26(1), 119–131.

[42] Stedinger, J. R., Vogel, R. M., Foufoula-Georgiou, E., 1993. Frequency analysis of extreme events. Handbook of Applied Hydrology, cap. 18, Ed. D.A. Maidment, McGraw-Hill, New York.

[43] Stedinger, J. R., Lu, L. H., 1995. Appraisal of regional and index flood quantile estimators, Stochastic Hydrol. Hydraul., 9(1), 49– 75.

[44] Sveinsson O. G. B., Boes, D. C., Salas, J. D., 2001. Population index flood method for regional frequency analysis. Water Resour. Res. 2001;37:2733–48.

[45] Tropeano, D., Turconi, L., Sanna, S. 2004. Debris flows triggeredby the August 29, 2003 cloudburst in Val Canale, Eastern Italian Alps. In: Proceedings of the International Symposium INTERPRAEVENT 2004, Riva del Garda (Italy), 24–27 May 2004.

[46] Vicens, G. J., I., Rodriguez-Iturbe, I., Shaake Jr., J. C., 1975. A Bayesian framework for the use of regional information in hydrology, Water Resour. Res., 11(3), 405–414.

[47] Villi, V., Caleffa, G., Gatto, G., Mori, G., 1986. Distribuzione spazio temporale delle piogge intense nel Triveneto- cartografia. Quaderno di Ricerca no. **7**., C.N.R and Regione Veneto (in italian).

[48] Wallis, J.R., Schaefer, M.G., Barker, B.L., Taylor, G.H., 2007. Regional precipitation-frequency analysis and spatial mapping for 24-hour and 2-hour durations for Washington State. Hydrology and Earth System Sciences 11 (1), 415–442.

4 Flash flood warning based on rainfall depth-duration thresholds and soil moisture conditions[3]

4.1 Introducion

Given the specific space-time scales of flash flood events, at least two features characterise flash flood forecasting with respect to riverine flood forecasting and point out to their larger uncertainty. These are: i) the short lead time, which implies both the integration of meteorological and hydrologic forecast, and the difficulties of using data assimilation procedures based on real time observed discharges to reduce uncertainty in hydrologic predictions, and ii) the need to provide local forecasts, which means that, on one hand, the rainfall must be monitored and forecasted on a wide range of space/time scales, and, on the other hand, every tributary of a monitored basin can be considered as a potential target for flood warning. In this sense, flash flood forecasting exemplifies the ungauged basin prediction problem under extreme conditions.

The assessment of the susceptibility to flash flood, by taking time-varying hydrologic characteristics such as soil moisture status and snowcover into account before the potential event, is a critical step to anticipate the locations of the river system which may be hitted by the flood. Even though the occurrence, location and (or) timing of the flash flood is still uncertain, this information may provide enough lead time so that flash flood mitigation measures can be planned and managed in an anticipatory rather than responsive manner. Lead time in these cases may be comprised between one day and few hours. The provision of information about susceptibility to flash flood is one of the objectives of the Flash Flood Guidance system, which is operating in the United States since 1970s (Mogil et al., 1978 [28]). According to Georgakakos (2006 [20]), the US National Weather Service relies routinely on Flash Flood Guidance (FFG, hereinafter) computations to produce flash flood watches and warnings. FFG is the depth of rain of a given duration, taken as uniform in space and time on a certain basin, necessary to cause minor flooding at the outlet of the considered basin. This rainfall depth, which is computed by running in inverse mode a lumped hydrological model, is compared to either real time-observed or forecasted rainfall of the same duration and on the same basin. If the nowcasted or forecasted rainfall depth is greater than the FFG, then flooding in the basin is considered likely. Georgakakos (2006 [20]) provided the theoretical basis of developing operational flash flood guidance systems by using analytical methods. Ntelekos et al. (2006 [36]) analysed uncertainty propagation within a simplified FFG system.

Apart from their extensive use in the United States (Georgakakos, 2006 [20]) and in Central America (Georgakakos, 2004 [19] ; Sperfslage et al., 2004 [40]), in Europe, the

[3] The study described in this chapter has been proposed in Norbiato et al. (2007c [35])

Integrated Project FLOODSite (http://www.floodsite.net) among others aims at assessing the advantage for using the rainfall threshold approach as an alternative to the traditional ones in the case of flash floods.

Alternatives to the FFG have been proposed in the last years, generally taking advantage from the development of spatially distributed hydrological models (Moore et al., 2006 [31]; Reed et al., 2007 [38]; Bloeschl et al., 2007 [4]). However, development of the FFG concept is still ongoing. It is recognised that the FFG provides a useful concept that simplifies communication about the hydrological status of basins from hydrologists to meteorologists and that it represents a potential benchmark for further development and intercomparison purposes.

The objective of this chapter is to evaluate a threshold-based flash flood warning approach based on FFG by considering a wide range of climatic and physiographic European conditions, and by focusing on ungauged basins. More specifically, system results have been evaluated at gauged interior sites that were not used to calibrate the lumped hydrological model. At these sites, the model parameters were regionalised by transposition from the parent basin, and by using GIS-based techniques to derive basin-specific parameters for simulation of snow melt dynamics and flow routing. Results derived in this way are considered indicative of expected performance at ungauged locations, under the conditions that model calibration may be carried out at larger spatial scales and that computed parameters may be transposed at smaller spatial scales.

Two alternative ways to compute soil moisture status were considered. The first consists on transpose soil moisture status, further than model parameters, from parent basins to interior basins. This technique has obvious advantages in terms of operational implementation, by reducing computational efforts to obtain FFG at several interior sites. However, soil moisture status may be biased when used at the scale of the specific interior basin, due to use of precipitation and evaporation estimates which are representative at the scale of the parent basin but potentially not at the scale of the interior basins. As a second alternative, the use of time-constant soil moisture status as an input to the threshold-based flash flood warning system was evaluated. This alternative is representative of time-constant precipitation depth-durations thresholds and it is obtained by setting the values of the model soil moisture status on their time-average value. Assessment of this procedure allows to evaluate the decrease in accuracy associated to lack of information about the temporal variation of soil moisture status before the flood event.

The simulation experiments described in this chapter are designed to understand the potential benefits and limitations of the flash flood warning approach and to guide further development. More specifically, modelling experiments address the four questions below.

1. Which is the impact on FFG technique accuracy due to of time-uniform precipitation? This issue is approached by comparing threshold-based results with those obtained by using the hydrological models with the observed precipitation input.

2. How simulation accuracy at ungauged interior points, simulated by using transposed parameters from parent basins, compare with results obtained for parent basins where calibration has been carried out?

3. Which is the decrease in simulation accuracy associated to transposing both parameter and soil moisture from the larger scale parent basins?

4. How technique performance degrades when a time-constant soil moisture status is used?

4.2 Study Areas and Data

Data from two distinct European regions were used in this study: north eastern Italy (with eight basins) and central France (with three basins). Figure 4-1 shows the location of the basins. Table 4-1 provides more detailed basin information, with Table 4-2 and Table 4-3 providing information on the length period with hourly data considered and division among calibration and validation period. Table 4-4 provides the information about the topological connection between parent basins and nested basins. Two parent basins contain two nested basins each, and other two parent basins contain one nested basin each.

Drainage area is comprised between 116 km^2 and 3244 km^2 for the parent basins, and between 7.3 km^2 and 233 km^2 for the nested basins. The size of the largest basin (Loire river at Bas-en Basset, with 3244 km^2) is at the limit of the spatial scales usually met for flash flood analysis. This case has been used here to assess the performance of the system with increasing the basin scale. The second largest basin is the Dunierés at Vauberlet, with 233.4 km^2.

The topography of these basins is in general rather complex, with some high altitude basins (Ridanna, Cordevole at Saviner, Cordevole at Vizza), characterised by top altitudes exceeding 3000 m a.s.l., and elevation range comprised between 800 and 2000 m. Floods in some of these basins may be influenced by snow accumulation and melt. Even though only rarely these floods are short and intense enough to be characterised as flash floods, snow-related processes are important elements for characterisation of the seasonal hydrological balance. It has been decided therefore to include dynamics of snow accumulation and melt in the modelling strategy.

In general, the river regime of these river systems is altered in a negligible way by management activities, such as artificial reservoirs and diversions. However, the regime of the Brenta river is influenced by two relatively large natural lakes (Caldonazzo and Levico), with 77 km^2 area drained by the lakes. In this case, the influence of the natural lakes on the river regime has been taken into account by subdividing the basin into subunits and simulating the effects of the lakes. Artificial reservoirs exist on the Loire river. The 200 km^2 upstream part of the Loire watershed is equipped with dams for hydropower plants and 350 km^2 of the Lignon watershed downstream Le Chambon sur Lignon is controlled by a dam built for the water supply of the City of Saint Etienne. These reservoirs are managed to be as “transparent” as possible during floods; as a consequence, their influence on flood flows is very limited especially at Bas-en-Basset. No significant dams exist on the Gagne and Dunieres river systems.

Karstified aquifer influence the runoff response for specific portions of the Posina and Brenta river systems.

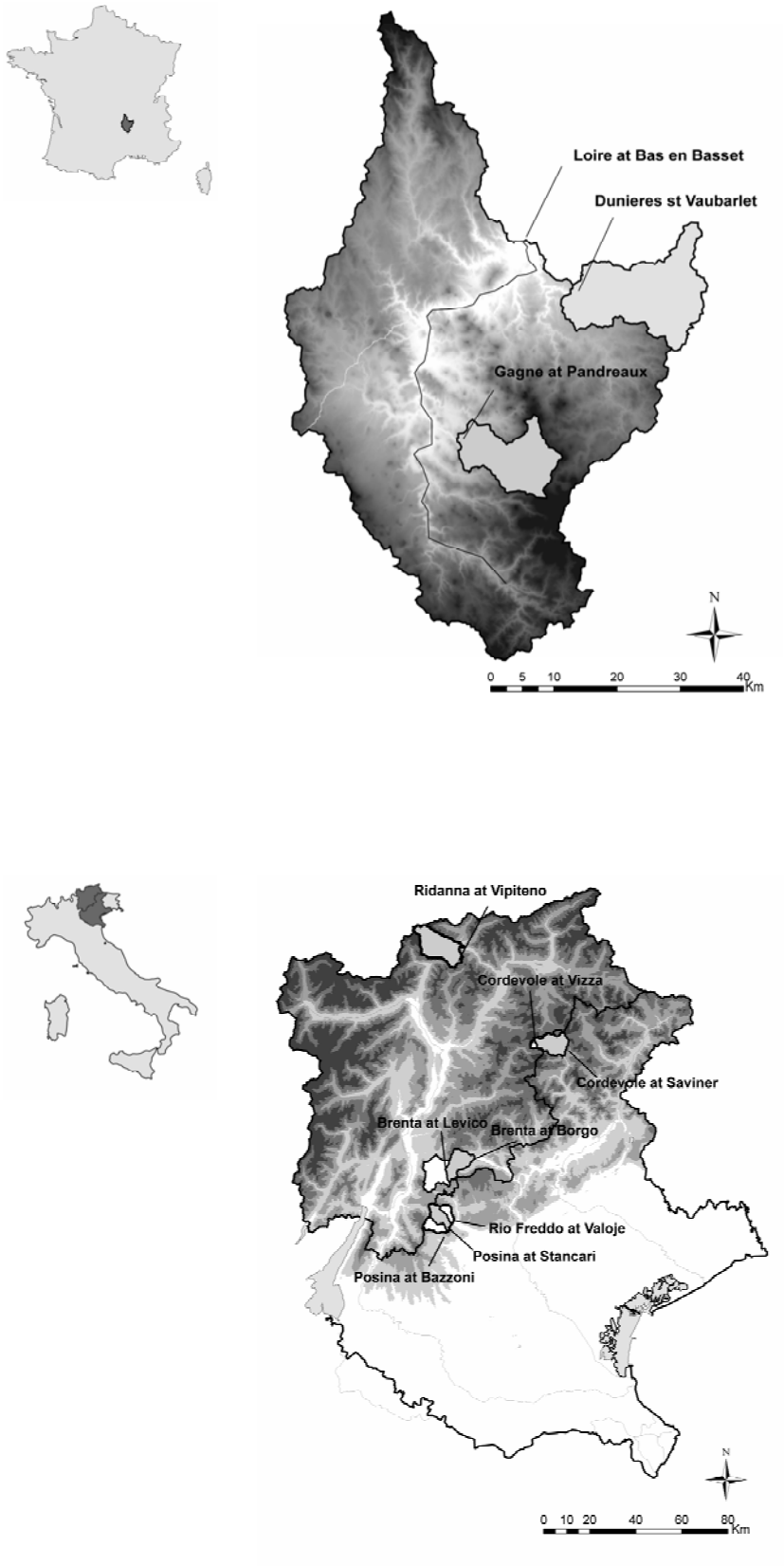

Figure 4-1. Study basins and their location in France and Italy

Table 4-1. Basins characteristics

Station name	Basin number	Area (km^2)	Elevation range (m)	Mean Annual Rainfall (mm)	Mean Annual Runoff (mm)	Runoff Coefficient
Loire at Bas-en-Basset	1	3244	450 – 1800	888	361	0.41
Cordevole at Saviner	2	109	1025 - 3200	1110	770	0.69
Posina at Stancari	3	116	388 – 2300	1645	1000	0.61
Brenta at Borgo	4	213.7*	380 - 2400	1068	650	0.61
Ridanna at Vipiteno	5	210.2	940 - 3600	1271	1016	0.80
Gagne at Pandreaux	6	121.9	600 – 1500	909	393	0.43
Dunieres at Vauberlet	7	233.4	584 - 1400	939	391	0.42
Cordevole at Vizza	8	7.3	1810 - 3200	1145	880	0.77
Posina at Bazzoni	9	38.8	453 - 2300	1717	1086	0.63
Rio Freddo at Valoje	10	22.2	390 - 2000	1549	835	0.54
Brenta at Levico	11	113*	435 - 2000	1088	-	-

* In the case of Brenta basin 77km^2 of the area is drained by natural lakes.

Table 4-2. Periods with data considered: parent basins

Station name	Basin number	Periods with hourly data considered	Calibration period	Validation period
Loire at Bas-en-Basset	1	1/10/1990 - 1/10/2003	1/10/1997 1/10/2003	1/10/1990 30/09/1997
Cordevole at Saviner	2	1/10/1993 - 1/10/2000	1/10/1993 30/09/1997	1/10/1997 1/10/2000
Posina at Stancari	3	1/10/1992 - 1/10/2000	1/10/1992 30/09/1996	1/10/1996 1/10/2000
Brenta at Borgo	4	1/10/1994 - 1/10/2005	1/10/1994 30/09/2001	1/10/2001 1/10/2005
Ridanna at Vipiteno	5	1/10/1992 - 1/10/2004	1/10/1992 30/09/1997	1/10/1997 1/10/2004

Table 4-3. Periods with data available: interior points

Station name	Basin number	Periods with hourly data available
Gagne at Pandreaux	6	1/10/1998 - 1/10/2003
Dunierés at Vauberlet	7	1/10/1990 - 1/10/2003
Cordevole at Vizza	8	1/10/1992 - 1/10/2000
Posina at Bazzoni	9	1/10/1993 - 1/10/2000
Rio Freddo at Valoje	10	1/10/1993 - 1/10/2000
Brenta at Levico	11	1/10/1994 - 1/10/2005 (only flood data)

Table 4-4. Relationship among parent and nested basins

Parent basins	Nested basins
1	6, 7
2	8
3	9, 10
4	11
5	-

Annual runoff coefficient range from rather low values (around 0.42) for the French basins to relatively high values for some Italian high altitude basins (0.8 for Ridanna). The Budyko's climatic classifications scheme (Budyko, 1974 [8]) has been applied to compare and contrast the climatic characteristics of these basins. This is achieved by presenting the specific response of each of these basins on the Budyko curve (Figure 4-2), which is a plot that expresses E/P, the ratio of average annual actual evapotranspiration (E) to average annual precipitation (P) as a function of EP/P, the ratio of average annual potential evapotranspiration (EP) to average annual precipitation (P). Actual evapotranspiration (E) for each basin was derived as the long-term difference between P and R (runoff) for the basins. Figure 4-2 shows clearly that the Italian basins (2, 3, 4, 5, 8, 10) represent a wet climate, whereas the French basins (1, 6, 7) have a medium climate.

Figure 4-2 shows also significant climate variability among parent and nested basins. This is the case for Cordevole at Saviner (2) and at Vizza (8), where differences are due mainly to different elevation ranges among parent and interior basin, and for Posina at Stancari (3) and Rio Freddo (10), where differences are mainly due to the differentiated impact of the karstified aquifer.

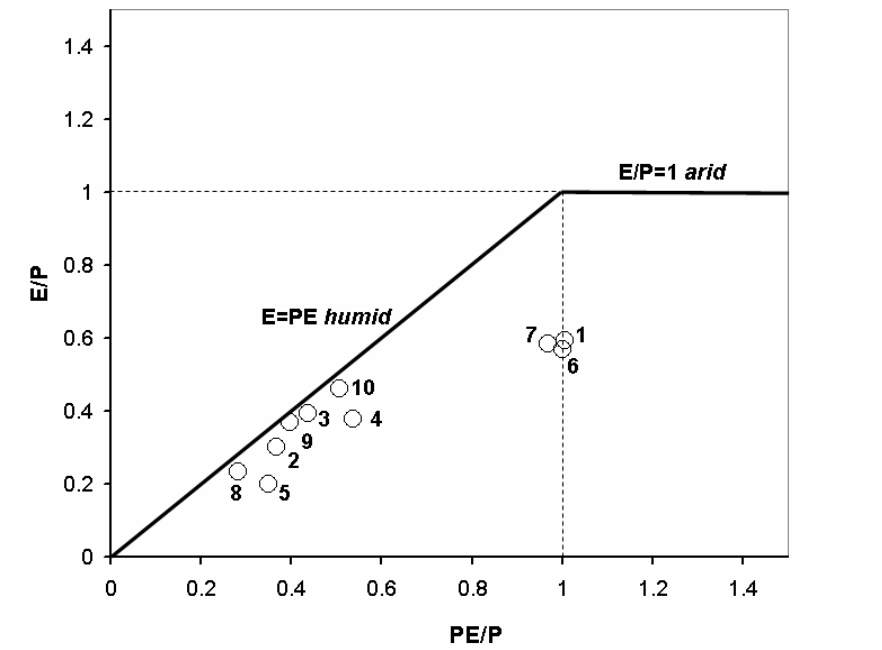

Figure 4-2. Plot of mass balance data from the study basins on the Budyko curve.

The length of the hourly record of streamflow, precipitation and temperature data ranges from 5 to 13 years, with a total of 101 years. The data were quality controlled and as a results part of the record was set to missing. Basin-averaged precipitation estimates were obtained based on rain gauge stations by using a Thiessen technique, with densities ranging from 1 station per 15 km^2 (Brenta river basin) to 1 station per 140 km^2 (Loire river basin).

The stage-discharge relationship at the interior streamflow gauge of Brenta at Levico is considered exceedingly uncertain for low flows. Due to this reason, only flood discharge data were used.

Digital Elevation Model (DEM) at four different resolutions were used: 75 m for the French basins, 30 m for Brenta and Ridanna, 25 m for Cordevole and 20 m for Posina.

4.2.1 Rationale for basins selection

The study basins in Figure 4-1 were selected for several reasons. First, these basins had the data required to conduct the intercomparison, with concurrent time series of hourly rainfall, temperature and discharge data made available for the basin outlets and selected interior points. The quality of the data available is representative of operational conditions, subject to complexities due to rough orography and high space-time variability. Lack of significant modification of the streamflow due to reservoirs and diversions simplifies the intercomparison study.

A second critical criterion for selection is the observation of past flash flood events in these basins and their representativeness of conditions leading to flash flood.

Finally, the selected parent basins contain internal points having observed streamflow data, allowing to develop study questions regarding the prediction of interior hydrologic processes.

The Ridanna basin has no interior gage locations. This basin represents an additional case for testing the threshold methodology over a high-altitude alpine basin frequently hitted by small scale flash flood, usually triggering shallow landsliding and debris flows.

Lastly, the hydrometeorology of flash flooding in these areas has been widely studied. Borga and Vizzaccaro (1997 [6]) and Dinku et al. (2002 [16]) analysed estimation uncertainties of flood-generating storms based on raingauges and radar observations for the upper Astico river system (Posina). In the same region, Borga et al. (2000 [7]) and Hossain et al. (2004 [22]) examined the impact of errors in radar-based rainfall estimates on flood prediction uncertainty.

4.3 The threshold-base technique

The threshold-based technique applies to a given basin and for a given rainfall duration, and it is based on the comparison between the FFG and the either real time-observed or forecasted rainfall. If the nowcasted or forecasted rainfall depth is greater than the FFG, then flooding in the basin is considered likely. It is important to recognise that the FFG technique does not predict flash flood timing, but only that a flood threat is imminent. The major effort within the FFG is the correct assessment of the flood magnitude, while the correct timing forecast is left to the monitoring activity triggered by the flash flood alert.

In this study, the FFG is obtained by running a lumped hydrological model for several hypothetical rainfall amounts for the selected rainfall duration and given current soil moisture conditions. Five rainfall durations are considered: one, three, six, twelve and twenty four hours. The lumped soil-moisture accounting hydrological model used in the methodology is described next.

4.3.1 Description of the hydrological model

The model used in this study is a semi-distributed conceptual rainfall-runoff model, following the structure of the PDM (Probability Distributed Moisture) model (Moore, 1985 [30]). A detailed description of the implemented hydrological system is reported in detail in Degli Esposti (2005 [15]). The model runs on a hourly time step and consists of a snow routine, a soil moisture routine and a flow routing routine. The snow routine represents snow accumulation and melt by using a distribution function approach based on a combined radiation index degree-day concept (Cazorzi and Dalla Fontana, 1986 [9]). Snow melt is computed as follows:

$$M = \begin{cases} f_m EI\,(T_h - T_0) & T_h > T_0 \\ 0 & T_h \le T_0 \end{cases} \qquad (4.1)$$

where M is the melt rate [mm h^{-1}], T_h is the hourly mean temperature [°C], T_0 [°C] is a threshold temperature beyond which melt is assumed to occur, f_m is a melt factor and EI [J m^{-2} h^{-1}] is an energy index which represents the potential radiation energy (variable in time) for a given site in the basin. EI is computed for each topographic element of the basin

taking into account solar altitude angle, optical depth of the atmosphere, elevation, aspect, slope and shading effects. The basin is subdivided into temperature bands (generally ranging 200 m in elevation), and for each band the empirical distribution of the energy index is used in the lumped form of the snow melt module. It means that each elevation band is subdivided in a fixed number of energy band whose limits correspond to different quantiles of the energy index empirical distribution. For each energy band snow accumulation, melt and refreezing are evaluated and then aggregated at the basin scale.

Catch deficit of the precipitation gauges during snowfall is corrected by a snow correction factor, *SCF*. A threshold temperature interval *TR−TS* is used to distinguish between rainfall, snowfall and a mix of rain and snow. The model includes routines able to compute runoff produced during rain-on-snow events, to propagate the exceed liquid water in the snow cover through it and to simulate the refreezing processes.

Potential evapotranspiration is estimated by using the Hargreaves and Samani method (Hargreaves and Samani, 1982 [21]).

The soil moisture routine uses a probability distribution to describe the spatial variation of water storage capacity across a basin. Saturation excess runoff generated at any point in the basin is integrated over the basin to give the total direct runoff entering the fast response pathways to the basin outlet. Drainage from the soil is subdivided into a subsurface and a baseflow component. Storage representations of the fast, medium(subsurface flow) and slow response pathways yield a fast, medium and slow response at the basin outlet which, when summed, gives the total basin flow. The PDM model configuration used here employs a Pareto distribution of storage capacity, *c*. This has the distribution function

$$F(c) = 1 - \left[1 - \left(c / c_{\max}\right)\right]^{b} \tag{4.2}$$

where c_{max} [mm] is the maximum storage capacity in the basin and the parameter *b* [-] controls the degree of spatial variability of storage capacity over the basin. The instantaneous rate of fast runoff generation from the basin is obtained by multiplying the rainfall rate by the proportion of the basin which is saturated.

Losses due to evaporation are calculated as a function of potential evaporation and the status of the soil moisture store. The dependence of evaporation loss on soil moisture content is introduced by assuming the following simple function between the ratio of actual to potential evaporation, *E/EP*, and soil moisture deficit, S_{max}-*S(t)*:

$$\frac{E(t)}{EP(t)} = 1 - \left\{ \frac{\left[S_{\max} - S(t)\right]}{S_{\max}} \right\}^{b_e} \tag{4.3}$$

where S_{max} [mm] is the total available basin storage, b_e [-] is an exponent coefficient and *S(t)* [mm] is the basin moisture storage at time *t*. Drainage to the slow flow path, *d* [mm h^{-1}], is represented by a function of basin moisture storage *S(t)* such that

$$d = \left(k_g\right)^{-1} \left[S(t) - S_t\right]^{b_g} \tag{4.4}$$

where the parameters are a time constant k_g [h mm $^{bg-1}$], an exponent coefficient b_g [-] and a threshold storage S_t [mm] below which there is no drainage.

Loss due to subsurface flow are calculated by means of the following equation:

$$Qsubsurface = Q_0 \cdot \exp^{(-(S_{\max} - S_t))/m} \quad (4.5)$$

where Q_0 [mmh^{-1}] and m [mm] are model parameters related to soil hydraulic properties and topography according to the TOPMODEL concepts (Beven and Wood, 1983 [1]; Wolock, 1993 [42]). $S_{\max} - S_t$ is the basin average soil moisture deficit.

The slow or base flow component, q_s [mm h^{-1}], of the total runoff is assumed to be routed through an cubic storage which is in general more suitable to represent the groundwater emptying (Moore et al., 2002 [31]) such that

$$q_b = kS^3 \quad (4.6)$$

where S_s [mm] is the depth of storage and k_s [h^{-1}mm^{-2}] is the decay parameter of the store.

Direct runoff from the proportion of the basin where storage capacity has been exceeded is routed by means of a geomorphology-based distributed unit hydrograph. With this procedure, a geomorphologic filter based on a threshold drainage area (A_{th}) is used to distinguish hillslopes and channel network starting from the space-filling representation of the drainage system directly obtainable from DEMs (Montgomery and Foufoula-Georgiou, 1993 [29]; Da Ros and Borga, 1997a [13]). The routing time of each site in the basin is evaluated assigning different typical velocity values in each pixel pertaining to the basin and classified as hillslope or channel. The two velocities, v_h and v_c, used to describe the flow routing process in each of the two components of the drainage system are assumed here constant; they maintain a physical meaning as the average velocities on hillslopes and in channel network. Total runoff is computed as the sum of slow, subsurface flow and fast runoff.

4.4 Assessment methodology

4.4.1 Model application

Three different strategies were considered to implement the methodology: i) model parameter calibration; ii) model parameter transposition from parent basin to interior sites; iii) model parameter and soil moisture status transposition from parent basins to interior points. These strategies can be described as follows.

Model parameter calibration

The goal of calibration is to adjust the model's parameters to decrease the difference between observed and simulated streamflow values. The closeness of fit can be checked qualitatively (e.g. plots of observed and simulated hydrographs) or quantitatively (residual statistics such as the Bias, Nash-Sutcliffe efficiency, etc.). In this study, the Shuffled Complex Evolution-University of Arizona (SCE-UA, Duan et al., 1992 [17]) global optimization algorithm was used for calibration of the hydrological model parameters over the five parent basins. The SCE-UA global search procedure is based on the downhill

simplex method (Nelder and Mead, 1965 [34]), combined with a random search procedure and the idea of complex shuffling. Even though the final objective of the study is to obtain a good description of flood events, equal weight was placed to the reconstruction of low flows, in an effort to improve the description of soil moisture conditions before the flood events.

The following objective functions were used during the optimization process for this study:

1: the Nash and Sutcliffe (1970 [33]) coefficient of efficiency defined as:

$$E_{NS} = 1 - \frac{\sum_{i=1}^{n}(O_i - S_i)^2}{\sum_{i=1}^{n}(O_i - O_{ave})^2} \tag{4.7}$$

where O_i is the hourly *i-th* observed discharge, S_i is the simulated discharge, and O_{ave} is the mean value of the observed discharges. The coefficient of efficiency was selected because it is dimensionless and is easily interpreted. If the model predicts observed streamflow with perfection then E_{NS}=1. If E_{NS}<0 then the model's predictive power is worse than simply using the average of the observed values.

2: the relative bias (RB) defined as:

$$RB = \frac{\sum_{i=1}^{n}(S_i - O_i)}{\sum_{i=1}^{n}O_i} \tag{4.8}$$

RB is a measure of total volume difference between observed and simulated streamflows, and is important in the evaluation of simulations from continuous hydrologic models.

A simple split sample test (Klemes, 1986 [23]) was considered for calibration and validation of the hydrological model. The test involves dividing the available data into two sets, one used for parameter estimation (calibration period) and the other for validation (validation period).

Model parameter transposition

The process of transferring information (such as basin model parameter values) from neighbouring basins to the basin of interest is generally referred to as hydrological regionalisation (Bloeschl and Sivapalan, 1995 [2]). Numerous regionalisation methods have been proposed in the literature for the case of basin model parameters (Bloeschl, 2005 [3]). Merz and Bloeschl (2004 [27]) examined the performance of various methods of regionalising the parameters of a conceptual basin model in 308 Austrian basins. They concluded that the methods based on spatial proximity performed better than those based on physiographic basin attributes. Similar finding were reported by Kokkonen et al. (2003 [24]) and Parajka et al. (2005 [37]). Kokkonen et al. (2003 [24], p. 2219), concluded that "when there is a reason to believe that, in the sense of hydrological behaviour, a gauged

basin resembles the ungauged basin, then it may be worthwhile to adopt the entire set of calibrated parameters from the gauged basin instead of deriving quantitative relationships between basin descriptors and model parameters". One of the advantages of the similarity approach may be that the complete set of model parameters is transposed from a donor basin.

In this study, a similarity approach was used for the parameter estimation of the interior gauges based on transposing the complete set of parameters from the parent basin to the interior basin. This verification strategy aims to obtain results which are indicative of expected performance at ungauged locations, under the conditions that model calibration may be carried out at larger spatial scales and that computed parameters may be transposed at smaller spatial scales.

Model parameter and model soil moisture status transposition

With this strategy, FFG values are obtained at interior sites based on transposing both model parameters and soil moisture status from the parent basin. This implies that the model is run based on input data (precipitation and temperature) for the parent basin. This methodology has obvious advantages in terms of operational implementation, by reducing computational efforts to obtain FFG at several interior sites. The model is run only at the level of the parent basin, and FFG computations are carried out for the specific interior sites. On the other hand, the quality of the model-based soil moisture status estimates obtained in this way may be altered. Biases in rainfall and temperature accumulate over weeks and months and soil moisture status are not as accurate as those obtained by running the model over the specific interior basins.

Figure 4-3 shows one year of simulation results at the outlet for the Cordevole basin at Vizza. Figure 4-3(a) shows simulation results with model parameter transposition from Cordevole at Saviner, whereas Figure 4-3(c) shows simulation results with model parameter and soil moisture status transposed from Cordevole at Saviner. Figure 4-3(b) and Figure 4-3(d) report simulation residuals in the two cases, respectively. These figures show that for this basin the two approaches yield hydrologically acceptable representations of the watershed behavior. At this scale, the two hydrographs appear visually similar. Only small differences can be seen, e.g. model with parameter transposition is biased low during the autumn floods (5900-6500), whereas model with parameter and soil moisture status is biased high during the same period. Figure 4-3(e) shows relative soil moisture content of the PDM storage obtained from model parameter transposition at Vizza and from model simulation at Saviner. This figure show clearly that there is a large difference between the two soil moisture statuses during the period from October (6500), when snow accumulation starts on the basin, to late March (1800) when snowmelt begins. This difference is due to the different impact that solid precipitation has on the hydrological behavior. For Vizza, almost all precipitation after October fall in solid phase, providing negligible input to the soil moisture store. On the contrary, on the lower basin closed at Saviner most of the precipitation falls in liquid form and feeds the PDM storage.

However, this bias has apparently a negligible impact on the simulation of the summer and fall floods, since the hydrological status of the two basins is reset during snowmelt. A smaller bias can be identified during the summer period, this being explained by the different precipitation and evaporation accumulations on the two basins.

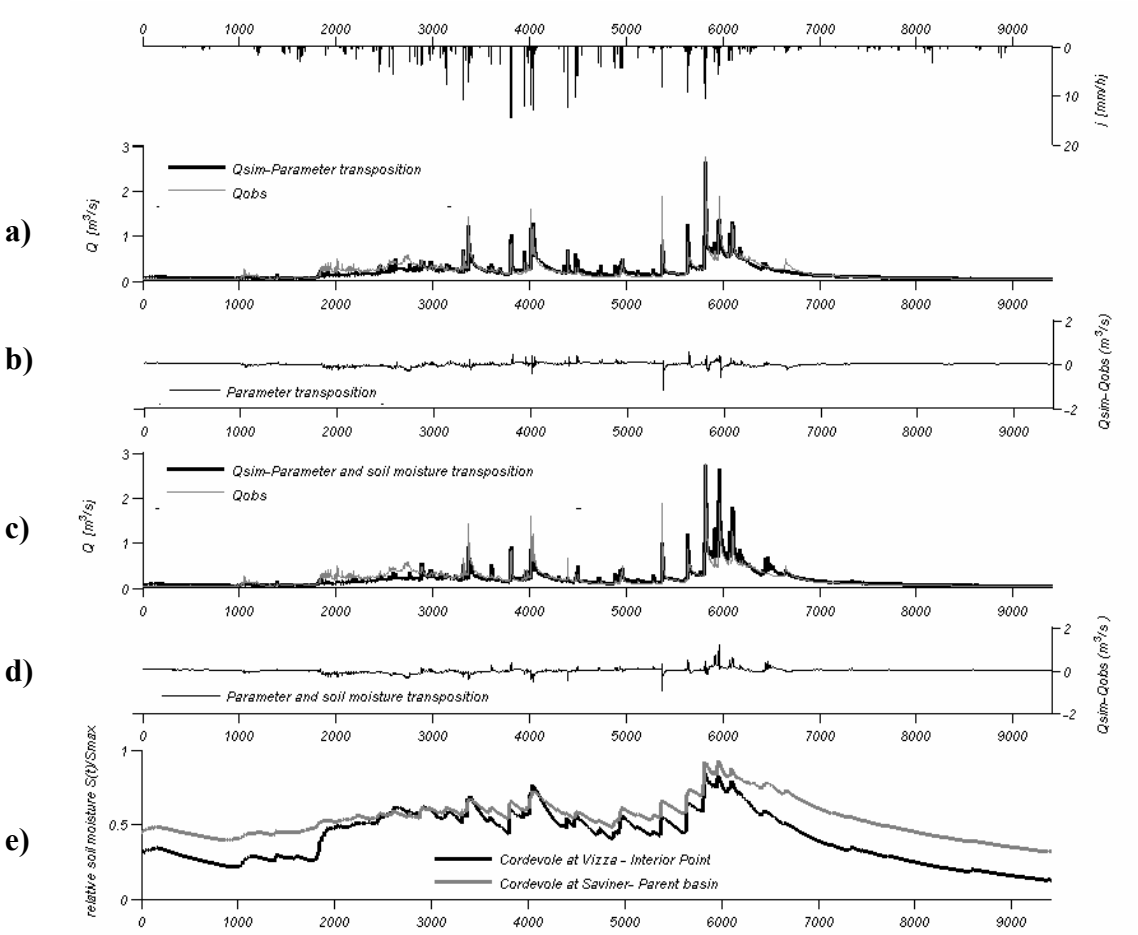

Figure 4-3a-e. One year (01.01.1993-31.12.1993) of hourly results at the outlet for the Cordevole river at Vizza (a) simulation results with model parameter transposition from Cordevole at Saviner; (b) simulation residuals, (c) simulation results with model parameter and soil moisture transposition from Cordevole at Saviner; (d) simulation residuals (e) relative soil moisture content of the PDM storage obtained from model parameter transposition at Vizza and from model simulation at Saviner.

4.4.2 FFG assessment

Five rainfall durations are considered for computation of the FFG: one, three, six, twelve and twenty four hours. The model is run continuously in time, and five values of FFG are computed each day (at 12:00) for each considered basin. Selection of the time during the day when FFG is computed has been shown to have negligible impact on final results. For the considered day, the FFG values are compared with the maximum estimated areal precipitation over the corresponding five durations. The technique predicts the exceedance of the threshold flooding (i.e.,a flash flood warning would be issued) when estimated precipitation exceeds FFG for at least one precipitation duration.

Assessment of the quality of flash flood forecasts based on FFG estimates is obtained by using contingency tables. Contingency tables are highly flexible methods that can be used to estimate the quality of a deterministic forecast system (Mason and Graham, 1999 [26]) and, in their simplest form, indicate its ability to anticipate correctly the occurrence or non occurrence of predefined events. A four-cell contingency table can be constructed which depicts the relationship between the forecasts and the events. Consider a set of forecasts that can have only two alternatives (e.g., yes, no) (Table 4-5). Let:

- X denote the number of positive forecasts that correspond to an occurrence of the event (hits);
- Y denote the number of events that occurred in conjunction with a negative forecasts (missed events);
- Z denote the number of positive forecasts that were not accompanied by an event (false alarms);
- W denote the number of negative forecasts that did not have any associated events.

Table 4-5. Four-cell contingency table used in the study

	FORECASTS	
EVENTS	**YES**	**NO**
YES	*X*	*Y*
NO	*Z*	*W*

These statistics can be used to summarise the contingency table:

- the probability of detection (POD). It is the ratio of correctly forecasted events to the total number of events

$$POD = \frac{X}{X + Y} \tag{4.9}$$

the range of values for POD goes from 0 to 1, the latter value being desirable. A POD of one means that all occurrences of the event were correctly forecast.

- the false alarm rate (FAR). It is the ratio of the number of false alarms to the total number of predicted events:

$$FAR = \frac{Z}{X + Z} \tag{4.10}$$

The range of values for FAR goes from 0 to 1, the former value being desirable. A FAR of zero means that in the verification sample, no non-occurrences of the event were forecast to occur.

Neither POD or FAR can give a complete picture of forecasting success; it is therefore desirable to include a statistic depending on both POD and FAR. This is the critical success index (CSI) (Schaefer, 1990 [39]; Wilks, 1995 [41]). The CSI is the ratio of correctly forecasted events to the total number of event forecasts that were either made (X+Z) or needed (Y):

$$CSI = \frac{X}{Y + X + Z} = \frac{1}{POD^{-1} + (1 - FAR)^{-1} - 1} \tag{4.11}$$

For either a zero POD or a unit FAR, the value of CSI is uniquely equal to zero, since there are no hits. The range of values for CSI goes from 0 to 1, the latter value being desirable.

Results obtained from the threshold-based methodology are compared with corresponding results from two alternatives methodologies. With the first alternative, FFG is contrasted with the temporal-detailed hydrological model (*Model*, hereafter). This provides the study with an evaluation of the assumption of time-uniform rainfall implied by the FFG. Scores statistics are obtained by comparing streamflow predicted by the model with the observed events, for each day, in terms of exceedance of the flooding threshold.

With the second alternative, FFG is contrasted with use of a time-constant soil moisture status as an input to the threshold-based flash flood warning system. This alternative is representative of time-constant depth-durations precipitation thresholds (*Constant*, hereafter). These constant depth-duration precipitation values are derived by setting the values of the model soil moisture status to those corresponding to the annual average discharge value. Assessment of this procedure allows the study to evaluate the degradation of accuracy associated to the loss of information about the temporal variation of antecedent soil moisture status.

4.4.3 Threshold flooding conditions

In this study the FFG is computed based on two different threshold flooding conditions. The first one (called hereafter High Threshold – HT) is based on the bankfull flow, characterised by 2-year return time. Carpenter et al. (1999 [9]) suggest that a 2-year flood is a reasonable threshold to use for flood warnings given that the flood flow associated with damage or hazard is often a little higher than bankfull flow. Use of this definition led to identification of 55 flood events exceeding the basin-specific thresholds, over the whole archive of streamflow data. However, use of this definition may give rise to sampling problems for the basins characterised by short data record length, due to the small number of local flood events. Owing to this reason, we use also a Low Threshold (LT), characterised by a return time around 0.5 year, corresponding to 223 flood events exceeding the threshold.

The assessment strategy comprises therefore three different procedures for model implementation, three different procedures for FFG assessment, and two threshold flooding conditions.

In the assessment procedure report below, system performances obtained on interior basins are compared with those obtained on parent basins. This implies that system performances on parent basins is comparable to the one that would have been attained on interior basins, in the case of model parameter calibration. Our results, which are not reported here for the sake of brevity, show that score statistics obtained on interior basins are within the range of those of parent basins, when model parameter calibration is carried out.

4.5 Results

4.5.1 Model application

Results on the three different methodologies used for model implementation are reported in Table 4-6 and Table 4-7 where the coefficient of efficiency (E_{NS}) and the relative bias (RB) are reported for the whole data period. For the parent basins, where the model has been calibrated, results concerning both the calibration and the independent validation period are also reported. Efficiency values for calibration and validation are relatively homogeneous, with the exception of Brenta at Borgo, where the validation period was considerably wetter than the calibration period. Efficiency is lower than average for the largest basin considered in the study (Loire at Bas-en-Basset, (1)) and for Brenta at Borgo (4). For the Loire basin, this suggests that there may be a mismatch between time and space scales of the hydrological model representation for this basin. In other words, the size of this basin and its inherent spatial variability are such that a lumped representation of precipitation and hydrological processes does not ensure a correct description of hourly streamflow temporal variability. In the case of the Brenta river, relatively poor model accuracy is due to the combined influence of lake storage, on one hand, and karstified aquifer, on the other.

Inspection of results reported for the interior gauges by using transposition of model parameters shows that efficiencies are generally degraded. Comparing overall efficiency computed on the whole simulation period shows that the coefficient of efficiency decreases by 23%, from 0.74 to 0.57. Ranking of efficiencies is not always respected when moving from parent to interior points: efficiency of model application at interior points with high (low) parent efficiency, is not always high (low). For instance, Rio Freddo at Valoje (10) is characterised by the lowest efficiency (0.20), whereas the parent (Posina at Stancari, (3)) has the highest efficiency (0.86). This may be due to the effect of the karstified aquifer, which influences Rio Freddo more significantly than its parent. The bias (both high and low) is also inflated when moving from parent to interior points.

Table 4-6. Model validation and calibration results. Parent basins

Parent basins	Calibration period		Validation period		Whole simulation period	
	E_{NS}	RB (%)	E_{NS}	RB (%)	E_{NS}	RB (%)
1	0.72	7	0.65	-4.25	0.66	2.33
2	0.72	5.35	0.75	0.78	0.73	3.42
3	0.76	1.1	0.77	2.2	0.86	2.31
4	0.71	2.64	0.54	8.74	0.64	5.02
5	0.80	1.36	0.78	-2.45	0.8	3.56

Table 4-7. Model validation results. Interior Points

Interior Points	parameter transposition		parameter and soil moisture transposition	
	E_{NS}	RB (%)	E_{NS}	RB (%)
6	0.64	-4.3	0.61	-13.2
7	0.46	-8.1	0.40	-15.2
8	0.69	1.4	0.75	-8.2
9	0.65	-6.2	0.68	-12.1
10	0.4	9.3	0.20	18.2
11	-	-	-	-

In spite of these observations, it is interesting to note that for three interior basins efficiency is larger than 0.6. This supports the view than transposing parameters from a donor to a similar basin has the potential to ensure reasonable performances in regionalisation efforts, even at the hourly time step used in this study.

Transposition of both model and soil moisture status values parameters is associated to a further slight degradation of efficiency (from 0.57 to 0.53) and to a large inflation of bias, with RB values up to 18.2%. This is clearly an effect of using biased soil moisture values in the model framework.

4.5.2 FFG assessment

Results concerning the threshold-based methodology are reported by using FAR and POD scores for each basin in Figure 4-4a-c, for i) parent basins, ii) interior points with model parameters transposition, and iii) interior points with model parameter and soil moisture status transposition, respectively. For each type of model application, the three different strategies of FFG assessment and the two flooding thresholds are considered. Corresponding CSI values are reported in Figure 4-5a-c, which report scatter plot of CSI values from FFG versus CSI values obtained from model application and use of constant threshold.

Parent basin: model parameter calibration

Results reported in Figure 4-4(a) with application of the Flash Flood Guidance shows that good results are generally obtained for the high flooding threshold. In this case, POD is always higher than 0.6, and FAR is less than 0.5 (with the exception of Brenta, with FAR equal to 0.72). For two basins (Posina at Stancari (3) and Ridanna (5)), POD is larger than 0.64 and FAR is less than 0.19. Performances are slightly degraded for some basins when using the low flooding threshold. This is the case for Posina (3) and Ridanna (5), with an

increase of FAR, and for Cordevole (2), with a decrease of POD. However, this does not occur for the Loire (1) and for Brenta at Borgo (4). Inspection of model simulations (not reported here) shows that this is an effect of modelling uncertainties of relatively small rain-on-snow events during the snowmelt season. As such, these effects have more impact on basins more affected by snow-related processes. The influence of these events is larger for the LT scenario than for the HT scenario.

Comparison of score statistics obtained by using the Flash Flood Guidance with those resulting from direct model application shows a slight degradation of system performance. This provides an indication that the use of time-uniform rainfall in the FFG context has a limited impact on forecast accuracy, at least for the parent basin. CSI values in Figure 4-5(a) for Model application range between 0.4 and 0.8, whereas corresponding values for FFG range between 0.22 and 0.7. It is interesting to note that the CSI ranking is very similar to the ranking of the same basins in terms of model efficiencies, with Posina (3) and Ridanna (5) ranking high and Loire (1) and Brenta (4) ranking low. This means that, as expected, high (low) efficiency in model application translates into high (low) CSI values.

System performances degrade considerably when a constant depth-duration precipitation threshold is used. In this case, POD is always less than 0.6, and FAR may be as high as one. CSI values are less than 0.4, with most of the basins comprised between 0 and 0.3. This shows, as expected, that information on antecedent soil moisture status is essential for flash flood forecasting in these humid to medium climate basins.

Interior points: model parameter transposition

Results reported for the interior points by using transposition of the model parameters from the parent basins show that the variability in performances (for instance, CSI) among the various basins increases considerably, with respect to parent basins. Whereas this may be due to differences between parent and interior basins, we note here that absence of local calibration may introduce random error and bias which translate into inflated variability in performances between basins. For two interior basins (Dunières (7) and Brenta at Levico (11)) CSI is rather low, with values less than 0.3 for both FFG and Model. One of these basins, Dunières, ranks low also in terms of model efficiency. The three basins which rank high in terms of model efficiency (Cordevole at Vizza (8), Posina at Bazzoni (9) and Gagne (6)) have also relatively high CSI. In general, CSI at interior points with high (low) parent CSI, is also high (low).

Basin size and climate have apparently no impact on CSI. Medium size basins, characterised by humid and medium climate, may exhibit high (Gagne (6) and Posina at Bazzoni (9)) and low (Brenta at Levico (11) and Dunières (7)) CSI values. A small size basin like Cordevole at Vizza (8) range in between these two extremes.

For interior points, results obtained from FFG are generally comparable with those obtained the model, as already observed for parent basins. However, one exception can be noted: Cordevole at Vizza (8). This interior points have the smallest basin area compared to the other basins. Since small spatial scale implies reduced response times, this means

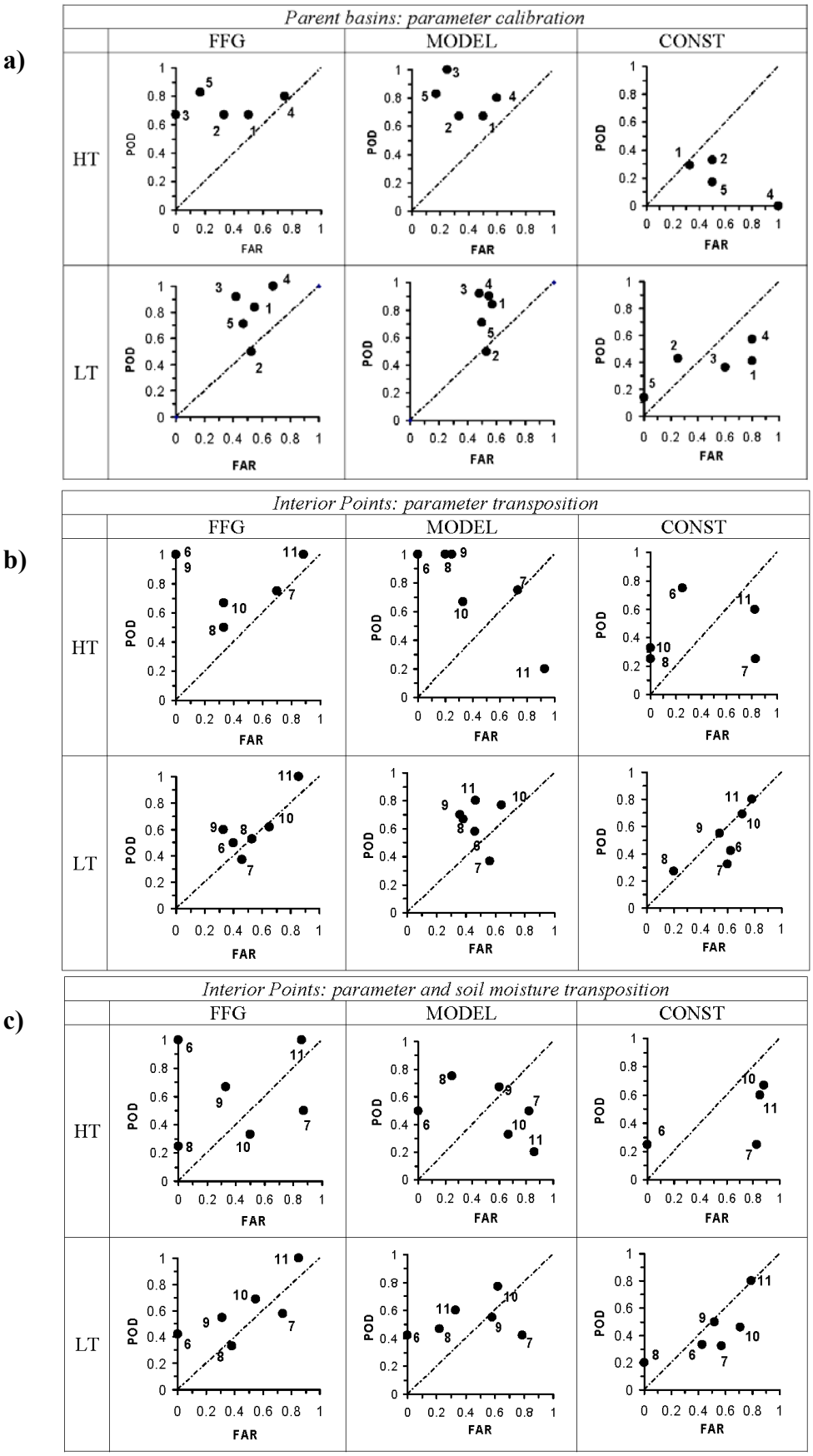

Figure 4-4a-c. Evaluation of the threshold-based technique for: a) parent basin with model calibration; b) interior basins with model parameter transposition; c) interior basins with both model parameter ans soil moisture status transposition. POD and FAR scores are plotted.

a)

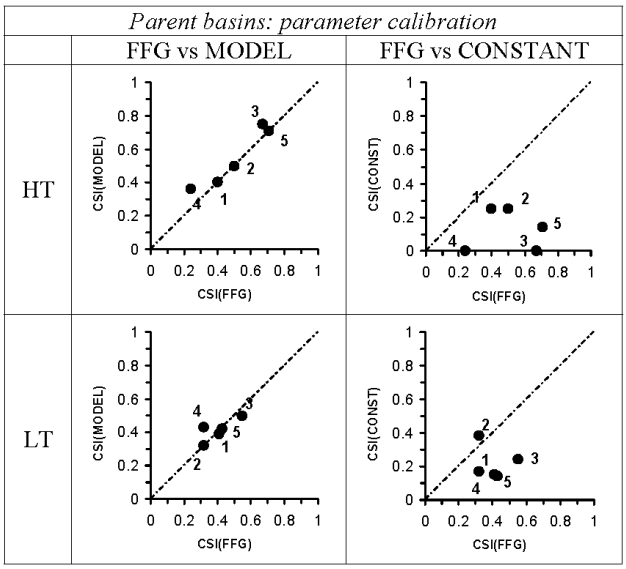

b)

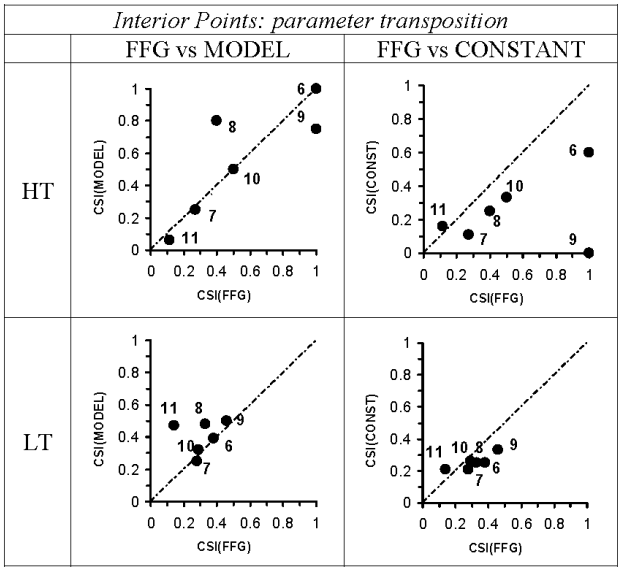

c)

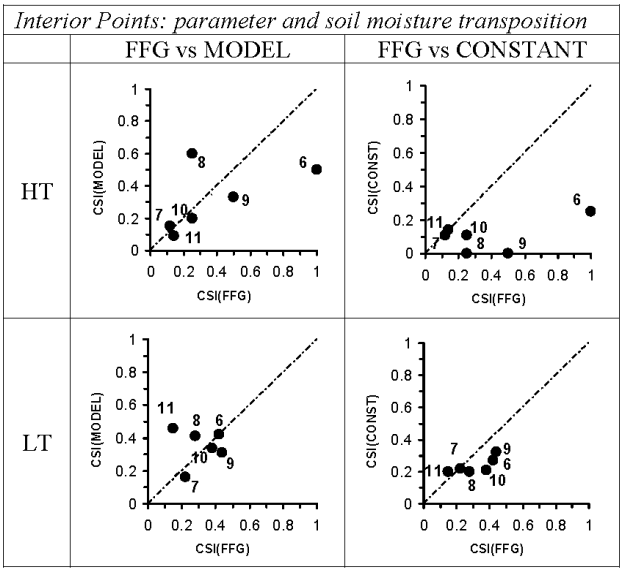

Figure 4-5a-c. Evaluation of the threshold-based technique for: a) parent basin with model calibration; b) interior basins with model parameter transposition; c) interior basins with both model parameter ans soil moisture status transposition. CSI scores are plotted.

that safe implementation of the FFG concept, as described in this study, may be limited by scale considerations, at least with comparison to model application.

As observed for parent basins, CSI degrades markedly when using a constant depth-duration precipitation threshold.

Interior points: model parameter and soil moisture status transposition

Use of soil moisture status transposition from parent basins (added to use of parameter transposition) produces a remarkable deterioration of system performance with respect to parameter transposition, as can be noted in the CSI plots. This is due to the biased character of these estimates, which are obtained by using estimates of precipitation and temperature from the parent basins.

Even in this case, it is observed that CSI degrades markedly when using a constant depth-duration precipitation threshold. This suggests that even a poor estimate of temporal variability of soil moisture, as the one derived from the parent basins, may improve markedly above the condition of no-information on antecedent soil moisture status.

Overall score statistics

Analysis of results reported in the previous sections show that score values obtained for the high flooding threshold exhibit always more dispersion than corresponding scores obtained for the low threshold. This is clearly an effect of the sampling problem which arise in these computations. Use of a high flooding threshold generally results in the analysis of a small sample of events which may prevent reliable characterization of the system performance. Lowering the threshold incorporates more events into the analysis, hence mitigating the sampling problem. However, this choice exposes one to the risk of including small flood events which are not representative of the dynamics under study. To increase reliability of high threshold statistics, we analyse overall score statistics computed on all the considered basins. Overall score statistics are computed based on one overall contingency table generated from all basins considered in the study. The overall score statistics are reported in Figure 4-6a-c and Figure 4-7a-c, for POD/FAR and CSI, respectively.

For parent basins and the high threshold, FFG is characterised by a POD of 0.76 with FAR of 0.48. In this case, CSI is equal to 0.43. For interior basins and high threshold, with parameters transposed by parent basins, POD increases to 0.85, but at the expenses of increasing FAR to 0.68. The overall CSI is equal to 0.28, in this case. This shows that the deterioration of performances following application of FFG to ungauged basins (with parameter transposition) is not negligible, and amounts to 35% (assuming that overall system performances on parent basins is comparable to the one that would have been attained on interior basins, in the case of model parameter calibration).

For interior basins, with parameters and soil moisture status transposed by parent basins, POD reduces to 0.64, while FAR increases to 0.73. The overall CSI is equal to 0.22 in this case and shows a decrease of 21% with respect to the case of parameter transposition.

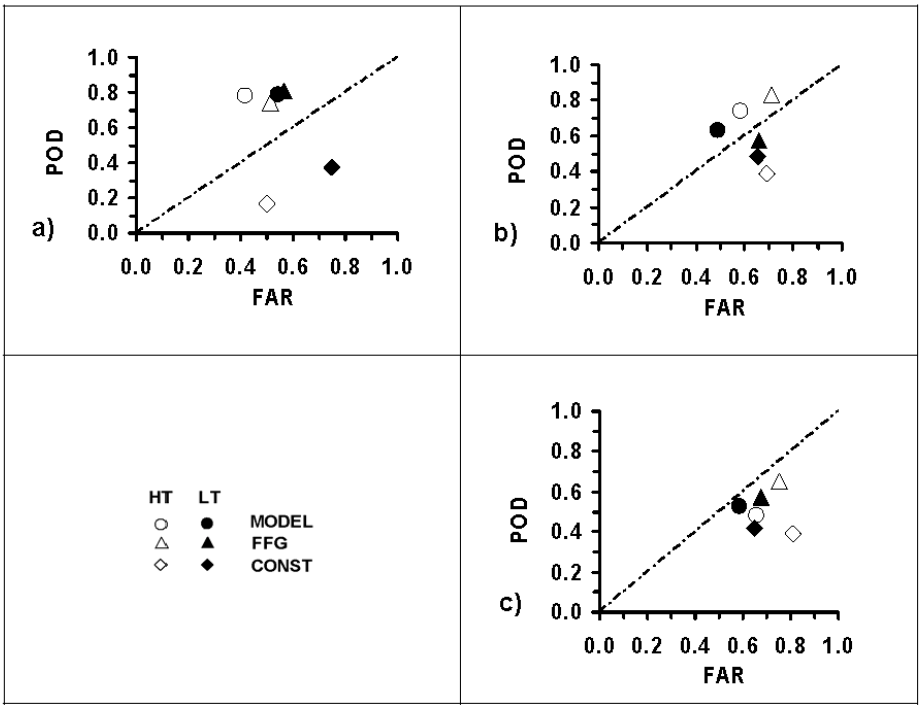

Figure 4-6a-c. Overall assessment of the threshold-based technique for: a) parent basin with model calibration; b) interior basins with model parameter transposition; c) interior basins with both model parameter and soil moisture status transposition. POD and FAR scores are plotted.

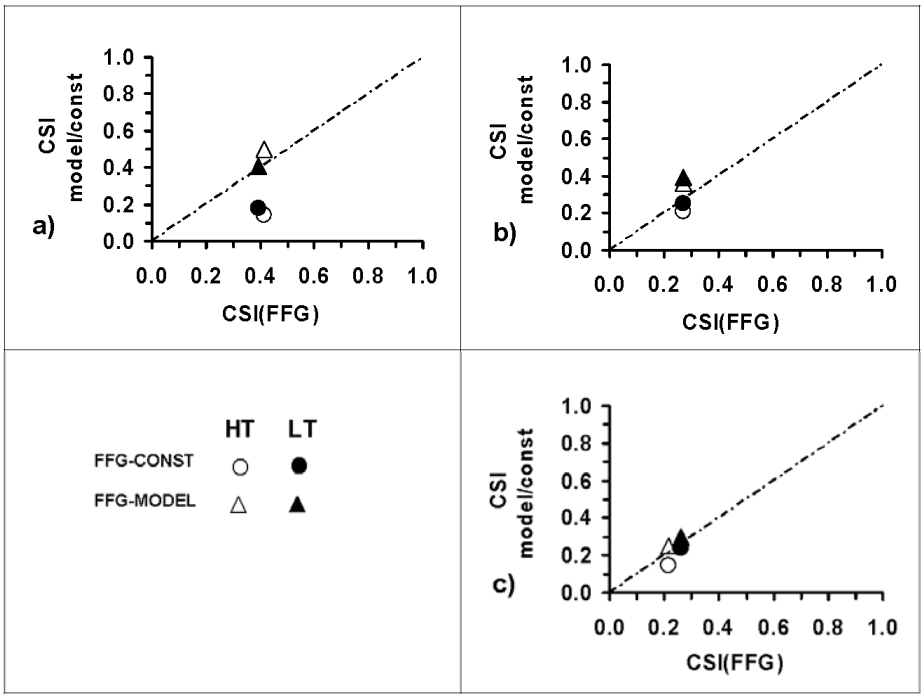

Figure 4-7a-c. Overall assessment of the threshold-based technique for: a) parent basin with model calibration; b) interior basins with model parameter transposition; c) interior basins with both model parameter and soil moisture status transposition. CSI scores are plotted.

Differences between FFG and direct model application are rather modest, and decrease with decreasing the accuracy of model application. The percent difference amounts to 18% for the parent basins, to 15% for interior basins with parameter transposition, and to 12% for interior basins with parameter and soil moisture status

transposition. This is not unexpected, showing that the impact on system performances due to the use of time-uniform precipitations reduces when other sources of uncertainties, related to lack of calibration and biases in the soil moisture estimations, become more significant.

Performance differences between FFG and use of constant depth-duration precipitation threshold are very high for the parent basins and decrease with decreasing the model accuracy. The percent difference amounts to 53% for the parent basins, to 25% for interior basins with parameter transposition, and to 19% for interior basins with parameter and soil moisture status transposition.

It is noted that differences between results obtained for the high and the low threshold are relatively low for the case of parent basins and for interior basins with parameter transpositions. These differences become comparable to those which arise among the various procedures for the case of model parameter and soil moisture status transposition.

4.6 Conclusions and future works

A threshold-based flash flood warning approach has been developed and tested on a wide range of climatic and physiographic European conditions, and by focusing on ungauged basins. The system is derived from the Flash Flood Guidance approach. The FFG is the depth of rain of a given duration, taken as uniform in space and time on a certain basin, necessary to cause minor flooding at the outlet of the considered basin. This rainfall depth, which is computed based on a lumped hydrological model, is compared to either real time-observed or forecasted rainfall of the same duration and on the same basin. If the nowcasted or forecasted rainfall depth is greater than the FFG, then flooding in the basin is considered likely.

The study provides an assessment of this technique based on operational quality data from eleven basins (six nested included in five larger parent basins) located in two European regions: north-eastern Italy and central France. The model used in this study is a semi-distributed conceptual rainfall-runoff model, following the structure of the PDM (Probability Distributed Moisture) model. System performances are evaluated by means of categorical statistics, such as the Critical Success Index (CSI).

Four questions posed in the Introduction were investigated to help understand the potential limitations and benefits of the FFG approach and guide further research and development. The experiments yielded the following answers:

1. Comparison of score statistics obtained by using the Flash Flood Guidance with those resulting from direct model application shows a slight degradation of system performance. Differences between FFG and direct model application are rather modest, and decrease with decreasing the accuracy of model application. The percent difference amounts to 18% for the parent basins, to 15% for interior basins with parameter transposition, and to 12% for interior basins with parameter and soil moisture status transposition. This is not unexpected, showing that the impact on

system performances due to the use of time-uniform precipitations reduces when other sources of uncertainties, related to lack of calibration and biases in the soil moisture estimations, become more significant.

2. Results show that overall CSI is equal to 0.43 for the parent basins, where the hydrological model has been calibrated. CSI reduces to 0.28 for the interior basins, when model parameters are transposed from parent basins. This shows that the deterioration of performances following application of FFG to ungauged basins (with parameter transposition) is not negligible, and amounts to 35% (assuming that overall system performances on parent basins is comparable to the one that would have been attained on interior basins, in the case of model parameter calibration).

3. For interior basins, with parameters and soil moisture status transposed by parent basins, CSI reduces to 0.22 and shows a decrease of 21% with respect to the case of parameter transposition.

4. Performance differences between FFG and use of constant depth-duration precipitation threshold are very high for the parent basins and decrease with decreasing the model accuracy. The percent difference amounts to 53% for the parent basins, to 25% for interior basins with parameter transposition, and to 19% for interior basins with parameter and soil moisture status transposition. This suggests that even a poor estimate of temporal variability of soil moisture, as the one derived from the parent basins, may improve markedly above the condition of no-information on antecedent soil moisture status.

These results show clearly that the performance of the FFG system hinges on the accurate representation of the initial soil moisture conditions. This shows that system improvements could be expected by additional work on real-time updating of model status. A natural choice would be to adjust the basin soil moisture state by making use of runoff data in a real time mode. The rationale of this is that runoff is usually an excellent indicator of the basin soil moisture state. An updating method widely used is the Kalman Filter which consists of weighting measurements and simulation, the weight (or Kalman gain) being a function of the measurement error and the model error (Da Ros and Borga, 1997b [14]). Additional work should focus on the value of real-time updating for ungauged basins (by transposing updated soil moisture status to interior points) and at various spatial scales.

Further work should also focus on use of simpler modelling concepts that makes more proper use of constant precipitation depth thresholds (Martina et al., 2006 [25]) and which incorporate knowledge about flash flood related damages. Along this line, a research effort is now underway to evaluate the effectiveness of using model-based constant precipitation depth thresholds (variable on a monthly basis) which are based on monthly averaged soil moisture status and which incorporate a Bayesian utility function minimization.

4.7 References

[1] Beven, K. J., Wood, E. F., 1983. Catchment geomorphology and the dynamics of runoff contributing area. J. Hydrology, 65, 139-158.

[2] Bloeschl, G., Sivapalan, M., 1995. Scale issues in hydrological modelling – a review. Hydrol. Proc., 9, 251–290, 1995.

[3] Bloeschl, G., 2005. Rainfall-runoff modelling of ungauged basins. Article 133 in: Encyclopedia of Hydrological Sciences, M. G. Anderson (Managing Editor), J. Wiley & Sons, Chichester, pp. 2061-2080.

[4] Blöschl, G., Reszler, C., Komma, J., 2007. A spatially distributed flash flood forecasting model. Submitted to Environmental Modelling & Software.

[5] Borga, M., 2006. HYDRATE Project: Description of work. University of Padova, 256 pp.

[6] Borga, M., Vizzaccaro, A., 1997. On the interpolation of hydrologic variables: formal equivalence of multiquadratic surface fitting and kriging. Journal of Hydrology., 195, 160-171.

[7] Borga, M., Anagnostou, E.N., Frank, E., 2000. On the use of real-time radar rainfall estimates for flood prediction in mountainous basins. Journal of Geophysical Research., 105, D2, 2269-2280.

[8] Budyko, M. I., 1974. Climate and life. Academic Press, New York.

[9] Carpenter, T.M., Sperfslage, J.A., Georgakakos, K.P., Sweeney, T., Fread, D.L., 1999. National threshold runoff estimation utilizing GIS in support of operational flash flood warning systems. Journal of Hydrology, 224, 21–44.

[10] Cazorzi, F., Dalla Fontana, G., 1996. Snowmelt modelling by combining air temperature and a distributed radiation index. Journal of Hydrology, 181, 169–187.

[11] Collier, C., 2007. Flash flood forecasting : What are the limits of predictability? Quarterly Journal of the Royal Meteorological Society. Q. J. R. Meteorol. Soc., vol. 133, no 622A, pp. 3-23 .

[12] Creutin, J.D., Borga, M., 2003. Radar hydrology modifies the monitoring of flash flood hazard. Hydrological Processes, 17, 7, 1453-1456, doi 10.10002/hyp.5122.

[13] Da Ros, D., Borga, M., 1997a. Use of digital elevation model data for the derivation of the geomorphologic instantaneous unit hydrograph. Hydrological Processes, 11, 13-33, 1997.

[14] Da Ros, D., Borga, M., 1997b. Adaptive use of a conceptual model for real time flood forecasting. Nordic Hydrology, 28(3), 169-188, 1997.

[15] Degli Esposti, S., 2005. Flood forecasting and catchment hydrology in hilly and mountainous regions. PhD dissertation. Department of Land and Agroforest Environments, University of Padova.

[16] Dinku, T., Anagnostou, E.N., Borga, M., 2002. Improving radar-based estimation of rainfall over complex terrain. Journal of Applied Meteorology, 41(12), 1163–1178.

[17] Duan, Q., Sorooshian, S., Gupta, V.K., 1992. Effective and efficient global optimization for conceptual rainfall-runoff models. Water Resources Research, 28(4), 265–284.

[18] Georgakakos, K. P., 1992. Advances in forecasting flash floods. In Proceedings of the CCNAA-AIT Joint Seminar on Prediction and Damage Mitigation of Meteorologically Induced Natural Disasters, 21-24 May 1992, National Taiwan University, Taipei, Taiwan, 280-293.

[19] Georgakakos, K.P., 2004. Mitigating adverse hydrological impacts of storms on a global scale with high resolution, global flash flood guidance, Abstracts Volume of International Conference on Storms/AMOS-MSNZ National Conference, 5–9 July. Autralian Meteorological Society, Brisbane, Australia pp. 23 – 30.

[20] Georgakakos, K. P., 2006. Analytical results for operational flash flood guidance. Journal of Hydrology, 317 (1-2), 81-103, doi:10.1016/j.jhydrol.2005.05.009.

[21] Hargreaves, G. H., Samani, Z. A., 1982. Estimating potential evapotranspiration. J. Irrig. Drain. Div., 108, 225–230.

[22] Hossain, F., Anagnostou, E.N., Dinku, T., Borga, M., 2004. Hydrological model sensitivity to parameter and radar rainfall estimation uncertainty. Hydrological Processes, 18-17, 3277-3291, 10.1002/hyp.5659.

[23] Klemes, V., 1986. Operational testing of hydrological simulation models. Hydrol. Sci. J., 31, 13-24.

[24] Kokkonen, T.S., Jakemann, A.J., Young, P.C., Koivusalo, H.J., 2003. Predicting aily flows in ungauged basins: model regionalisation from basin descriptors at the Coweeta Hydrologica Laboratory, North Carolina. Hydrol. Processes, 17, 2219-2238, DOI:10.1002/hyp.1329,2003.

[25] Martina, M.L.V., Todini, E., Libralon, A., 2006. A Bayesian decision approach to rainfall thresholds based flood warning. Hydrol. Earth Syst. Sci., 10, 413–426.

[26] Mason, S. J., Graham, N. E., 1999. Conditional Probabilities, Relative Operating Characteristics and Relative Operating Levels, Weat. Forecast., 14, 713–725, 1999.

[27] Merz, R., Blöschl, G., 2004. Regionalisation of basin model parameters, Journal of Hydrology, 287, 95-123, DOI:10.1016/j.jhydrol.2003.09.028.

[28] Mogil, H. M., Monro, J. C., Groper, H. S., 1978. NWS's flash flood warning and disaster preparedness programs. Bulletin of the American Meteorological Society, 59, 690-699.

[29] Montgomery, D.R., Foufoula-Georgiou, E., 1993. Channel network source representation using digital elevation models. Water Resources Research, 29(12), 3925–3934.

[30] Moore, R.J., 1985. The probability-distributed principle and runoff production at point and basin scales. Hydrol. Sci. J., 30, 273-297.

[31] Moore, R.J., Bell, V.A., 2002. Incorporation of grounddwater losses and well data in rainfall-runoff models illustrated using PDM. Hydrology and hearth System Sciences, 6 (1), 25-38, 2002.

[32] Moore, R.J., Cole, S.J., Bell, V.A. and Jones, D.A., 2006. Issues in flood forecasting: ungauged basins, extreme floods and uncertainty. In: K.N.N. Tchiguirinskaia andT.P. Hubert (Editors), 8th Kovacs Colloquium. Frontiers in flood research IAHS, Paris, pp. 103-122.

[33] Nash, J.E., Sutcliffe, J.E., 1970. River flow forecasting through conceptual models, Part I: A discussion of principles. Journal of Hydrology, 10, 282–290.

[34] Nelder, J.A., Mead, R., 1965. A simplex method for function minimization. Computer Journal, 7(4), 308–313.

[35] Norbiato, D., Borga, M., Degli Esposti, E., Gaume, E., Anquetin, S., 2007c. Flash flood warning based on rainfall depth-duration thresholds and soil moisture conditions: An assessment under European conditions. Journal of Hydrology. Submitted article.

[36] Ntelekos, A. A., Krajewski, W. F., Georgakakos, K. P,. 2006. On the uncertainties of flash flood guidance. Towards probabilistic forecasting of flash floods. Journal of Hydrometeorology, 896–915.

[37] Parajka, J., Merz, R., Blöschl, G., 2005. A comparison of regionalisation methods for basin model parameters. Hydrology and Earth System Sciences, 9, 157-171.

[38] Reed, S., Schaake, J., Zhang, Z., 2007. A distributed hydrologic model and threshold frequency-based method for flash flood forecasting at ungauged locations. Journal of Hydrology, 337 (3), p.402-420.

[39] Schaefer, J.T., 1990. The Critical Success Index as an indicator of warning skill. Weather and Forecasting, 5, 570-575.

[40] Sperfslage, J. A., Georgakakos, K. P., Carpenter, T. M., Shamir, E., Graham, N. E., Alfaro, R., Soriano, L., 2004. Central America Flash Flood Guidance (CAFFG) User's Guide. HRC Limited Distribution Report No. 21. Hydrologic Research Center, San Diego, CA, 82 pp.

[41] Wilks, D. S., 1995. Statistical Methods in the Atmospheric Sciences, An Introduction. Academic Press, New York, 238-250.

[42] Wolock, D. M., 1993. Simulating the variable-source-area concept of stream-flow generation with the watershed model TOPMODEL. Water Resour. Invest. Rep., U.S. Geol. Surv., 93-4124.

5 Controls on event runoff coefficients in the eastern Italian Alps[4]

5.1 Introduction

Predicting flood response in ungauged basins is emerging as one of the major issues in the hydrological science (Sivapalan et al., 2003 [27]). Predictions are particularly difficult to make in alpine regions where data are sparse and the spatial variability of both precipitation and physical controls on runoff generation is enormous. The event runoff coefficient, defined as the portion of rainfall that becomes direct runoff during an event (Blume et al., 2007 [2]), is a key concept in hydrology and an important diagnostic variable on basin response, particularly if a range of basins and a range of events are to be compared by a single indicator (Merz et al., 2006 [16]). Analysis of event runoff coefficient may provide essential insight on how different landscape 'filter' rainfall to generate runoff and to explain the observed differences with basin characteristics (Blume et al., 2007 [2]). Quantifying process control on space and time variability of runoff coefficient may therefore contribute to isolate flood generating mechanisms both in time (summer vs winter, rainfall vs. snowmelt, etc), and also in space (different climate, geology, soils, vegetation, etc.) (Fiorentino and Jacobellis, 2001 [10]).

There exists a substantial body of work on controls of runoff coefficient variability at the regional scale. Scale dependency of runoff coefficient to plot and basin area has been examined from Wainwright and Parsons (2002 [31]) and Cerdan et al. (2004 [7]), who both identified a significant decrease in the runoff coefficient as area increases. Furthermore, Cerdan et al.(2004 [7]) was able to show that at the scale of 10 km^2 the percentage of arable land is a driving factor of runoff response. Gottschalk and Weingartner (1998 [11]) examined runoff coefficients of 192 flood events in 17 Swiss basins which they used in a derived flood frequency model. They fitted a Beta function to the distribution of runoff coefficients in each basin and interpreted the parameters for different hydrologic regions in Switzerland. They concluded that the differences in runoff coefficients can be explained by topographic characteristics such as altitude and slope and to some degree by stream network density and geology. This approach was substantially extended by Merz et al. (2006 [16]), who analysed a total of about 50000 events in 337 Austrian basins with basin areas ranging from 80 to 10000 km^2 over the period 1981-2000. They found that, in the type of climate and at the scale of the basins examined in their work, the main controls on event runoff coefficients were the climate and the runoff regime through the seasonal basin water balance and hence antecedent soil moisture conditions in addition to event characteristics. Basin characteristics such as soils and land use affected runoff coefficients to a lesser degree.

The aim of this study is to analyse the process controls of runoff coefficients using data from 14 basins, located in the eastern Italian Alps, with area ranging from 7 to 600

[4] The study described in this chapter will be proposed in Norbiato et al. (2008a [22])

km^2. A total of 535 events have been back calculated from hourly runoff data, hourly precipitation data and model-based estimates of snowmelt over the period 1989-2004. A continuous soil moisture accounting model was applied to each basin to derive initial soil moisture conditions prior to each event. Basins were classified according to the permeability characteristics of the lithological units, as inferred from geological surveys, and according to the soil moisture capacity, inferred from analysis of the flow duration curve. The statistical characteristics of the distribution functions of the runoff coefficients as well as the effect of event rainfall characteristics, climate, geology, land use and antecedent soil moisture conditions on the runoff coefficients are examined.

5.2 Study basins: morphology, climate, land use and geology

The location of the 14 basins used in this study is shown in Figure 5-1. Some of these basins (13, 14, 11 e 12) have just been analysed in Chapter 4 to test the FFG methodology. Table 5-1 provides more detailed basin information. For the sake of clarity, basins are sequentially numbered as indicated in Table 5-1. Basin drainage area is comprised between 7.3 km^2 and 608.4 km^2. The topography is rather complex with altitudes ranging from 388 m a.s.l. (lowest altitude of Posina) to 3700 m a.s.l. (highest elevation of Aurino at Cadipietra). Measured runoff represents well the natural runoff variability, since management activities, such as artificial reservoirs and diversions, alter in a negligible way the river regime. Five basins are included in four larger parent basins (Basins 1 and 3 are included in Basin 2; Basins 5, 9 and 14 are included in Basins 4, 10 and 13, respectively).

Basin number	Station name
1	Aurino at Cadipietra
2	Aurino at San Giorgio
3	Riva at Seghe
4	Gadera at Mantana
5	San Vigilio at Longega
6	Casies at Colle
7	Rienza at Monguelfo
8	Anterselva at Bagni
9	Plan at Plan
10	Passirio at Saltusio
11	Ridanna at Vipiteno
12	Posina at Stancari
13	Cordevole at Saviner
14	Cordevole at Vizza

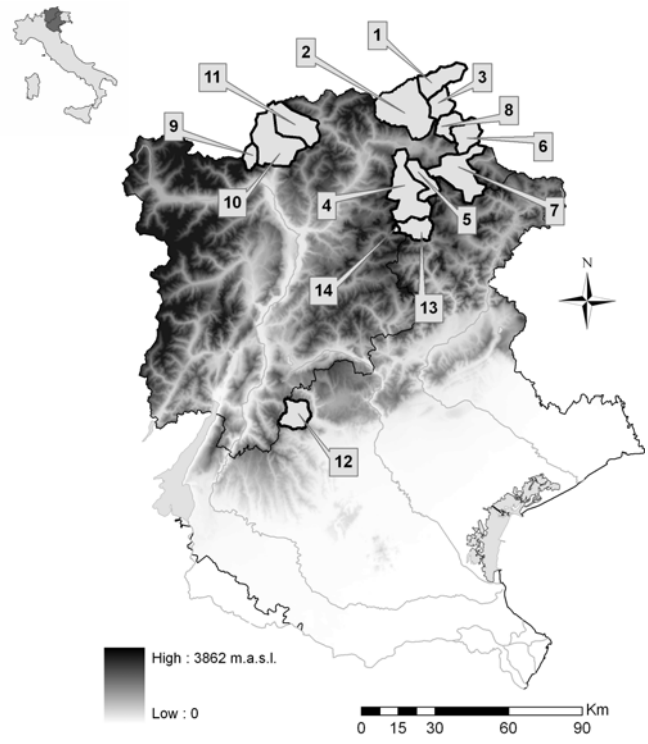

Figure 5-1. Study basins and their location in Italy

Table 5-1. Basins characteristics

Basin number	Station name	Area (km^2)	Elevation range (m a.s.l.)	Mean annual precipitation (mm)	Mean annual runoff (mm)	Annual runoff coefficient	Mean value of maximum annual flood (m^3/s)	Mean value of maximum annual flood / mean discharge
1	Aurino at Cadipietra	149.8	1035-3400	1520	1276	0.84	40.3	6.7
2	Aurino at San Giorgio	608.4	816-3400	1351	1033	0.76	136.4	6.6
3	Riva at Seghe	91.4	1520-3400	1659	1283	0.77	36.5	9.7
4	Gadera at Mantana	396.7	814-3200	963	623	0.65	62.0	7.9
5	San Vigilio at Longega	105.5	1010-3000	900	560	0.62	4.6	2.4
6	Casies at Colle	117.4	1196-2800	993	669	0.67	15.8	6.2
7	Rienza at Monguelfo	268.6	1096-3200	980	621	0.63	20.1	3.7
8	Anterselva at Bagni	82.4	1091-3200	1050	780	0.74	12.6	6.2
9	Plan at Plan	49.0	1575-3200	1520	1255	0.83	26.2	8.9
10	Passirio at Saltusio	342.4	442-3400	1580	1238	0.78	202.1	14.9
11	Ridanna at Vipiteno	210.2	940-3600	1375	1019	0.74	79.6	11.6
12	Posina at Stancari	116.0	388-2300	1708	1000	0.59	111.4	33.2
13	Cordevole at Saviner	109.0	1025-3200	1120	770	0.69	30.7	11.4
14	Cordevole at Vizza	7.3	1810-3200	1218	866	0.71	2.6	12.5

Examination of Table 5-1 shows that these basins exhibit significant variability in terms of hydrological response. A parameter which describes this variability is the ratio between the mean value of maximum annual flood and the annual average discharge.

Table 5-1 shows that basins with similar drainage area, such as Basin 5 (San Vigilio at Longega), Basin 12 (Posina at Stancari) and Basin 13 (Cordevole at Saviner) (with areas ranging from 105.5 to 116.0 km^2) are characterised by values of the ratio ranging over more than one order of magnitude (from 2.4 to 33.4). This variability implies that different processes are responsible for flood runoff generation across these basins. Qualitative information gathered by means of site visits was used to make educated guesses about the hydrological processes driving runoff generation during flood events. According to this information, for example, the response of the Posina basin is dominated by quick subsurface flow and surface runoff generated on saturated areas, whereas response of the San Vigilio basin is delayed and attenuated thanks to large groundwater storage.

Estimates of basin-averaged mean annual precipitation (MAP) amounts reported in Table 5-1 are obtained by using the Thiessen technique, with densities ranging from 1 station per 4 km^2 (Basin 14 – Cordevole at Vizza) to 1 station per 150 km^2 (Basin 1 –

Aurino at Cadipietra) and using corrections for snowfall catch deficit (Sevruk et al., 1998 [26]). Basin-avaraged mean annual precipitation ranges from 900 mm to 1708 mm. Precipitation is larger for the basin located in the forealpine regions (Basin 12) and for some of the basins most exposed to the *stau* effect (Basins 3 and 10). It is intermediate for the basins located in the Dolomite region exposed to humid and warm winds from the Adriatic sea (Basins 13 and 14) and for the other basins exposed to the *stau* effect (Basins 1, 2, 9 and 11). Precipitation is significantly lower in basins of Val Pusteria (Basins 4 to 8), due to the dual sheltering effect of the mountainous ranges to both the north and the south.

We applied the Budyko's climatic classifications scheme (Budyko, 1974 [5]) to display the climatic characteristics of these basins. This is achieved by presenting the specific response of each basin on the Budyko curve (Figure 5-2), which is a plot that expresses E/P, the ratio of average annual evapotranspiration (E) to average annual precipitation (P) as a function of EP/P, the ratio of average annual potential evapotranspiration (EP) to average annual precipitation (P). Actual evapotranspiration (E) for each basin was derived as the long-term difference between P and R (runoff) for the basins, whereas potential evapotranspiration was computed based on the Hargreaves method (Hargreaves and Samani, 1982 [12]). Figure 5-2 shows clearly that all the basins are characterised by a wet climate and that the ratio of evapotranspiration to precipitation is controlled generally by basin elevation. This control is reflected in the pattern of mean annual runoff coefficients, which range from 0.59 (Basin 12, Posina) to 0.84 (Basin 1, Aurino at Cadipietra).

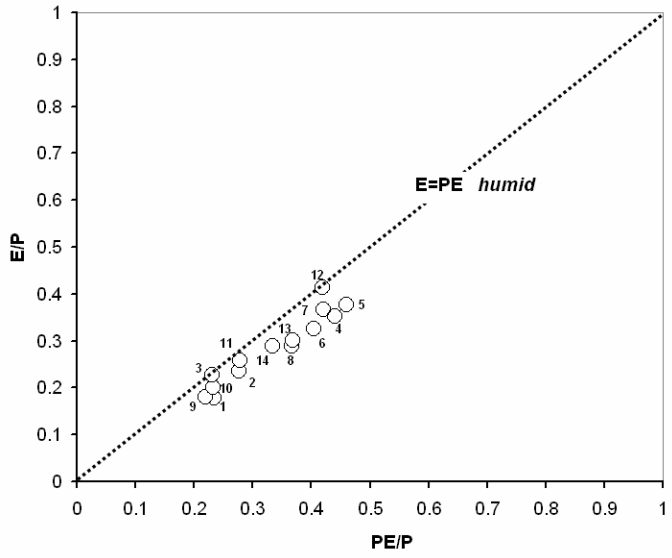

Figure 5-2. Plot of mass balance data from the study basins on the Budyko curve

Figure 5-3 shows the mean monthly values of liquid precipitation, solid precipitation and runoff related to their mean annual values. All the alpine basins are characterised by peaks of precipitation and runoff in the summer months. Basin 12 (Posina at Stancari) shows two maximum values of mean monthly rainfall, the most important in autumn and the minor one during spring. The significance of snowfall implies that both the seasonal

hydrological balance and the flood regime in these basins are influenced by snow accumulation and melt.

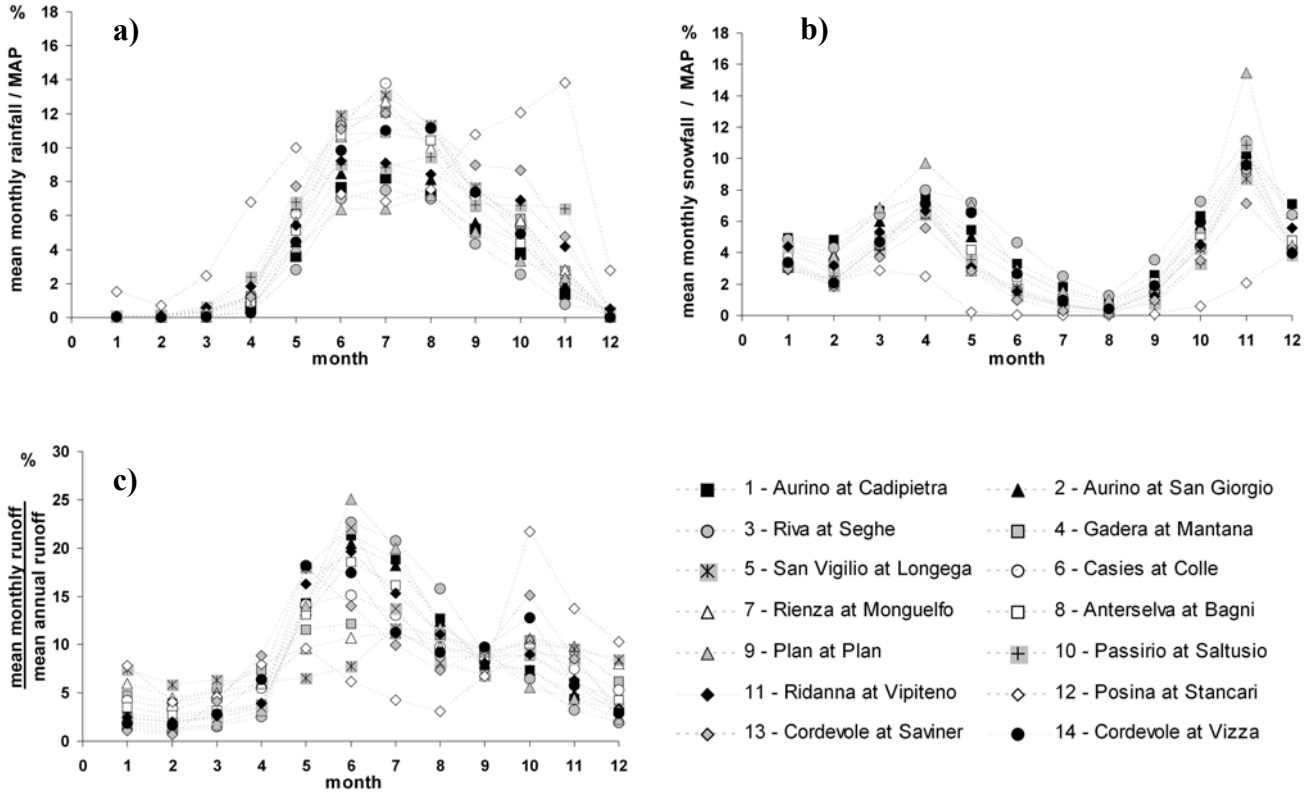

Figure 5-3. a) mean monthly rainfall over MAP; b) mean monthly snowfall over MAP; c) mean monthly runoff over mean annual runoff.

Grassland, sparsely vegeteated area (including outcrop rocks), coniferous and mixed forests are the most important type of land use in these basins (Table 5-2). Outcrop rocks cover a considerable portion of Basins 4 (Gadera at Mantana), 5 (San Vigilio at Longega) and 7 (Rienza at Monguelfo) and are strongly influenced by secondary permeability effects. The most significant glaciated area (6%) is located on the Basin 9 (Plan at Plan) while Basin 12 (Posina at Stancari) is characterised by a wide forested area (74%). Sparsely vegetated area dominates on Basin 3 (Riva at Seghe) (61%).

For the purposes of this study, the study basins were classified according to the permeability characters of the prevailing lithological units, using the 1:100,000 scale geologic map of Italy. Metamorphic and sedimentary rock units are prevailing across the study basins. Igneous rocks, mainly represented by dykes intruding sedimentary rocks and/or scanty levels of tonalites within metamorphic rocks, are relatively rare. The most common metamorphic rocks cropping out in the study basins are gneiss (in the varieties of orthogneiss and paragneiss, respectively), phyllites and micaschists. Calc-schists, prasinites and serpentinites are also found, although to a lesser extent. These rock types are characterized by a low to very low permeability. These units prevail on Basins 1, 2, 3, 6, and 8 to 11.

Table 5-2. Land use for the study basins

Basin number	Station name	Discontinuos urban fabric	Arable land	Grassland	Coniferous forest	Broad leaved and mixed forest	Glaciers	Sparsely vegetated areas
1	Aurino at Cadipietra	0%	0%	36%	22%	1%	3%	38%
2	Aurino at San Giorgio	0%	1%	30%	30%	3%	4%	32%
3	Riva at Seghe	0%	0%	26%	12%	1%	0%	61%
4	Gadera at Mantana	1%	0%	26%	41%	8%	0%	24%
5	San Vigilio at Longega	1%	0%	20%	34%	11%	0%	34%
6	Casies at Colle	0%	0%	37%	43%	0%	0%	20%
7	Rienza at Monguelfo	1%	0%	19%	51%	6%	0%	23%
8	Anterselva at Bagni	0%	0%	27%	40%	1%	0%	32%
9	Plan at Plan	0%	0%	41%	3%	0%	6%	50%
10	Passirio at Saltusio	0%	0%	43%	24%	3%	2%	28%
11	Ridanna at Vipiteno	0%	0%	44%	26%	3%	5%	22%
12	Posina at Stancari	0%	0%	22%	3%	71%	0%	4%
13	Cordevole at Saviner	0%	0%	43%	32%	10%	0%	15%
14	Cordevole at Vizza	0%	0%	66%	1%	0%	0%	33%

The sedimentary rocks prevail on Basins 13 and 14, and belong to the typical Permian-Triassic dolomite series. This includes a wide range of rock types: dolostones, bedded limestones, sandstones, conglomerates, pyroclastic products, sequences of carbonate-terrigenous deposits and evaporitic rocks. These units are characterized by a medium permeability. Sedimentary rocks found in Basin 12 are saccharoidal, stratified or massif dolostones with scanty strips of grey limestones with marly and clayey levels. When they are not subject to karst processes or fractured (which are present in a subbasin of this basin), these rock types show a low to medium permeability. Both metamorphic and carbonate rocks are present in Basins 4, 5 and 7, where significant karst processes are found, implying high permeability (Van de Griend et al., 1986 [30]).

Based on these analyses, a 'permeability index' has been derived for each basin. The index summarises in a qualitative ranking the permeability characteristics and ranges from 1 to 3, representing conditions of low, intermediate and high permeability, respectively (Table 5-3).

Table 5-3. Permeability index

Basin number	Station name	Permeability index
1	Aurino at Cadipietra	1 – Low permeability
2	Aurino at San Giorgio	1 – Low permeability
3	Riva at Seghe	1 – Low permeability
4	Gadera at Mantana	3 – High permeability
5	San Vigilio at Longega	3 – High permeability
6	Casies at Colle	2 – Intermediate permeability
7	Rienza at Monguelfo	3 – High permeability
8	Anterselva at Bagni	2 – Intermediate permeability
9	Plan at Plan	1 – Low permeability
10	Passirio at Saltusio	1 – Low permeability
11	Ridanna at Vipiteno	1 – Low permeability
12	Posina at Stancari	1 – Low permeability
13	Cordevole at Saviner	2 – Intermediate permeability
14	Cordevole at Vizza	2 – Intermediate permeability

5.3 Computation of event runoff coefficients

Runoff coefficients were computed over the period ranging from 1989 to 2004. The length of the hourly record of streamflow, precipitation and temperature available for each basin ranges from 10 to 15 years.

A combination of three different approaches was used to calculate runoff coefficients and initial basin soil moisture conditions. A continuous soil moisture accounting model was applied to each basin to trace the soil moisture conditions of basins in a continuous way and to estimate event water input to basins in forms of rainfall, snowfall and snowmelt. Observed runoff was then separated into baseflow and direct flow, and flood events were identified. At the scale of each flood event a simple event rainfall-runoff model was fitted to the direct hydrograph, following Merz et al. (2006 [16]). In this runoff model, the runoff coefficient appears explicitly as a model parameter and can hence be estimated by optimising an objective function. This procedure is less sensitive to the choice of the start and end points of the events than the usual ratio of volumes (Merz et al., 2006 [16]).

The baseflow separation method, the event separation method, the estimation of the runoff coefficient and the continuous soil moisture accounting model are described in the following sections.

5.3.1 The baseflow separation method

The baseflow separation is carried out by means of an automatic method which applies simple smoothing and separation rules to the total streamflow hydrograph (Institute of Hydrology, 1980 [13]; Nathan and McMahan, 1990 [21]). The basis of the technique may be described as follows. First the minima of 5-day nonoverlapping periods are found for the entire period of record. Next, this minima series is searched for values that are less than 1.11 times the two outer values; such central values are defined as turning points. The baseflow hydrograph is then constructed by simply connecting all the turning points.

Figure 5-4 shows the application of this technique to three different basins for the same period (26 June– 6 August 1997, characterised by several short-duration storms) to three different basins with similar drainage area (Basin 5, 13 and 12). Rainfall input in Basin 5 produces a slow increase in baseflow, until a certain threshold is reached. When this threshold is exceeded (with the storm of 28th of July), the basin generates direct runoff. This behaviour is clearly due to the large groundwater storage (largely karstified) characterising this basin. Production of direct runoff volumes is both more continuous and important for Basins 13 (Cordevole at Saviner) and 12 (Posina at Stancari). Figure 5-4 shows that the baseflow separation technique corresponds to what one would separate manually by visual inspection for three very different baseflow behaviours.

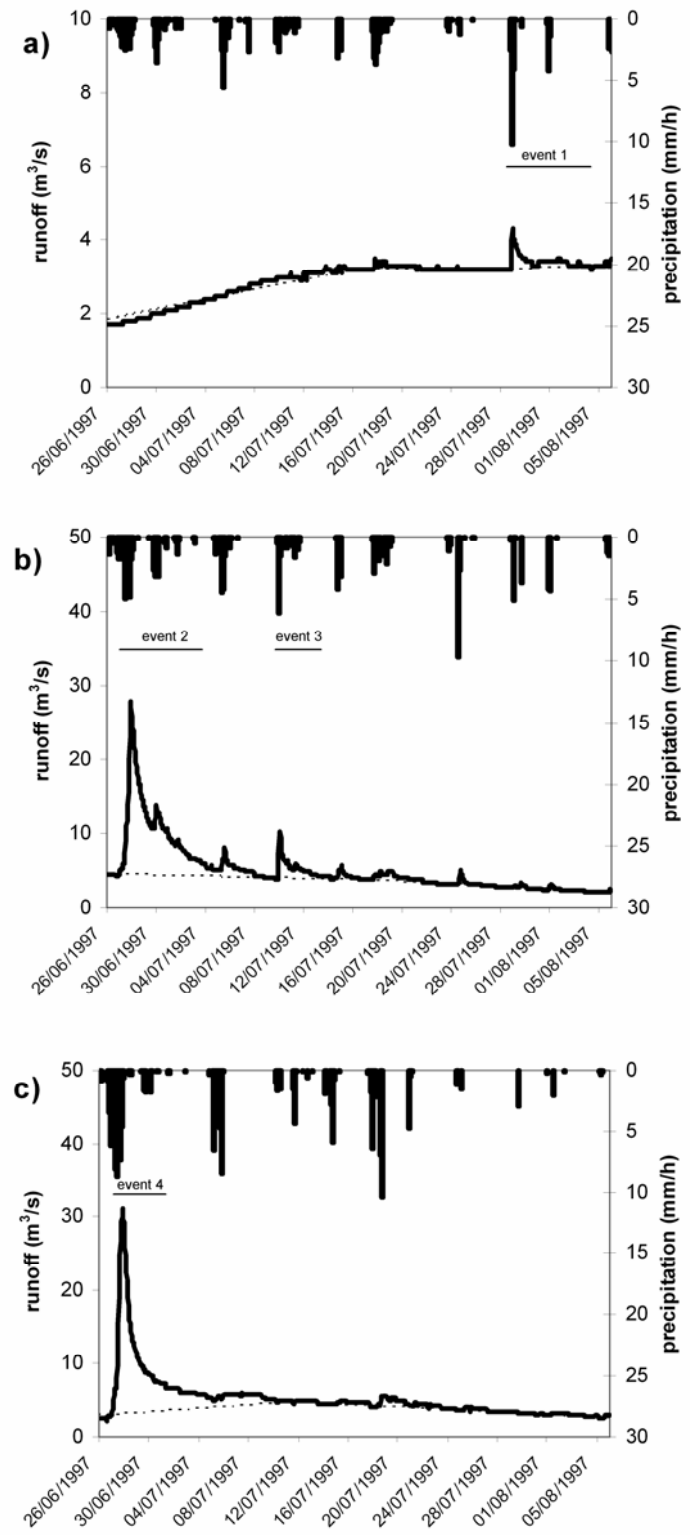

Figure 5-4. Separation of baseflow and runoff events. a) Basin 5 (San Vigilio at Longega), b) Basin 13 (Cordevole at Saviner), c) Basin 12 (Posina at Stancari).

5.3.2 The event separation method

The event separation method, which is based on the methodology used by Merz et al. (2006 [16]), consists of three steps: i) screening of peak flows to identify potential event

peak flows; ii) determination of starting time for each event; iii) determination of the time corresponding to the end of the event.

For a peak flow to be the peak flow of a flood event, two conditions should be met: i) the ratio of direct runoff to baseflow at the peak time should be larger than 0.5 (for Basin 5 this threshold was set to 0.2 due to the particularly weak hydrological response); ii) there should not exist larger flow in the previous and following 12 h.

The determination of the start and end point of each event follows an iterative procedure and requires the estimation of a characteristic time scale $t_c^{'}$, computed according to Merz et al.(2006 [16]). The parameters of the iterative procedure are η_j and ε_j. For each peak flow, the start of an event is searched backwards from t_p to $t_p - \eta \cdot t_c^{'}$. The start of an event was assumed to be that time t_s for which

$$q^d(t_s) < \varepsilon_j \cdot q^d(t_p) \tag{5.1}$$

where $q^d(t_s)$ is the direct runoff at time t_s and $q^d(t_p)$ is the direct runoff at time of peak t_p, i.e. the time where the direct runoff becomes small compared to the direct runoff at the time of the flow peak. If no starting point is found, the search is repeated and η_j and ε_j are gradually increased in five iterations (j=1 to 5) to η_j=0.5; 1.0; 1.5; 2.0; 2.5 and ε_j=0.01; 0.03; 0.1; 0.2; 0.4, respectively. With this iterative approach, the direct runoff at the beginning of an event is as small as possible but if no such point in time is found, a higher direct runoff is allowed.

In a similar fashion, the time t_e of the end of each event is identified by searching in the time window comprised between t_p and $t_p + 4\eta_j \cdot t_c^{'}$. All potential events for which the beginning and end points could be identified, for which the peak flow at time t_p is larger than any other discharge within the event, and for which $t_p - t_s > 3h$ and $t_e - t_p > 6h$, are considered acceptable events.The estimation of the characteristic time scale $t_c^{'}$ is based on the same parameters used by Merz et al. (2006 [16]).

5.3.3 Estimation of the runoff coefficient

A simple rainfall runoff model was used to calculate the runoff coefficient of each identified event. The model is composed by a linear storage with storage parameter k_d and a constant runoff coefficient r_c. The direct runoff over the time period $t_s - t_e$ was simulated with basin rainfall plus snowmelt inputs (as computed based on the water balance model described below) over the time period $t_s - t_c^{'}/10$ to $t_e - t_c^{'}/10$. The Shuffled Complex Evolution optimisation scheme (Duan et al., 1992 [9]) was used to calibrate the two model parameter minimizing the root mean square difference between the observed direct runoff hydrograph and the simulated direct runoff hydrograph. The parameter r_c ranged between 0 and 1 while k_d ranged between $0.5\,t_c^{'}$ and $40\,t_c^{'}$.

In this study only the runoff coefficients for which the root mean square error of the fitting was less than 70% of the average direct runoff were considered. Moreover, with the aim to select the more important events, for each basin the largest 3·N events, which passed the statistical analysis, were retained (N is the number of years of recorded data). Following this procedure, the runoff coefficient for a total of 535 events was computed.

5.3.4 The continuous soil-moisture accounting hydrological model

The continuous hydrological model used in this study is the semi-distributed conceptual rainfall-runoff model which has been described in Chapter 4. For model application, the topography was described by using Digital Elevation Model (DEM) data at three different resolutions: 25 m for Basins 13 and 14, 20 m for Basin 12, 30m for Basins 1 to 11.

The Shuffled Complex Evolution optimisation method (Duan et al., 1992 [9]) was used in combination with a manual calibration to estimate the hydrological model parameters over the 14 basins. In an effort to improve the description of soil moisture conditions before the flood events equal weight was placed to the reconstruction of low flows.

The following objective functions were used during the optimization process for this study:

1: the Nash and Sutcliffe (1970) coefficient of efficiency defined as:

$$E_{NS} = 1 - \frac{\sum_{i=1}^{n}(O_i - S_i)^2}{\sum_{i=1}^{n}(O_i - O_{ave})^2} \tag{5.2}$$

where O_i is the hourly *i-th* observed discharge, S_i is the simulated discharge, and O_{ave} is the mean value of the observed discharges. The coefficient of efficiency was selected because it is dimensionless and is easily interpreted. If the model predicts observed streamflow with perfection then E_{NS}=1. If E_{NS}<0 then the model's predictive power is worse than simply using the average of the observed values.

2: the relative bias (RB) defined as:

$$RB = \frac{\sum_{i=1}^{n}(S_i - O_i)}{\sum_{i=1}^{n}O_i} \tag{5.3}$$

RB is a measure of total volume difference between observed and simulated streamflows, and is important in the evaluation of simulations from continuous hydrologic models. A simple split sample test (Klemes, 1986 [15]) was considered for calibration and validation of the hydrological model. The test involves dividing the available data into two sets, one used for parameter estimation (calibration period) and the other for validation (validation period).

Information on the length period with hourly data available and division among calibration and validation period are reported in Table 5-4. PDM verification statistics for

both the calibration and the independent validation period, as well as for the whole data period, are reported in Table 5-5.

Table 5-4. Periods with data available

Basin number	Station name	Periods with hourly data available	Calibration period	Validation period
1	Aurino at Cadipietra	1/10/89-31/12/2004	1/10/89-30/09/97	1/10/97-30/09/2004
2	Aurino at San Giorgio	1/10/89-31/12/2004	1/10/89-30/09/97	1/10/97-30/09/2004
3	Riva at Seghe	1/10/89-31/12/2004	1/10/89-30/09/97	1/10/97-30/09/2004
4	Gadera at Mantana	1/10/89-31/12/2004	1/10/89-30/09/97	1/10/97-30/09/2004
5	San Vigilio at Longega	1/10/89-30/09/97 1/10/2002-31/12/2004	1/10/89-30/09/97	1/10/2002-30/09/2004
6	Casies at Colle	1/10/89-31/12/2004	1/10/89-30/09/97	1/10/97-30/09/2004
7	Rienza at Monguelfo	1/10/89-31/12/2004	1/10/89-30/09/97	1/10/97-30/09/2004
8	Anterselva at Bagni	1/10/89-31/12/2004	1/10/89-30/09/97	1/10/97-30/09/2004
9	Plan at Plan	1/10/94-31/12/1997 1/10/2002-31/12/2004	1/10/94-30/09/97	1/10/2002-30/09/2004
10	Passirio at Saltusio	1/10/94-31/12/2004	1/10/94-30/09/99	1/10/99-30/09/2004
11	Ridanna at Vipiteno	1/10/89-31/12/2004	1/10/89-30/09/97	1/10/97-30/09/2004
12	Posina at Stancari	1/10/92-31/12/1999	1/10/92-30/09/96	1/10/96-30/09/2000
13	Cordevole at Saviner	1/10/92-31/12/2003	1/10/92-30/09/98	1/10/98-30/09/2004
14	Cordevole at Vizza	1/10/92-31/12/2003	1/10/92-30/09/98	1/10/98-30/09/2004

Table 5-5. Continuous soil moisture accounting model validation and calibration results

Basin Number	Calibration period		Validation period		Whole simulation period	
	E_{NS}	RB (%)	E_{NS}	RB (%)	E_{NS}	RB (%)
1	0.78	8.75	0.69	1.36	0.74	5.29
2	0.65	9.40	0.61	7.63	0.63	8.54
3	0.75	10.48	0.64	2.52	0.71	6.85
4	0.75	3.32	0.40	-0.32	0.56	1.50
5	0.66	-4.53	0.48	0.80	0.63	-4.03
6	0.78	1.99	0.79	-0.81	0.78	0.73
7	0.81	-5.52	0.52	-1.47	0.65	-3.51
8	0.53	9.25	0.73	0.03	0.65	4.60
9	0.69	3.62	0.51	10.30	0.60	6.96
10	0.73	9.40	0.81	8.55	0.78	8.94
11	0.54	4.16	0.78	-2.45	0.67	2.87
12	0.76	1.10	0.77	2.22	0.86	2.31
13	0.62	5.95	0.79	11.81	0.73	9.10
14	0.67	1.41	0.63	-3.72	0.65	-1.07

Efficiency values in calibration are larger than 0.5 and overall Efficiency is around 0.70. When moving from calibration to validation, the overall Efficiency decreases to 0.65 with Basin 4 (Gadera at Mantana) displaying the worst performances (ENS=0.4). This may be due to the effect of the karstified aquifer, which influences a portion of this basin. Hydrological response changes widely across this basin in relation to its local geological characteristics, and this enhances the difficulties of the simulation by means of a lumped model. Estimation of snow accumulation in high altitude basins, and in particular the

temporal variability of the SCF parameter (Snow Correction Factor), adds to the difficulties related to the geological heterogeneity of the study basins and limits the accuracy of the water balance model.

Inspection of results reported for the whole simulation period shows an overall Efficiency of 0.68 with 40% of the basins characterised by Efficiency grater than 0.7. Bias values for calibration and validation range between -5% and 11%.

5.4 Results

The cumulative distribution functions of the event runoff coefficients for the study basins are shown in Figure 5-5 while corresponding summary statistics are reported in Table 5-6.

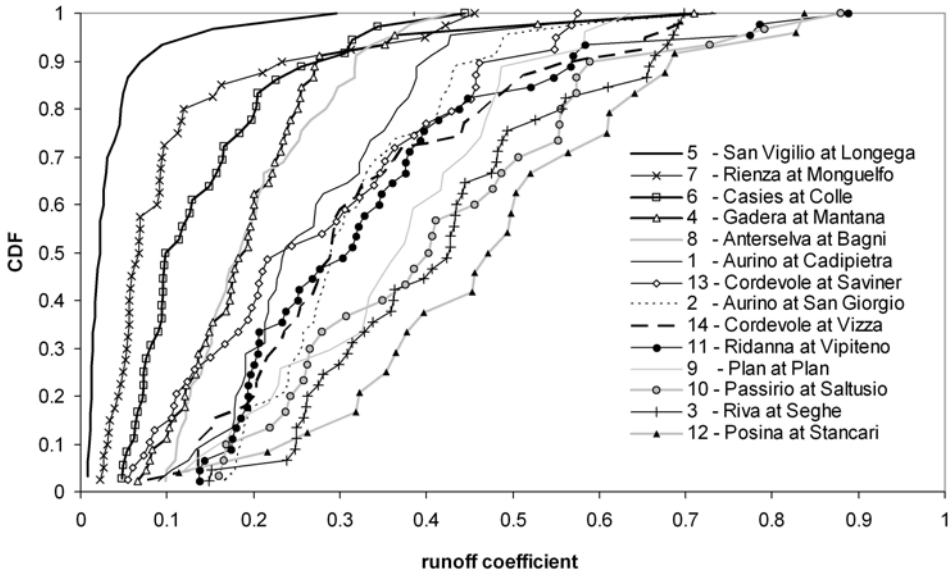

Figure 5-5. Distribution function of the event runoff coefficients for the study basins

Table 5-6. Statistical characteristics of the event runoff coefficient distribution functions

Basin number	Station name	Number of events	Mean	Skewness	CV
1	Aurino at Cadipietra	45	0.28	1.4	0.43
2	Aurino at San Giorgio	45	0.32	1.13	0.38
3	Riva at Seghe	45	0.42	0.30	0.36
4	Gadera at Mantana	45	0.20	2.45	0.55
5	San Vigilio at Longega	30	0.04	3.59	1.50
6	Casies at Colle	36	0.14	1.49	0.64
7	Rienza at Monguelfo	40	0.11	2.12	1.00
8	Anterselva at Bagni	45	0.21	0.82	0.38
9	Plan at Plan	27	0.37	-0.03	0.38
10	Passirio at Saltusio	30	0.42	0.62	0.45
11	Ridanna at Vipiteno	45	0.34	1.34	0.53
12	Posina at Stancari	24	0.48	0.13	0.38
13	Cordevole at Saviner	39	0.28	0.37	0.57
14	Cordevole at Vizza	39	0.33	0.85	0.48

Results reported in Table 5-6 shows that the average values of runoff coefficient ranges more than one order of magnitude, from 0.04 (Basin 5) to 0.48 (Basin 12). This points out to the large variability of the hydrological response in the study area. Interestingly, Basin 5 and Basin 12 are respectively the driest and the wettest basins in the study set. Both coefficient of variation and skewness of the distributions decrease with the increasing of the mean value, as shown in Figure 5-6a-b.

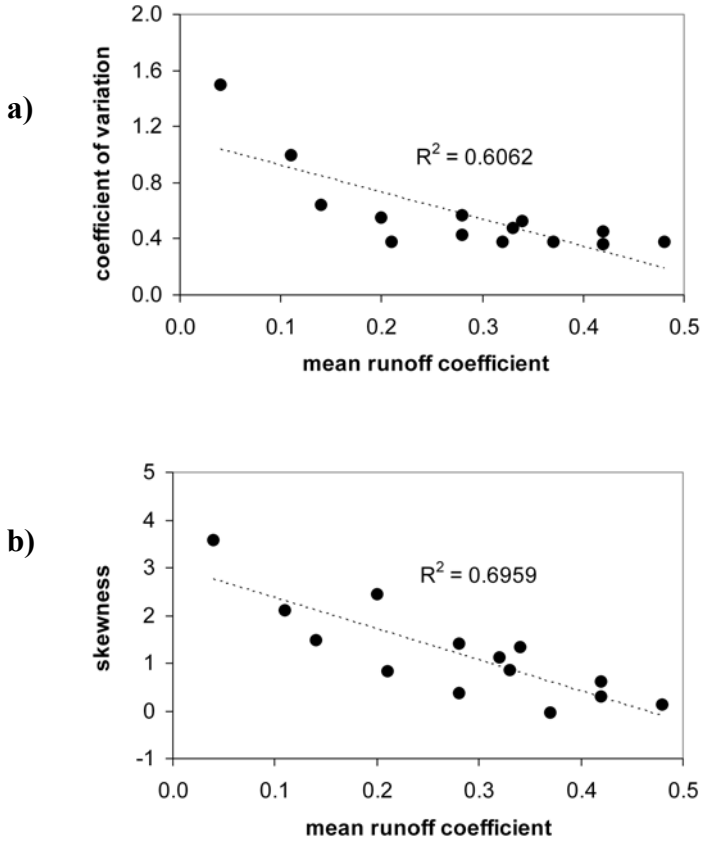

Figure 5-6a-b. Mean runoff coefficients plotted versus: a)coefficients of variation of runoff coefficient distributions; b) skewness of runoff coefficient distributions.

These results are consistent with those reported by Merz et al. (2006 [16]). Basins with high mean value of runoff coefficient are characterised by distribution functions which are almost uniform. Conversely, basins with low mean values of runoff coefficient exhibit often highly skewed distribution functions and large outliers. The overall mean value of the runoff coefficient is 0.28, whereas mean coefficient of variation is 0.57 and mean skewness is 1.18. These values are intermediate between those reported by Merz et al. (2006 [16]), who reported 0.4 and 0.84 for mean value and skewness, respectively, for their alpine region, and Gottschalk and Weingartner (1998 [11]), who reported a mean value of 0.1 for their alpine region and of 0.19 for their southern alpine region. One reason for these differences is the use of different procedures for the computation of the event runoff coefficient, which may give raise to vastly different results, as shown by Blume et

al. (2007 [2]). Other reasons may be found when examining the physical characteristics of the study basins. Snow and glacier melt has an important role on distribution of runoff coefficients in the alpine basins analysed by Merz et al. (2006 [16]), by increasing the antecedent soil moisture through snow and ice melt. This effect, which increases the value of the runoff coefficients, is likely to be less important in our study.

Results from this analysis are reported with more detail for three basins having similar drainage area (Basin 5, 12 and 13, with area ranging from 105 to 116 km^2)(Figure 5-7a-c), but vastly differing hydrologic response. Basin 5 (San Vigilio at Longega) and 12 (Posina at Stancari) represent two end members as far as runoff ratio distribution is concerned, as mentioned above, whereas Basin 13 (Cordevole at Saviner) has intermediate response.

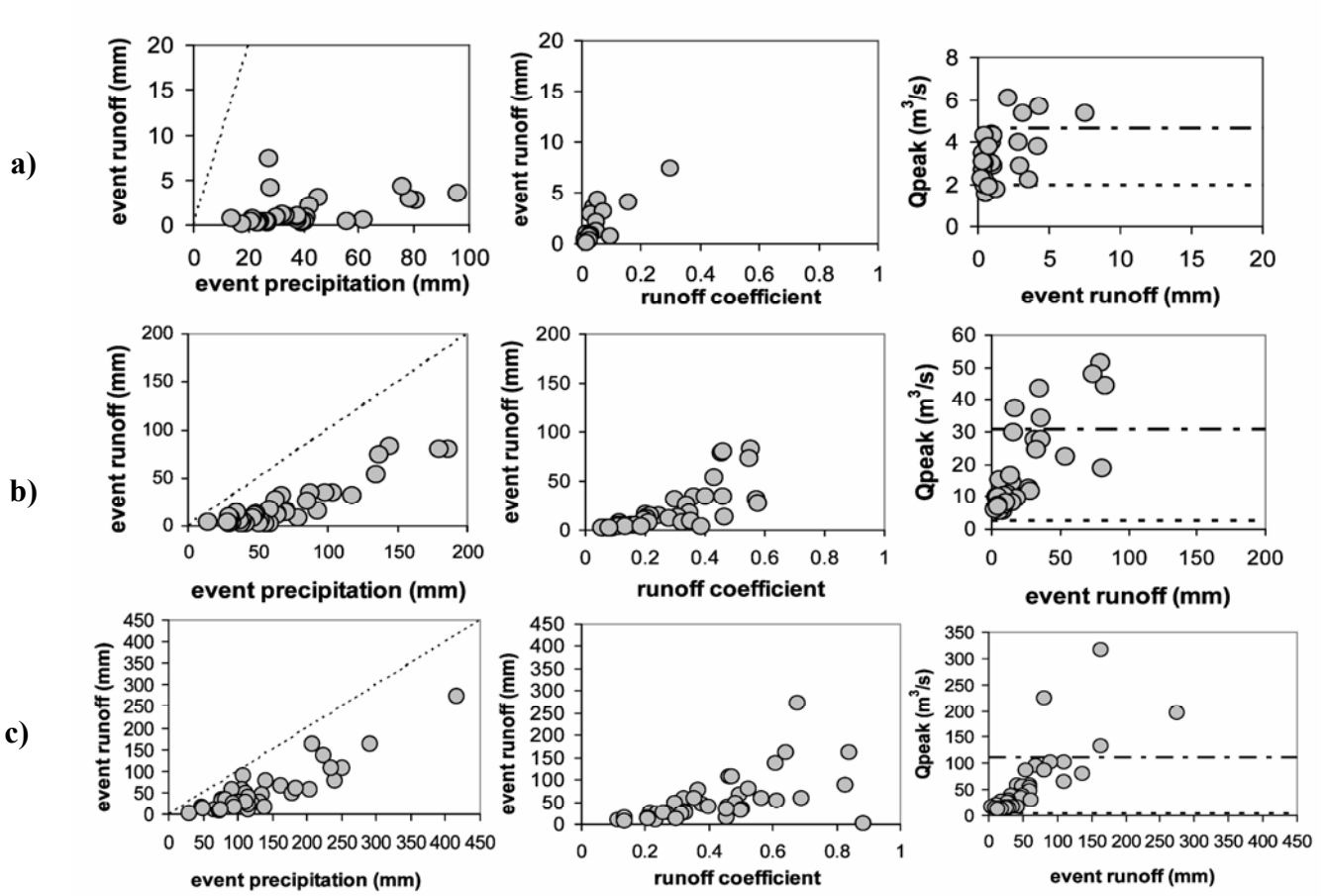

Figure 5-7a-c. Event runoff depth vs. event rainfall depth; event runoff depth vs. runoff coefficient; flood peak vs. runoff depth (with indication of the mean runoff coefficient, the mean maximum annual flood and the mean flood), for three representative basins: a) Basin 5 (San Vigilio at Longega), b) Basin 13 (Cordevole at Saviner), c) Basin 12 (Posina at Stancari). Note the change of scale for the three basins.

On the left panel, direct runoff depths have been plotted against the event precipitation depths, showing the large variability of the climatic forcing, with maximum estimated event precipitation increasing from 100 mm on the San Vigilio to 420 mm on the Posina. Examination of this panel shows also that dependence of runoff depths on rainfall depths increases when moving from San Vigilio to the Posina. Examination of the central panel, where runoff coefficients are reported against corresponding runoff depths, shows

that runoff coefficients increases with increasing runoff depths, as expected, implying the strong nonlinearity of the rainfall-runoff process. However, it is interesting to note on the San Vigilio that runoff coefficients vary in a relatively small range until a runoff threshold is exceeded, after which they show a sudden increase. While this behaviour is expected in basins influenced by a large groundwater storage (and in particular on karstified basins, Phillips, 2006 [23]), this provides also an explanation for the large outliers reported for this basin. On the right panel, event discharge peaks have been plotted against the corresponding runoff depths to provide insight on how the shape of the hydrograph varies with runoff volume (Michaud and Sorooshian, 1994 [17]). Examination of this panel shows that the linearity of the relationship between peak discharges and runoff depths increases when moving from the San Vigilio to the Posina. This agrees with the flashy character of the Posina runoff response, which contrasts with the delayed and multipeaked response of the San Vigilio, where runoff is generated only with long-lasting rainfall events.

The large variability emerging from this analysis needs an explanation in terms of hydrological, climatological, geological and land use properties. These controls are evaluated in the following sections.

5.4.1 The role of climate

Climate variability strongly impacts upon the mechanisms of flood generation in two ways: in a direct way through the variability of storm characteristics and indirectly through the seasonality of rainfall and evapotranspiration which then affect the antecedent basin conditions for individual storm events (Sivapalan et al., 2005 [28]). Mean areal precipitation (MAP) is used here to describe the climate variability across the basins. Figure 5-8 shows that mean event rainfall generally increases with MAP (even though in a nonlinear way) across the study basins. This shows that MAP can be used to surrogate, at least partially, the characteristics of storm events leading to floods.

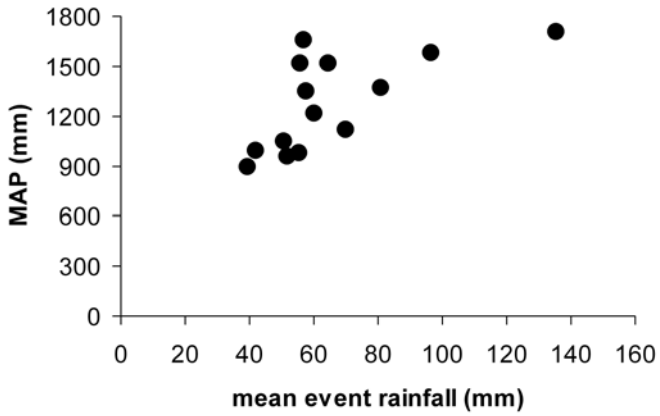

Figure 5-8. Relationship between mean event rainfall and MAP for the study basins

Basin mean runoff coefficients are reported against MAP in Figure 5-9. This figure shows that a significant linear relationship may be found between these two variables for the study basins (R^2=0.83; least squares linear regression is significant at 1% level). The significance of this relationship means that MAP influences the distribution of runoff coefficients not only through the characteristics of the flood-generating storm events, but also by controlling the variability of the initial conditions. By increasing MAP, it becomes more likely that initial conditions are wet, thus enhancing runoff generation. This means also that with increasing MAP, less is the probability to have outlying values of runoff coefficient, leading to distribution functions that are less skewed. These results agree with those obtained by Merz et al. (2006 [16]), who also found that MAP is an important control on the statistical characteristics of the runoff coefficients, and that mean event runoff coefficient increases by increasing MAP.

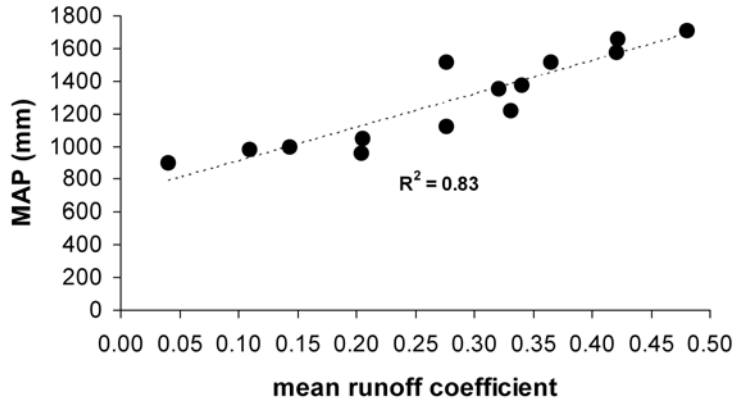

Figure 5-9. Mean runoff coefficients versus MAP for the study basins

5.4.2 The role of geology

Given the significant control exerted by MAP on runoff coefficient distribution, the role of geology has been assessed taking into account the influence of MAP. In Figure 5-10 the mean runoff coefficients have been plotted against MAPs by using different grey gradation to signify variation of permeability index (Table 5-3). Figure 5-10 shows that runoff coefficient increases with permeability ranking (from high permeability to low permeability), as expected. It is important to note that in general terms the most (less) permeable basins are also those characterised by low (high) MAP. This is an important non-physical feature of the sampling structure of our study that needs to be accounted for in the analysis. Since the two controls act in the same way, the influence of geology on runoff coefficients can be isolated only by comparing basins with similar MAP. This is the case for the Basins 4 to 8, 13 and 14, with MAP ranging between 900 and 1200 mm. For these basins, the runoff coefficient increases with decreasing the permeability, as expected, with the exception of Basins 4. For this last basin, the geological classification may be not completely representative of the geological complexity of this basin. Less permeable basins have larger runoff coefficients, as expected, but our data and the geological

classification considered here cannot be used to isolate the individual effect of geology and climate in these cases. A counterintuive situation is reported for Basins 1 and 13, where Basin 1 has lower permeability and higher MAP than Basin 13. In spite of these characteristics, which would suggest an higher runoff coefficient for Basin 1 with respect to Basin 13, the mean observed runoff coefficient is the same (even though the cumulative distribution is rather different, Figure 5-5). Overall, these observations suggest that the significance of the linear relationships reported in Figure 5-10 reflects the control of both climate and geology on runoff coefficient, and that geology represents an important control on runoff coefficient, at least when MAP is less than 1200 mm. However, the predictive power of the relationship reported in Figure 5-10 has important limitations, which depends on uncertainties in the geological/climatic classification and on the influence of other unaccounted physical controls on runoff coefficient distribution.

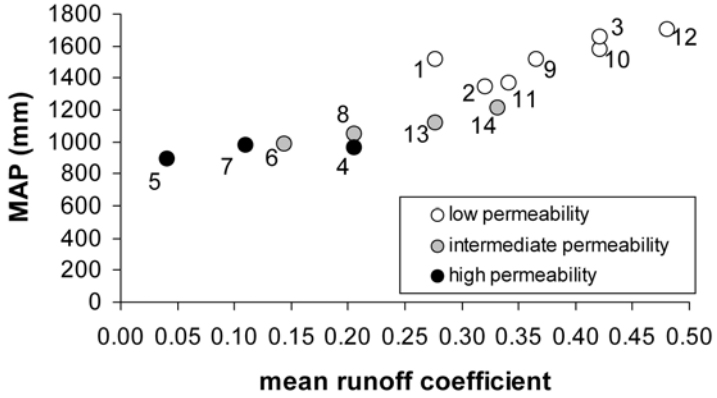

Figure 5-10. Mean runoff coefficients versus MAP for the study basins stratified by permeability index.

5.4.3 The role of land use

There is rich literature on land use change effects on runoff generation during flood events, including Jones (2000 [14]), Bronstert et al. (2002 [3]), Robinson et al., (2003 [25]), Andreassian (2004 [1]) and Bloeschl et al. (2007 [4]). However, probably the most widely used procedure to index the effects of soils and land use on runoff coefficient is the US-SCS curve number method (US-SCS, 1972 [29]; Ponce and Hawkins, 1996 [24]). The SCS method provides a procedure for estimating the curve number from soil type and land use and antecedent rainfall. Once the curve number is known it can be used to estimate event runoff depth from event rainfall depth for an ungauged basin.

In this study we used the SCS curve number to isolate the potential effect of soil and land use variability on event runoff coefficient distribution. The SCS curve number was computed from soil and land use data. The soil map was reclassified to obtain the soil groups map (US-SCS, 1972 [29]) which, combined with the land use map, yielded a Curve Number map. Finally, the average Curve Number was computed for every basin. Since the Curve Number is used here as an index of the mean basin response, average antecedent rainfall conditions are assumed for all basins. For every basin, Figure 5-11 shows the 90%,

50% and 10% quantiles of the runoff coefficient distribution functions against the basin average Curve Number. The highest Curve Numbers would be expected to be associated with the highest runoff coefficients. However, this is not fully borne out in the results reported in Figure 5-11.

For instance, the smallest value of Curve Number is reported for Basin 12 (Posina at Stancari), which is characterised by the largest runoff coefficient. Land use in Basin 12, in fact, is dominated by forests. Consequently the SCS method predicts relatively small values of curve number as forest soils are usually highly permeable. However, in this basin soil permeability seems to have relatively little effect on the runoff coefficients with respect to storm event and climatic characteristics. On the other hand, four basins like Basins 4, 5, 7 and 10, whose mean runoff coefficients span almost the complete range of computed runoff coefficients, are characterised by very similar values of curve number.

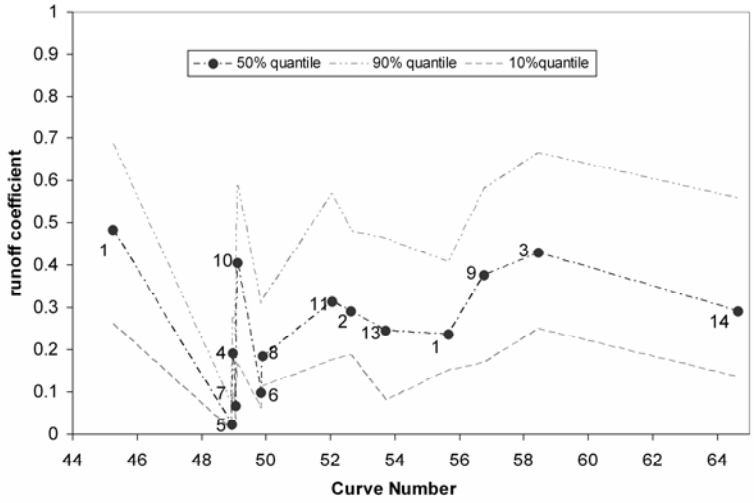

Figure 5-11. Quantiles of runoff coefficient distributions versus the SCS Curve Number

This shows that land use effect on runoff coefficients, as indexed by the SCS-CN method, is outweighed by climatic and geologic effects. This probably depends, among other things, on the way rock outcrops have been considered in the computation of the Curve Number. With this method, rock outcrops are generally associated to almost impervious surfaces with high values of curve number. However, insight obtained from site visits as well as previous results on the role of geology have shown that runoff generation from rock outcrops depends heavily on the lithological units, with the rainfall flux being completely and fastly drained in karstified limestones and through faults and fissures of limestones and dolomites (such as those present on the San Vigilio basin).

5.4.4 The role of initial soil moisture conditions

Evaluation of the role of initial soil moisture conditions on distribution of event runoff coefficient requires consideration of two factors: basin soil moisture capacity and antecedent soil moisture conditions. The rationale for the selection of these factors is that the impact of antecedent soil moisture conditions is expected to increase with increasing the soil moisture capacity. In this study, the basin soil moisture capacity was indexed based on the flow duration curve. The flow duration curve shows the percentage of time during

which any selected discharge may be equalled or exceeded; a log-normal transformation for the flow data is normally applied to linearise the resulting curve. Past studies (Institute of Hydrology, 1980 [13]) have shown that when low flows are expressed as a percentage of the long-term mean flow (standardised), the dependencies on the climatic variability and on the scale effect of basin area are minimised. The shape of the standardised flow-duration curve indicates the characteristic response of a basin to rainfall. The gradients of the log-normal standardised flow duration curves for a range of basins with differing geology (Figure 5-12) illustrate that impermeable basins have high gradient curves reflecting a very variable flow regime; low storage of water in the basin results in a quick response to rainfall and low flows in the absence of rainfall. Low gradient flow-duration curves indicate that the variance of daily flows is low, because of the damping effects of groundwater storages provided naturally, for example, by extensive karstified or limestone aquifers. The ratio of daily discharge which is exceeded 90% of the time to the median daily flow, Q_{90}/Q_{50}, has been used as an index of soil moisture capacity.

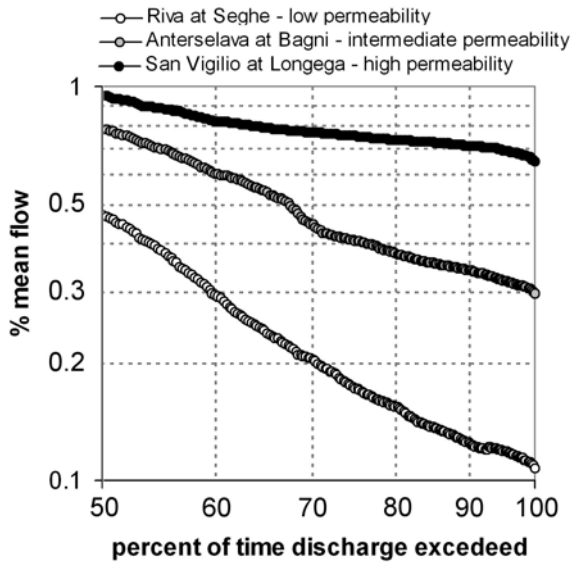

Figure 5-12. The influence of geology on the gradient of the standardised flow duration curve.

Values of the soil moisture capacity index (Q_{90}/Q_{50}) are reported for each basin in Table 5-7, which shows also the permeability index. In general there is a good correspondence between the permeability index and the soil moisture capacity index, with the last value increasing with the permeability ranking. An exception is represented by Basin 13, and, to a lesser degree, by Basin 8. Even though Basin 13 and 14 have similar geologic classification (with Basin 14 included in the larger parent Basin 13), Table 5-7 shows that it is likely that permeability of Basin 13 is lower than the one derived from the geologic classification.

Table 5-7. The soil moisture capacity index (Q_{90}/Q_{50}). The table reports also the permeability index.

Basin number	Station name	Q_{90}/Q_{50}	Permeability index
3	Riva at Seghe	0.26	1
14	Cordevole at Vizza	0.30	2
9	Plan at Plan	0.33	1
11	Ridanna at Vipiteno	0.39	1
1	Aurino at Cadipietra	0.41	1
10	Passirio at Saltusio	0.44	1
8	Anterselva at Bagni	0.44	2
12	Posina at Stancari	0.45	1
2	Aurino at San Giorgio	0.47	1
13	Cordevole at Saviner	0.51	2
6	Casies at Colle	0.52	2
7	Rienza at Monguelfo	0.58	3
4	Gadera at Mantana	0.58	3
5	San Vigilio at Longega	0.75	3

The initial soil moisture conditions have been derived by means of the continuous soil moisture accounting model, through examination of the relative soil moisture content of the PDM storage. Relative initial soil moisture conditions larger than the median value of the initial soil moisture distribution functions were considered “wet”, while lower values were considered “dry”. This afforded to split the flood events into two classes named “wet” and “dry”, according to the corresponding initial soil moisture conditions. Moreover, in order to isolate the effect of initial conditions with respect to the effect of rainfall depth, we considered only the basins for which the distributions of rainfall depths during dry and wet periods were similar. In these basins, the probability of having high or low rainfall depths is expected to be the same both in dry and wet periods. This led to exclude six basins (2, 6, 8, 9, 10 and 11) from the analysis.

In snow-affected basins, flood runoff generation is driven by two types of initial conditions: one is represented by the initial soil moisture, the other by the initial snowcover. To isolate the effect of initial soil moisture conditions, we considered the events less influenced by snowmelt. Figure 5-13 shows the distribution functions of the runoff coefficients classified by different ranges of the snowmelt volumes over total precipitation ratio.The runoff coefficients increase when the contribution of melt increases. This finding is in agreement with Merz et al. (2006 [16]), who found large runoff coefficients for rain-on-snow flood events. In this analysis we considered the events with snow melt depth lower than 33% of the event precipitation depth. These events represent 70% of the total events.

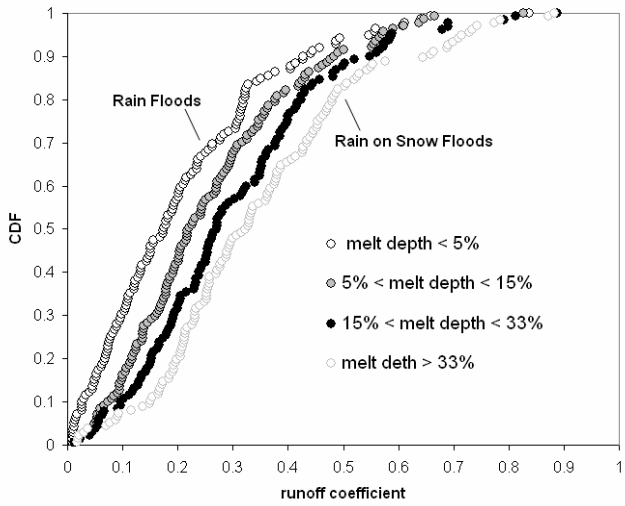

Figure 5-13. Distribution function of the event runoff coefficients for different percentages of snow melt over event rainfall depth

The role of the initial soil moisture conditions has been examined by contrasting the distribution function of the runoff coefficients for 'wet' events with respect to the distribution of the 'dry' events. This analysis is reported with some details in Figure 5-14 for three representative basins: Basin 5 (San Vigilio at Longega), Basin 13 (Cordevole at Saviner) and Basin 3 (Riva at Seghe). Basins 5 and 3 represent two end members as far as the soil moisture capacity index is concerned, with index values of 0.75 and 0.26, respectively. Basin 13 has an intermediate index value, amounting to 0.51. Figure 5-14 shows the distribution function of the initial relative soil moisture (left panel), the distribution functions of the event precipitation for 'dry' and 'wet' events (central panel) and the distribution functions of the event runoff coefficients for 'dry' and 'wet' events (right panel). Examination of the central panel shows that the distributions of rainfall depths during dry and wet periods is similar, as expected after the design of the analysis. The right panel shows that the distribution of 'wet' runoff coefficients differs with respect to the 'dry' one (with a shift towards higher values of runoff coefficient) only for the intermediate Basin 13. In the other two cases, the two distributions almost overlap. This behaviour is expected for Basin 3; in this case, the low soil moisture capacity minimises the effect of initial soil moisture conditions. However, it is not expected for Basin 5, characterised by high values of the soil moisture capacity index. To evaluate these aspects, we have computed the relative difference between the mean values of the distribution of 'wet' and 'dry' runoff coefficients for the various considered basins. The relative difference of the mean values (called 'relative difference' hereafter) is reported in Figure 5-15 together with the corresponding soil moisture capacity index.

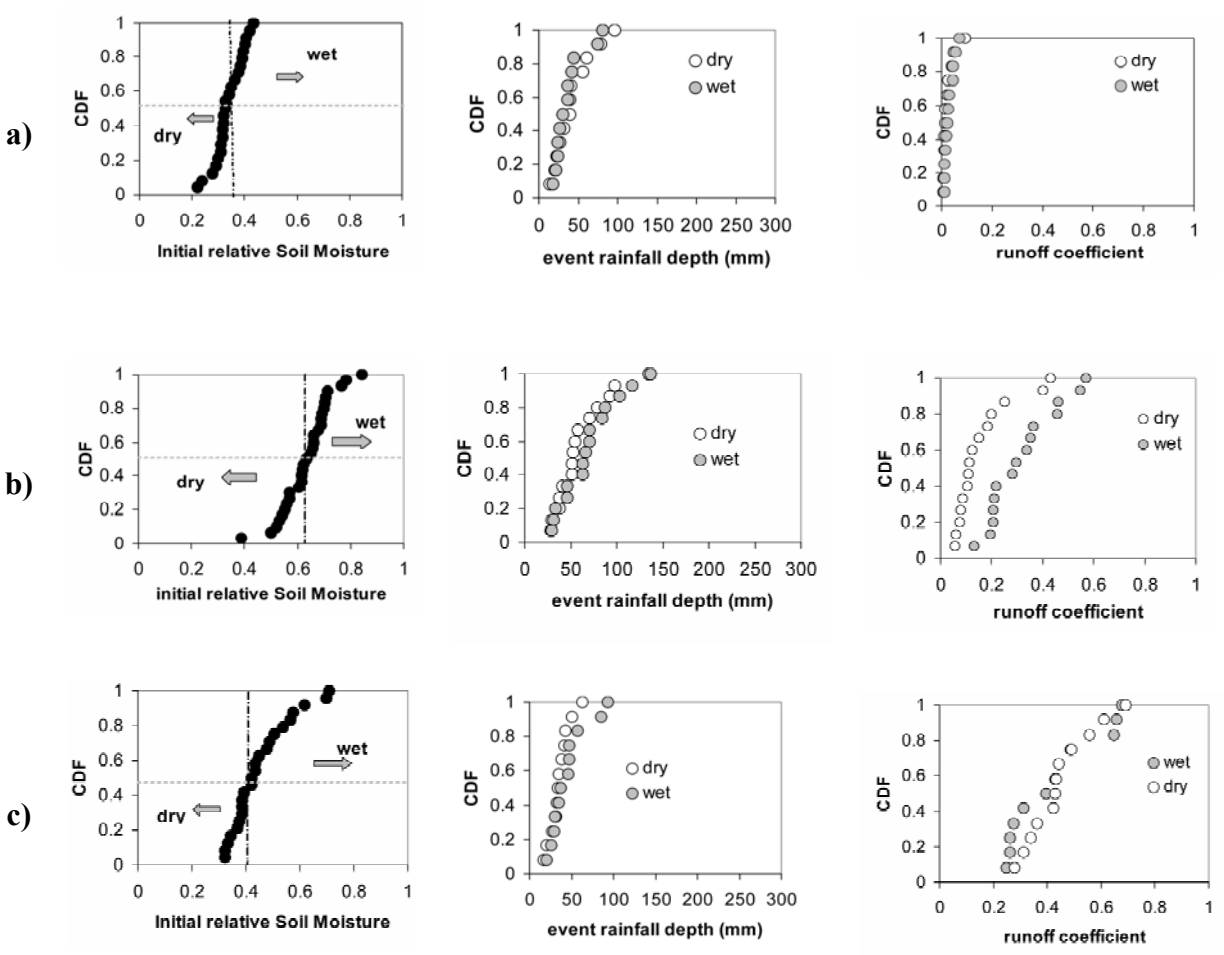

Figure 5-14a-c. Distribution functions of initial relative soil moisture, runoff coefficients and event rainfall depths for dry and wet periods. a) Basin 5 (San Vigilio at Longega), b) Basin 13 (Cordevole at Saviner, c) Basin 3 (Riva at Seghe).

Figure 5-15 shows that the influence of the initial soil moisture conditions does not increase with the soil moisture capacity. Actually it exists an optimum region of soil moisture capacity, as indexed by the capacity index, which maximises the impact of initial soil moisture conditions on runoff coefficient. According to this study, this optimum region ranges between index values of 0.35 and 0.55. For basins with larger index values (such as Basins 4, 7 and 5) the difference between mean values of 'wet' and 'dry' runoff coefficients is negligible. It is speculated that for these cases, characterised by large groundwater capacity (represented, for instance, by a karstified aquifer), the initial capacity is always larger than event precipitation, even in 'wet' conditions. In these cases, runoff is generated on the relatively small portions of the basin which are not intercepted by the karstified aquifer.

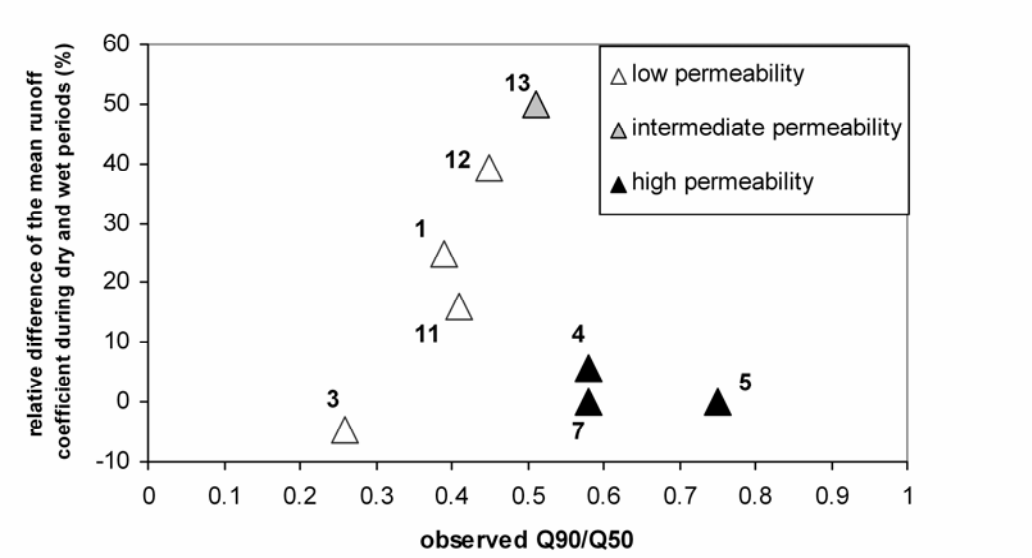

Figure 5-15. Optimum region of groundwater capacity, as indexed by the parameter Q90/Q50.

5.5 Conclusions

There are five principal observations from this work.

i. The large spatial variability in mean runoff coefficient, which ranges from 0.04 to 0.48, is relatively well explained by the mean annual precipitation. Runoff coefficients increase with mean annual precipitation. Variability and skewness of runoff coefficient distribution tend to reduce with increasing mean annual precipitation.

ii. Geological characteristics (as indexed through the 'permeability index') are a dominant control on runoff coefficient, at least for mean annual precipitation less than 1200 mm, through their direct effect on hydrologic pathways and storage properties. Basins characterised by high permeability index have low values of mean runoff coefficient. Less permeable basins have larger runoff coefficients, as expected, but our data and the geological classification considered here cannot be used to isolate the individual effect of geology and climate in these cases, since basins with low permeability index have also high mean annual precipitation.

iii. Land use, as indexed by the SCS curve number, influences runoff coefficient distribution to a lesser degree. This result seems to be related both to ambiguities in the SCS curve number-based indexing (particularly for rock outcrops) and to scale effects. Most of the basins considered here have areas exceeding 50 km^2. Some of the land use and soil characteristics are likely to average out over this basin size.

iv. An analysis of the runoff coefficients by flood type indicates that runoff coefficients increase with event snowmelt, and are relatively low for rain floods. The effect of snow processes mainly seems to be in increasing antecedent soil moisture.

v. Results show that it exists an optimum region of soil moisture capacity, as indexed by a flow duration curve-based index, which maximises the impact of initial soil moisture conditions on runoff coefficient. This means that the difference between

runoff coefficients characterised by wet and dry initial conditions is negligible for basins with very larger groundwater capacity (given by largely karstified aquifer) and for basins with reduced groundwater capacity. For basins characterised by intermediate conditions, the difference (and hence the impact of the initial soil moisture conditions) is relatively large.

5.6 References

[1] Andreassian, V., 2004. Waters and forests: from historical controversy to scientific debate. Journal of Hydrology, 291, 1–27.

[2] Blume, T., Zehe, E., Bronstert, A., 2007. Rainfall runoff response, event-based runoff coefficients and hydrograph separation. Hydrolog. Sci. J., 52(5), 843-862.

[3] Bronstert A., Niehoff, D., Bürger, G., 2002. Effects of climate and land-use change on storm runoff generation: present knowledge and modelling capabilities. Hydrological Processes, 16, 2, 509-529.

[4] Bloeschl, G. et al., 2007. At what scales do climate variability and land cover change impact on flooding and low flows? Hydrological Processes, 21, 1241–1247.

[5] Budyko, M. I.,1974. Climate and life. Academic Press, New York.

[6] Cazorzi, F., Dalla Fontana, G., 1996. Snowmelt modelling by combining air temperature and a distributed radiation index. Journal of Hydrology. 181, 169–187.

[7] Cerdan, O., Le Bissonnais, Y., Govers, G., Leconte, V., van Oost, K., Couturier, A., King, C., Dubreuil, N., 2004. Scale effects on runoff from experimental plots to basins in agricultural areas in Normandy. Journal of hydrology, 299, 4–14.

[8] Da Ros, D., Borga, M., 1997: Use of digital elevation model data for the derivation of the geomorphologic instantaneous unit hydrograph. Hydrological Processes, 11, 13-33.

[9] Duan, Q., Sorooshian, S., Gupta, S., Gupta, V.K., 1992. Effective and efficient global optimization for conceptual rainfall-runoff models. Water Resources Research 28(4), 265–284.

[10] Fiorentino, M., Iacobellis, V., 2001. New insights into the climatic and geologic controls on the probability distribution of floods. Water Resources Research, 37(3), 721– 730.

[11] Gottschalk, L., Weingartner, R., 1998. Distribution of peak flow derived from a distribution od rainfall volume and runoff coefficient, and a unit hydrogrph. Journal of hydrology, 208, 148-162.

[12] Hargreaves, G. H., Samani, Z. A., 1982. Estimating potential evapotranspiration. J. Irrig. Drain. Div., 108, 225–230.

[13] Institute of Hydrology, 1980. Low Flow Studies Report. Institute of Hydrology. Wallingford, UK.

[14] Jones, J., 2000. Hydrologic processes and peak discharge response to forest removal, regrowth, and roads in 10 small experimental basins, Western Cascades, Oregon. Water Resources Research 36: 2621–2642.

[15] Klemes, V., 1986. Operational testing of hydrological simulation models. Hydrol. Sci. J., 31, 13-24.

[16] Merz, R., Bloeschl, G., Parajka, J., 2006. Spatio-temporal variability of event runoff coefficients. Journal of Hydrology, 331, 591-604.

[17] Michaud, J. D., and S. Sorooshian, 1994: Comparison of simple versus complex distributed runoff models on a midsized, semiarid watershed. Water Resources Research, 30(3), 593–605.

[18] Montgomery, D.R., Foufoula-Georgiou, E., 1993. Channel network source representation using digital elevation models. Water Resources Research 29(12), 3925–3934.

[19] Moore, R.J., 1985. The probability-distributed principle and runoff production at point and basin scales. Hydrol. Sci. J., 30, 273-297.

[20] Nash, J.E., Sutcliffe, J.E., 1970. River flow forecasting through conceptual models, Part I: A discussion of principles. Journal of Hydrology, 10, 282–290.

[21] Nathan, R.J., McMahan T.A., 1990. Evaluation of automated techniques for baseflow and recession analysis. Water Resources Research. 26(7):1465-1473.

[22] Norbiato, D., Borga, M., Bloeschl, G., Merz, R., Carton, A., 2008a. Controls on event runoff coefficients in the eastern Italian Alps. To be submitted to Journal of Hydrology.

[23] Phillips, J.D., 2006: Evolutionary geomorphology: thresholds and nonlinearity in landform response to environmental change. Hydrol. Earth Syst. Sci., 10, 731–742, 2006.

[24] Ponce, V.M., R.H. Hawkins, 1996: Runoff curve number: Has it reached maturity?, J. Hydrologic Eng., 1, 1, 11-19.

[25] Robinson M, Cognard-Plancq A-L, Cosandey C, David J, Durand P, F¨uhrer H-W, Hall R, Hendriques MO, Marc V, Mccarthy R, McDonnell M, Martin C, Nisbet T, O'Dea P, Rodgers M, Zollner A. 2003. Studies of the impact of forests on peak flows and baseflows: a European perspective. Forest Ecology and Management, 186, 85–97.

[26] Sevruk, B., Paulais, M., Roulet, Y.-A., 1998. Correction of precipitation measurement using fresh snow as reference. In: Proceedings of the WMO Technical Conference on Meteorological and Environmental Instruments and Methods of Observation, TECO-98. WMO/TD-No. 877, Geneva, Switzerland, 349–352.

[27] Sivapalan, M., Takeuchi, K., Franks, S.W., Gupta, V.K., Karambiri, H., Lakshmi, V., Liang, X., McDonnell, J.J., Mendiondo, E.M., O'Connell, P.E., Oki, T., Pomeroy, J.W., Schertzer, D., Uhlenbrook, S., Zehe, E., 2003. IAHS decade on Predictions in Ungauged Basins (PUB), 2003-2012: shaping an exciting future for the hydrological sciences. Hydrological Sciences Journal, 48, 857-880.

[28] Sivapalan, M., G. Bloeschl, R. Merz, D. Gutknecht, 2005: Linking flood frequency to long-term water balance: Incorporating effects of seasonality. Water Resources Research, 41, W06012, doi:10.1029/2004WR003439.

[29] US-SCS, 1972. National Engineering Handbook Section 4 Hydrology. US Department of Agriculture.

[30] Van de Griend, A., E. Seyhan, G.B. Engelen, W. Geirnaert, 1986: Hydrological characteristics of an alpine glacial valley in the north Italian Dolomites. Journal of Hydrology, 88, 275-299.

[31] Wainwright, J., Parsons, A.J., 2002. The effect of temporal variations in rainfall on scale dependency in runoff coefficients, Water Resour. Res., 38(12), 1271.

6 Analytical solutions to a hillslope-storage kinematic wave model for subsurface flow and analysis of its hysteretic behaviour[5]

6.1 Introduction

Most hydrologic understanding is based at the point scale, whilst our needs for predictive modeling are at basin scales. There is an urgent need for improved hydrologic predictions at that scale. Solving this spatial scaling problem requires a new approach along different lines of research that coincide with the PUB (Prediction in Ungaged basins) scientific programme. Until now, observations of streamflow are required to calibrate the rainfall-runoff models, which are central to most strategies for hydrologic prediction. While the calibration on runoff data has served hydrology well in the past, this is not an option in ungauged basins. In ungauged basins other methods must be used and basin characteristics play a central role in this. Solving the scaling problem calls for new approaches in basin modelling. The new generation of models should be able to integrate, in a innovative way, the information concerning the geomorphic structure of a basin, which is the only one everywhere available, particularly in the case of ungaged basins.

The classical form of geomorphic information is a digital elevation model (DEM), and the classical way to use it for hydrological purposes is to build a two or threedimensional gridded spatially distributed hydrological model, where each grid cell has an associated topographic elevation, and water is allowed to flow from grid cell to grid cell. This can be considered as an explicit way of incorporating geomorphic data. In some sense, because grid cells are only linked through common boundaries, the larger scale spatial correlations and structures that exist in the geomorphic surface are ignored.

There are, however, alternative ways of applying geomorphic data in a more implicit way, that, by doing so, do respect these larger scale geomorphic structures. Thus far, Fan and Bras (1998 [13]) and the Hydrology and Quantitative Water Management (HWM) group of Wageningen University and then at the Arizona University have developed methods that account for the three-dimensional hillslope form while still using simple flow equations.

Recently, Troch et al. (2002 [28]) developed storage-based equations able to capture the flow processes of all elementary hillslopes by simple scaling laws pertaining to hillslope length, slope and form. Such a description can give rise to a new generation of distributed rainfall-runoff models because it captures the essential behaviour of the natural system while being low-dimensional and computationally efficient. Hillslope response has

[5] The stidy described in this chapter has been published in Norbiato et al. (2008b [23])

traditionally been studied by means of the hydraulic groundwater theory. Solving the three-dimensional Richards equation for different hillslopes within a basin is a complex task. Fan and Bras (1998[13]) presented a way to transfer the three-dimensional soil mantle into a one-dimensional profile. Continuity and a kinematic form of Darcy 's law lead to quasi-linear wave equations for subsurface flow, solvable with the method of characteristics. Adopting a power function of the form proposed by Di Stefano et al. (2000 [9]) to describe the bedrock slope, Troch et al. (2002 [28]) derive more general solutions to the hillslope-storage kinematic wave equation for subsurface flow, applicable to a wide range of complex hillslopes. Results concerning a development of this approach are the object of this chapter.

The subsurface flow dynamics is analysed by means of a simplified model based on the kinematic wave assumptions and using a method first proposed by Horton (1936 [18]) and then further developed by Fan and Bras (1998 [13]) to transfer the three-dimensional soil mantle into a one-dimensional profile. The hillslope-storage subsurface flow equation considered in this study takes into account the topographic controls exerted on the flow processes by the plan shape and profile curvature. General solutions to the hillslope-storage kinematic wave equations, are derived, adopting a second order polynomial function to describe the bedrock slope and an exponential function to describe the variation of the width of the hillslope with hillslope distance. These solutions, which are applicable to a wide range of hillslopes, affords a broad and clear view of the essential features of the problem and allows to derive two geometric parameters α and ψ which define the hydrological similarity between hillslopes with respect to their characteristic response.

Results of the application of this simplified model for subsurface flow processes show the existence of a hysteretic behaviour in the saturated storage - flux relationships at the hillslope scale. The influence of topographic factors on the hysteretic behaviour has been widely explored in the study.

Hysteresis is a common feature in several hydrological processes. It may occur in many input-output relationships between time-dependent quantities. In general, an input-output relationship is said to present hysteresis if the value of the output at a generic time does not only depend on the value of the input at the same instant, but also on the history of the input. As such, hysteresis identifies a class of strongly non linear processes, i.e. linearisation cannot encapsulate the observed phenomena (Flynn et al., 2003 [14] ; O'Kane and Flynn, 2007 [24]).

In hydrology, the hysteretic behaviour of the relation between water retention and soil-moisture tension has been studied for 70 years, dating back to the studies of Haynes (1930 [15]) and Richards (1941 [26]). In applying the Darcy-Richards equation it was found that the soil moisture characteristic curves that link soil moisture content, soil water potential and hydraulic conductivity, were not single valued but were rather different for wetting and drying.

Hysteresis has also been found to emerge at various space and time scales and in many different hydrological processes. Observations of hysteresis in the storage-surface discharge relationships have been reported by a number of authors. For instance, Myrabø

(1997 [20]) reported distinct hysteretic effects in discharge-groundwater level relationships in a number of small basins in Norway. This author showed that the behaviour of the discharge-groundwater relationship is dependent on location, antecedent conditions and size of response area before each precipitation event. Hysteretic relationships between streamflow and groundwater level were identified also by Kendall et al. (1999 [19]) for headwater basins in Vermont (USA). Clockwise hysteresis (higher groundwater level for given discharge on rising limb than at same discharge on falling limb) was reported for riparian sites, suggesting that the riparian zone was the dominant source area during the rising limb of the melt hydrograph. Hysteresis was counterclockwise at hillslope sites, suggesting that hillslope drainage controlled the snowmelt recession. Similar relationships were reported by Schumann and Hermann (2002 [27]) for two small mountainous basins in Germany.

Ewen and Birkinshaw (2006 [12]) examined hysteretic loops in storage-discharge plots based on runoff data from the Slapton Wood basin in UK. They identified a basic pattern of hysteretic loops, with higher groundwater mean volume for given discharge on rising limb than at same discharge on falling limb. Beven (2006 [4]) reported hysteretic behaviour associated with individual storms in plots of relative storage vs relative runoff for a number of small basins in UK.

A whole range of hydrological processes can either collectively or individually contribute to generate hysteresis at the basin scale. For instance, Beven (2006 [4]) mentioned "…the small scale matrix soil characteristics, the possibility of changing vertical and downslope connectivities of flow pathways as the soil dries and rewets, the development of the inter-unit patterns of antecedent wetness,…, the dynamics of contributing areas".

Chirico (2001 [8]) and Niedzialek and Ogden (2004 [22]), in separate studies focused on the saturation excess runoff generation mechanism, examined the relationship between small basin properties and the temporal growth and decay of saturated source areas. These authors used different physically-based hydrologic models and were able to show that the temporal evolution of the extent of saturated source area versus basin average soil water content during a number of wetting and drying cycles exhibits a wide variety of trajectories or hysteretic loops.

Chapman and Ong (2006 [6]) reported an hysteresis loop between dimensionless flow and mean flow depth from shallow groundwater, for rising and falling conditions by applying a shallow groundwater equation for flow over a convexo-concave continuous curvilinear bed.

These findings support the view that hysteresis in the relation between average saturated soil water content and hillslope subsurface flow may contribute to hysteresis emerging at the hillslope and at the basin scale and that hillslope geometry (together with other factors) may influence the structural characteristics of hysteresis.

6.2 The hillslope-storage kinematic wave model

The saturated component of the hillslope response has traditionally been studied by means of the hydraulic groundwater theory. To overcome difficulties associated with three-dimensional models, a series of low-dimensional hillslope models have been recently developed (Troch et al., 2002, 2004 [28][29]). These models are able to treat geometric complexity in a simple way by using a width weighting and depth averaging scheme which allows to map the three-dimensional soil mantle into a one-dimensional profile, resulting in a significant reduction in model complexity. This type of width weighting actually goes back to Horton (1936 [18]) and since then was further developed by Beven (1977 [1]) and by Fan and Bras (1998 [13]). One should note that these models are limited to the saturated component of the hillslope response and does not include the unsaturated component.

Fan and Bras (1998 [13]) introduced the soil moisture storage function S(x,t),

$$S(x,t) = w(x)h(x,t)\varepsilon \tag{6.1}$$

where w(x) is the width of the hillslope at flow distance x, measured along the horizontal, from the divide (the so-called hillslope width function), h(x) is the width-averaged water table height (measured along the vertical) at flow distance x, ε is drainable porosity and t is time (see also Figure 6-1 for a graphical definition of the width and soil depth function). This allows reformulating the three-dimensional flow problem as a one-dimensional flow problem. The propagation of soil moisture storage in space and time, S(x,t) is constrained by the continuity equation and Darcy's law.

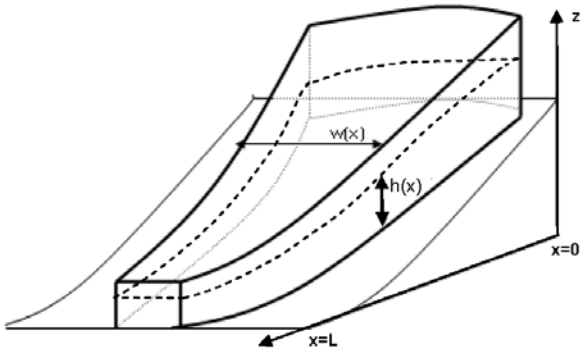

Figure 6-1. Three-dimensional view of a convergent hillslope

Along the hillslope the continuity equation reads

$$\frac{\partial S}{\partial t} + \frac{\partial Q}{\partial x} = r(t)w(x) \tag{6.2}$$

where r(t) is the recharge to the saturated layer and Q is the flow rate. Let us further assume that the flow rate Q is related to the storage S(x,t) through a kinematic form of Darcy's equation

$$Q = -k\frac{S}{\varepsilon}\frac{dz}{dx} \tag{6.3}$$

where z is the elevation of the bedrock above a given datum.

Combining (6.3) and (6.2) and assuming no spatial variability in k and ε provides a quasi-linear wave equation in terms of soil moisture storage

$$b(x)\frac{\partial S}{\partial x}+\frac{\partial S}{\partial t}=c(x,S) \tag{6.4}$$

where

$$b(x)=-\frac{kz'(x)}{\varepsilon} \tag{6.5}$$

and

$$c(x,S)=rw(x)+\frac{kz''(x)}{\varepsilon}S \tag{6.6}$$

and z' and z'' are first and second derivatives of the bedrock profile curvature function z(x) with respect to x..

In the following the profile curvature function given by Fan and Bras (1998 [13]) will be used.

$$z(x)=H+\beta x+\gamma x^2 \tag{6.7}$$

In Equation (6.7), values of β are always negative, values of $\gamma>0$ define concave profiles, $\gamma<0$ define convex profiles, and for $\gamma=0$ the profile is linear. A potential limitation of Equation (6.7) is that it cannot describe a convexo-concave hillslope profile. Research is on going toward identifying a proper S-shaped function that can be integrated out of (6.5) and (6.6). Furthermore, an exponential formulation for the width function is used, defined as (Troch et al., 2004 [28])

$$w(x)=C\exp(ax) \tag{6.8}$$

In Equation (6.8), *C* defines the width of the hillslope at the divide, and *a* represents the degree of convergence. Values of $a>0$ define divergent shapes, $a<0$ define convergent shapes, and for $a=0$ the shape is rectangular.

Because it has been assumed that the kinematic wave approximation holds, the analysis presented here is limited to moderate to steep slopes. The lower limit of relevant slopes is defined by the ratio of gravity drainage versus diffusion drainage (Beven, 1981 [2]), as well as by the ratio of water table gradients and bedrock gradients (Hilberts et al., 2004 [17]).

Since the kinematic form of Darcy's law has been formulated under the assumption of horizontal flow lines, there exists also an upper limit to the relevant bedrock slopes (Childs, 1971 [7]). However, Hilberts et al. (2004 [17]) have reported good accuracy for the kinematic wave model when applied to steep hillslopes with gradients of 30°.

6.2.1 Analytical solution using the method of characteristics

With the method of characteristics, Equation (6.4) can be written as two ordinary differential equations:

$$\frac{dx}{dt}=b(x)=-\frac{kz'}{\varepsilon}=-\frac{k(\beta+2\gamma x)}{\varepsilon} \tag{6.9}$$

$$\frac{dS}{dx} = \frac{c(x,S)}{b(x)} = -\frac{\varepsilon}{kz'} rw - \frac{z''}{z'} S \tag{6.10}$$

Equation (6.9) describes a family of curves in the (*x*, *t*) plane, called the characteristic curves, and (6.10) describes how the soil moisture wave, *S*, propagates along each curve. Figure 6-2 illustrates the method of the characteristics in the (x,t) plane. In Figure 6-2, T_r indicates the duration of the recharge event, T_c indicates the response time of the hillslope, which depends only on the geometric and hydraulic characteristics of the hillslope, T_1 is the sum of T_c and T_r, and L is length of the hillslope, measured along the horizontal.

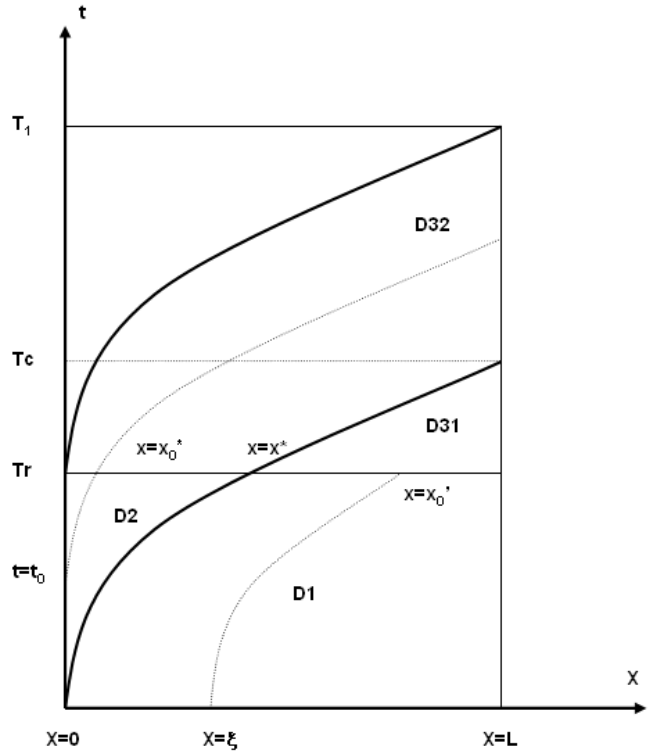

Figure 6-2. (x,t) plane with characteristic curves and domain definition

If the recharge rate *r(t)* is assumed constant during the recharge, an analytical solution for the storage *S* can be obtained. The following initial and boundary Dirichlet conditions were assumed:

$$S(x,0) = g(x) \quad 0 \le x \le L; \quad \text{with } g(0) = 0 \tag{6.11}$$

$$S(0,t) = g(0) = 0, \forall t \tag{6.12}$$

where L defines the length of the hillslope in the horizontal direction. Since the governing equation (6.4) is of first order only, the kinematic waves possess only one system of characteristics. This would also imply that kinematic waves travel in the downstream direction only, and that the solution of the equation does not require a downstream boundary condition. As a result, when the porous medium is cut at x=L by the bed of a stream or lake, it will overpredict the length of the seepage face at the downstream boundary, since it takes no account of downstream effects in the vicinity of the boundary (Beven, 1981 [2]).

The response time of the hillslope is obtained integrating equation (6.9) between x=0 and x=L with time t ranging between t=0 and t=T_c:

$$T_c = -\frac{\varepsilon}{2\gamma k}\ln\left(1+\frac{2\gamma L}{\beta}\right) \quad for\ \gamma \neq 0$$
$$T_c = -\frac{L\varepsilon}{\beta k} \quad for\ \gamma = 0 \qquad (6.13)$$

For $\gamma \neq 0$, the structure of this expression leads to the following geometric constraint

$$1+\frac{2\gamma L}{\beta} > 0$$

Since β is always negative, for convex hillslopes ($\gamma<0$) this inequality is always true, so there is no further constraint on β, γ or L. On the contrary, for concave hillslopes ($\gamma>0$), the constraint on the curvature is

$$\gamma < -\frac{\beta}{2L}\ .$$

The condition $\gamma = -\frac{\beta}{2L}$ represents a situation with horizontal bed for x=L. Note that the solutions investigated here are for absence of surface saturation. This means that the soil moisture capacity always exceeds the computed soil moisture. Analysis of hysteretic behaviour of the relationship between the saturated area and average hillslope soil moisture (Chirico, 2001 [8]; Niedzialek and Ogden, 2004 [22]) is beyond the scope of this study and will be presented in future works.

A condition of partial equilibrium is investigated and three domains are distinguished for soil moisture storage at x=L. The flowing results are obtained by the integration of equation (6.10) across the different characteristic curves through x=L at different time t and taking into account of the different numerical domains:

For $0 \le t \le T_r$ (domain D1 in Figure 6-2):

Domain D1 is defined by the characteristic curve t=t(x,0) and the line t=0 (initial condition), t=T_r, and x=L (outlet of hillslope). The following initial and boundary conditions are valid for domain D1:

$$t(\xi) = 0 \qquad 0 \le \xi \le L$$
$$S(\xi) = g(\xi) \quad 0 \le \xi \le L$$

where ξ is a parameter representing the intersection of a characteristic curve with the x-axis and it is obtained integrating equation (6.9) between x= ξ and x=L:

$$\xi = \left(L+\frac{\beta}{2\gamma}\right)\exp\left(\frac{2k\gamma}{\varepsilon}t\right)-\frac{\beta}{2\gamma} \quad for\ \gamma \neq 0$$
$$\xi = L+\frac{k\beta}{\varepsilon}t \quad for\ \gamma = 0 \qquad (6.14)$$

The solution in the D1 domain is then given by:

$$S(L,t) = -\frac{\varepsilon r}{k}\frac{[A(L) - A(\xi)]}{\beta + 2\gamma L} + g(\xi)\exp\left(\frac{2\gamma k}{\varepsilon}t\right) \; for\, \gamma \neq 0$$
$$S(L,t) = -\frac{\varepsilon r}{k}[A(L) - A(\xi)] + g(\xi) \; for\, \gamma = 0 \qquad (6.15)$$

where A(x) is the uphill drainage area at location x.

For $T_r \le t \le T_c$ (domain D31 in Figure 6-2):

Domain 31 is bounded by the characteristic curve passing through x* (see for definition Figure 6-2) and the curves x=L and t=T_r. The following initial and boundary conditions are valid for this domain:

$t(x_0^{'}) = T_r \quad x^* \le x_0^{'} \le L$

$S(x_0^{'}) = S(x_0^{'}, T_r)$

where $x_0^{'}$ is a parameter representing the intersection of the characteristic curve through ξ and t=T_r and it is obtained integrating equation (6.9) between x= $x_0^{'}$ and x=L:

$$x_0^{'} = \left(L + \frac{\beta}{2\gamma}\right)\exp\left(\frac{2k\gamma}{\varepsilon}(t - T_r)\right) - \frac{\beta}{2\gamma} \; for\, \gamma \neq 0$$
$$x_0^{'} = L + \frac{k\beta}{\varepsilon}(t - T_r) \; for\, \gamma = 0 \qquad (6.16)$$

The solution for this domain is given by:

$$S(L,t) = S(x_0^{'})\frac{\beta + 2\gamma x_0^{'}}{\beta + 2\gamma L} \; for\, \gamma \neq 0$$
$$S(L,t) = S(x_0^{'}) \; for\, \gamma = 0 \qquad (6.17)$$

where $S(x_0^{'}, t)$ is:

$$S(x_0^{'}, t) = -\frac{\varepsilon r}{k}\frac{[A(x_0^{'}) - A(\xi)]}{\beta + 2\gamma x_0^{'}} + g(\xi)\exp\left(\frac{2\gamma k}{\varepsilon}T_r\right), \; for\, \gamma \neq 0$$
$$S(x_0^{'}, t) = -\frac{\varepsilon r}{k}[A(x_0^{'}) - A(\xi)] + g(\xi), \; for\, \gamma = 0 \qquad (6.18)$$

For $T_c \le t \le T_r + T_c$ (domain D32 in Figure 6-2):

Domain D32 is bounded by the characteristic curve passing through x*, the characteristic curve passing through (0,T_r), and the curves x=L and t=T_r. The following initial an boundary conditions are valid for domain D32:

$t(x_0^*) = T_r \quad 0 \le x_0^* \le x^*$

$S(x_0^*) = S(x_0^*, T_r)$

where x_0^* is a parameter representing the intersection of the characteristic curve through t=t_0 and t=T_r:

$$x_0^* = \left(L + \frac{\beta}{2\gamma} \right) \exp\left(\frac{2k\gamma}{\varepsilon} \left(t - T_r \right) \right) - \frac{\beta}{2\gamma},\ for\ \gamma \neq 0$$
$$x_0^* = L + \frac{k\beta}{\varepsilon} \left(t - T_r \right),\ for\ \gamma = 0 \tag{6.19}$$

The solution for this domain is given by:

$$S(L,t) = S\left(x_0^*\right) \frac{\beta + 2\gamma x_0^*}{\beta + 2\gamma L}\ \ for\ \gamma \neq 0$$
$$S(L,t) = S(x_0^*)\ \ for\ \gamma = 0 \tag{6.20}$$

where $S\left(x_0^*, t\right)$ is obtained through the analysis of domain D2 (Figure 6-2).

Domain D2 is bounded by the characteristic curve through $t=t_0$ and $t=T_r$. The following initial an boundary conditions are used for domain D2:

$$\mathrm{t}(0) = \mathrm{t}_0 \quad 0 \le \mathrm{t}_0 \le \mathrm{T}_r$$
$$\frac{\mathrm{dS}}{\mathrm{dx}} = 0, \quad \mathrm{S}(0, \mathrm{t}) = \mathrm{g}(0) \tag{6.21}$$

where t_0 is a parameter representing the intersection of a characteristic curve with the t-axis and it is given by:

$$\mathrm{x} = \frac{\beta}{2\gamma} \left[\exp\left(\frac{2\gamma \mathrm{k}}{\varepsilon} \left(\mathrm{t}_0 - \mathrm{t} \right) \right) - 1 \right] \tag{6.22}$$

$S\left(x_0^*, t\right)$ then is obtained through:

$$S\left(x_0^*, t\right) = -\frac{\varepsilon r}{k} \frac{A\left(x_0^*\right)}{\beta + 2\gamma x_0^*},\ for\ \gamma \neq 0$$
$$S\left(x_0^*, t\right) = -\frac{\varepsilon r}{k} A\left(x_0^*\right),\ for\ \gamma = 0 \tag{6.23}$$

6.2.2 Determination of subsurface discharge at the hillslope outlet

The subsurface flow rate Q(L,t) at the hillslope outlet may be obtained by combining Eq. (6.3) and Eqs (6.15), (6.17) and (6.20). The area A(x) is different in the case of rettangular shape (a=0) and exponential shape (a≠0):

$$A(x) = \int_{\xi}^{x} w dx = \int_{\xi}^{x} c \exp(ax) dx = \frac{c}{a} \left(\exp(ax) - \exp(a\xi) \right) \text{ for } a \neq 0 \tag{6.24}$$

$$A(x) = cx \text{ for } a = 0 \tag{6.25}$$

When the exponential formulation of Eq. (6.8) is used to describe the width function, the following solutions are obtained:

For $0 \le t \le T_r$

$$Q(L,t)=-\frac{k}{\varepsilon}(\beta+2\gamma L)\left[g(\xi)\exp\left(\frac{2\gamma k}{\varepsilon}t\right)-\frac{\varepsilon rc}{ka}\frac{\exp(aL)-\exp\left(a\left(\frac{\beta}{2\gamma}+L\right)\exp\left(\frac{2\gamma k}{\varepsilon}t\right)-\frac{\beta}{2\gamma}\right)}{\beta+2\gamma L}\right]\quad\gamma\neq 0$$

(6.26)

$$Q(L,t)=r\left[\frac{c}{a}\left(\exp(aL)-\exp\left(a\left(L+\frac{k\beta t}{\varepsilon}\right)\right)\right)\right]+g(\xi)\quad\gamma=0$$

for $g(\xi)=0$ one obtains

$$Q(L,t)=\frac{rc}{a}\left(\exp(aL)-\exp\left(a\left(\left(\frac{\beta}{2\gamma}+L\right)\exp\left(\frac{2\gamma k}{\varepsilon}t\right)-\frac{\beta}{2\gamma}\right)\right)\right)\quad\gamma\neq 0 \qquad (6.27)$$

$$Q(L,t)=r\left[\frac{c}{a}\left(\exp(aL)-\exp\left(a\left(L+\frac{k\beta t}{\varepsilon}\right)\right)\right)\right]\quad\gamma=0$$

For $T_r\le t\le T_c$

$$Q(L,t)=-\frac{k}{\varepsilon}(\beta+2\gamma L)\left(\left(-\frac{\varepsilon rc}{ka}\frac{\left[\exp\left(a\left(\left(\frac{\beta}{2\gamma}+L\right)\exp\left(\frac{2\gamma k}{\varepsilon}(t-T_r)\right)-\frac{\beta}{2\gamma}\right)\right)-\exp\left(a\left(\left(\frac{\beta}{2\gamma}+L\right)\exp\left(\frac{2k\gamma}{\varepsilon}t\right)-\frac{\beta}{2\gamma}\right)\right)\right]}{\beta+2\gamma L}\right)+g(\xi)\exp\left(\frac{2\gamma k}{\varepsilon}T_r\right)\right)\quad\gamma\neq 0$$

$$Q(L,t)=r\left[\frac{c}{a}\left(\exp\left(a\left(L+\frac{k\beta}{\varepsilon}(t-T_r)\right)\right)-\exp\left(a\left(L+\frac{k\beta t}{\varepsilon}\right)\right)\right)\right]+g(\xi)\quad\gamma=0 \qquad (6.28)$$

for $g(\xi)=0$ one obtains

$$Q(L,t)=\frac{rc}{a}\left(\exp\left(a\left(\left(\frac{\beta}{2\gamma}+L\right)\exp\left(\frac{2\gamma k}{\varepsilon}(t-T_r)\right)-\frac{\beta}{2\gamma}\right)\right)-\exp\left(a\left(\left(\frac{\beta}{2\gamma}+L\right)\exp\left(\frac{2k\gamma}{\varepsilon}t\right)-\frac{\beta}{2\gamma}\right)\right)\right)\quad\gamma\neq 0$$

$$Q(L,t)=r\left[\frac{c}{a}\left(\exp\left(a\left(L+\frac{k\beta}{\varepsilon}(t-T_r)\right)\right)-\exp\left(a\left(L+\frac{k\beta t}{\varepsilon}\right)\right)\right)\right]\quad\gamma=0 \qquad (6.29)$$

For $T_c\le t\le T_r+T_c$

$$Q(L,t)=\frac{rc}{a}\left(\exp\left(a\left(\left(\frac{\beta}{2\gamma}+L\right)\exp\left(\frac{2\gamma k}{\varepsilon}(t-T_r)\right)-\frac{\beta}{2\gamma}\right)\right)-1\right) \quad \gamma\neq 0$$

$$Q(L,t)=r\left[\frac{c}{a}\left(\exp\left(a\left(L+\frac{k\beta}{\varepsilon}(t-T_r)\right)\right)-1\right)\right] \quad \gamma=0 \tag{6.30}$$

which is obviously independent from initial conditions.

6.2.3 Determination of the hillslope saturated moisture content

The hillslope saturated moisture content at time t, V(t), may be obtained by applying the mass conservation equation over the hillslope. However, the general solution for the hillslope saturated moisture content involves nonelementary integrals (i.e., there is no explicit formula in terms of elementary functions for the antiderivative). Owing to this reason, analytical solutions are provided here for two elementary cases: i) a=0, which represents a rectangular hillslope with any profile that conforms to Eq. (6.7), and ii) γ=0, which represents a planar hillslope with any planform that conforms to Eq. (6.8). These solutions are as follows:

For $0 \le t \le T_r$

$$\begin{aligned} a=0: &\quad V(Q(L,t))=V(0)-\frac{\varepsilon}{2\gamma k}Q(L,t)-rc\frac{\beta}{2\gamma}t \\ \gamma=0: &\quad V(Q(L,t))=V(0)-\frac{\varepsilon}{a\beta k}Q(L,t)-\frac{rc}{a}t \end{aligned} \tag{6.31}$$

For $T_r \le t \le T_c$

$$\begin{aligned} a=0: &\quad V(Q(L,t))=V(T_r)-\frac{\varepsilon}{2\gamma k}\left[Q(L,t)-Q(L,T_r)\right] \\ \gamma=0: &\quad V(Q(L,t))=V(T_r)-\frac{\varepsilon}{a\beta k}\left[Q(L,t)-Q(L,T_r)\right] \end{aligned} \tag{6.32}$$

For $T_c \le t \le T_r + T_c$

$$\begin{aligned} a=0: &\quad V(Q(L,t))=V(T_c)-\frac{\varepsilon}{2\gamma k}\left[Q(L,t)-Q(L,T_c)\right]+rc\frac{\beta}{2\gamma}(t-T_c) \\ \gamma=0: &\quad V(Q(L,t))=V(T_c)-\frac{\varepsilon}{a\beta k}\left[Q(L,t)-Q(L,T_c)\right]+\frac{rc}{a}(t-T_c) \end{aligned} \tag{6.33}$$

For the other cases, involving values of both a and γ different from zero, solutions will be provided in the following by means of numerical integration.

Inspection of the structure of Eq. (6.31)-(6.33) shows that the maximum value for the hillslope saturated moisture content (V_{max}) corresponds to a recharge duration at least equal to the T_c. It is interesting to note that the dimensionless hillslope saturated moisture content, obtained as $\sigma(t)=V(t)/V_{max}$, is function of the geometric parameters and of the dimensionless time $\tau=t/T_c$, and outflow $\varphi(t)=Q(L,t)/Q_{max}$, as follows (for $T_r=T_c$):

for $0 \le \tau \le 1$

$$a = 0: \quad \sigma(\tau) = \varphi(\tau)\left(\frac{2\frac{\gamma L}{\beta}}{2\frac{\gamma L}{\beta} - \ln\left(2\frac{\gamma L}{\beta}+1\right)}\right) - \tau\left(\frac{\ln\left(2\frac{\gamma L}{\beta}+1\right)}{2\frac{\gamma L}{\beta} - \ln\left(2\frac{\gamma L}{\beta}+1\right)}\right) \tag{6.34}$$

$$\gamma = 0: \quad \sigma(\tau) = \varphi(\tau)\left(\frac{\exp(aL)-1}{\exp(aL)-1-aL}\right) - \tau\left(\frac{aL}{\exp(aL)-1-aL}\right)$$

for $1 \le \tau \le 2$

$$a = 0: \quad \sigma(\tau) = 1 + (\varphi(\tau)-1)\left(\frac{2\frac{\gamma L}{\beta}}{2\frac{\gamma L}{\beta} - \ln\left(2\frac{\gamma L}{\beta}+1\right)}\right) + (\tau-1)\left(\frac{\ln\left(2\frac{\gamma L}{\beta}+1\right)}{2\frac{\gamma L}{\beta} - \ln\left(2\frac{\gamma L}{\beta}+1\right)}\right) \tag{6.35}$$

$$\gamma = 0: \quad \sigma(\tau) = 1 + (\varphi(\tau)-1)\left(\frac{\exp(aL)-1}{\exp(aL)-1-aL}\right) + (\tau-1)\left(\frac{aL}{\exp(aL)-1-aL}\right)$$

6.2.4 Dimensional inspection

This section aims to analyse the general character of topographic control on hillslope response. The objective here is to derive geometrical similarity parameters which can be used to understand landscape topographic control on hillslope response. Two ubiquitous parameters found in the previous sections are:

$$\alpha = aL$$

$$\psi = \ln\left(\frac{2\gamma L}{\beta}+1\right)$$

The divergency parameter α is related to the plan shape of the hillslope: values of $\alpha>0$ define divergent shapes, $\alpha<0$ define convergent shapes, and for $\alpha=0$ the shape is rectangular. The convexity parameter ψ is related to the curvature profile of the hillslope: values of $\psi<0$ define concave profiles, $\psi>0$ define convex profiles, and for $\gamma=0$ the profile is linear.

Using these parameters and the dimensionless variables already introduced in Section 6.2.3, it is possible to write Equations (6.26)-(6.30) in a compact manner as follows (for $T_r=T_c$):

$$\begin{aligned}
&\text{for } 0 \le \tau \le 1 \\
&\varphi(\tau) = \frac{1-\exp\left(-\alpha\left(\frac{1-\exp(-\psi\tau)}{1-\exp(-\psi)}\right)\right)}{1-\exp(-\alpha)} \\
&\text{for } 1 \le \tau \le 2 \\
&\varphi(\tau) = \frac{\exp\left(-\alpha\left(\frac{1-\exp(-\psi(\tau-1))}{1-\exp(-\psi)}\right)\right)-\exp(-\alpha)}{1-\exp(-\alpha)}
\end{aligned} \tag{6.36}$$

By taking the limit of divergency $\alpha \to 0$ we obtain

$$\begin{aligned}
&\text{for } 0 \le \tau \le 1 \\
&\varphi(\tau) = \frac{1-\exp(-\psi\tau)}{1-\exp(-\psi)} \\
&\text{for } 1 \le \tau \le 2 \\
&\varphi(\tau) = \frac{\exp(-\psi(\tau-1))-\exp(-\psi)}{1-\exp(-\psi)}
\end{aligned} \tag{6.37}$$

while, symmetrically, for convexity $\psi \to 0$, we obtain

$$\begin{aligned}
&\text{for } 0 \le \tau \le 1 \\
&\varphi(\tau) = \frac{1-\exp(-\alpha\tau)}{1-\exp(-\alpha)} \\
&\text{for } 1 \le \tau \le 2 \\
&\varphi(\tau) = \frac{\exp(-\alpha(\tau-1))-\exp(-\alpha)}{1-\exp(-\alpha)}
\end{aligned} \tag{6.38}$$

Finally, for both $\alpha \to 0$ and $\psi \to 0$ we obtain the dimensionless outflow for a planar and rectangular hillslope, as follows:

$$\begin{aligned}
&\text{for } 0 \le \tau \le 1 \\
&\varphi(\tau) = \tau \\
&\text{for } 1 \le \tau \le 2 \\
&\varphi(\tau) = 2-\tau
\end{aligned} \tag{6.39}$$

Equations (6.34)-(6.35) are then written as follows:

$$\begin{aligned}
&\text{for } 0 \le \tau \le 1 \\
&\text{a} = 0: \quad \sigma(\tau) = \varphi(\tau)\left(\frac{\exp(\psi)-1}{\exp(\psi)-1-\psi}\right) - \tau\left(\frac{\psi}{\exp(\psi)-1-\psi}\right) \\
&\gamma = 0: \quad \sigma(\tau) = \varphi(\tau)\left(\frac{\exp(\alpha)-1}{\exp(\alpha)-1-\alpha}\right) - \tau\left(\frac{\alpha}{\exp(\alpha)-1-\alpha}\right) \\
&\text{for } 1 \le \tau \le 2
\end{aligned} \tag{6.40}$$

$$a=0:\quad \sigma(\tau)=1+(\varphi(\tau)-1)\left(\frac{\exp(\psi)-1}{\exp(\psi)-1-\psi}\right)+(\tau-1)\left(\frac{\psi}{\exp(\psi)-1-\psi}\right)$$
$$\gamma=0:\quad \sigma(\tau)=1+(\varphi(\tau)-1)\left(\frac{\exp(\alpha)-1}{\exp(\alpha)-1-\alpha}\right)+(\tau-1)\left(\frac{\alpha}{\exp(\alpha)-1-\alpha}\right) \tag{6.41}$$

Since both the dimensionless outflow and volume may be expressed in terms of the variables α, ψ and τ, these results show that the dimensionless hillslope response depends only on the variables α and ψ. The dimensionless geometrical parameters α and ψ define therefore the hydrological similarity between hillslopes with respect to their characteristics response.

6.3 Analysis of the hysteretic behaviour for basic hillslope types

This section is devoted to the analysis of the relationship between the hillslope water content and the subsurface discharge at the base of the hillslope for various hillslope shapes. For this purpose, we analyse nine hillslopes defined by the parameters reported in Table 6-1. As suggested by Dikau (1989 [10]) and following Troch et al. (2002 [28]), these hillslopes are obtained by combining three plan and three profile curvatures, thus defining nine basic geometric relief forms (Figure 6-3). It has been assumed L=100 m, k=1 mh^{-1} , ε=0.3, r=1 mmh^{-1} and dry initial conditions. With this choice of hydraulic and geometrical parameters, the nine hillslope have the same response time T_c (equal to 164.8 h) and same area (equal to 3000 m^2). The drop in elevation between divide and outlet is 20m for cases 1, 3, 4, 6, 7 and 9; it is 18.2 m for cases 2, 5 and 8. For each hillslope, we examined response to 4 different recharge events, characterised by the same intensity and by duration equal to 0.25 T_c , 0.50 T_c , 0.75 T_c and 1.00 T_c , respectively.

Table 6-1. Geometrical parameters for the nine slopes

Nr	profile	plan	β (-)	γ (m^{-1})	C(m)	a(m^{-1})
1	Conc down	Divergent	-0.3	0.001	3.	0.036
2	Straight	Divergent	-0.182	0	3.	0.036
3	Conc up	Divergent	-0.1	-0.001	3.	0.036
4	Conc down	Straight	-0.3	0.001	30.	0
5	Straight	Straight	-0.182	0	30.	0
6	Conc up	Straight	-0.1	-0.001	30.	0
7	Conc down	Convergent	-0.3	0.001	120.	-0.038
8	Straight	Convergent	-0.182	0	120.	-0.038
9	Conc up	Convergent	-0.1	-0.001	120.	-0.038

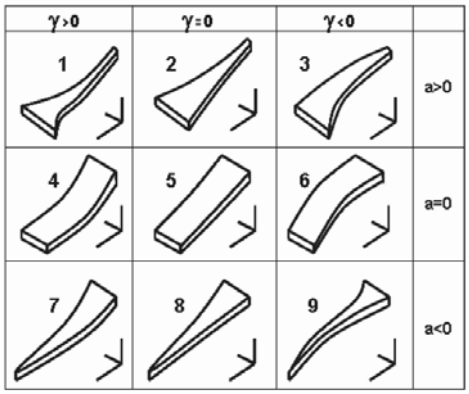

Figure 6-3. Three-dimensional view of the nine hillslopes considered in this study.

By using the analytical relationships presented in Section 6.2.3, and numerical integration for the cases with both a and γ different from zero, we derived the relationships between discharge and volume for the nine hillslopes. Figure 6-4 and Figure 6-5 summarise the main results from this experiment reporting the time series of outflow and soil moisture volume (Figure 6-4) and the looped response trajectories in the storage-flux (V-Q) plot (Figure 6-5) for the nine hillslopes. Figure 6-6 describes the trajectories of the dimensionless variables φ(t) and σ(t), for cases 1, 3, 7 and 9.

As expected, slope 5 shows the typical ramp response function for outflow. The diverging slopes (cases 1, 2 and 3) and, though to a lesser extent, even the straight and convex slope (case 6) have approximately a first-order step response function for subsurface drainage. This response is characterised by a quick rise at the beginning of the recharge event and a slow increase towards the end. The other hillslopes show exponential growth for outflow, with a slow increase at the beginning of the recharge event and a faster rise towards the end.

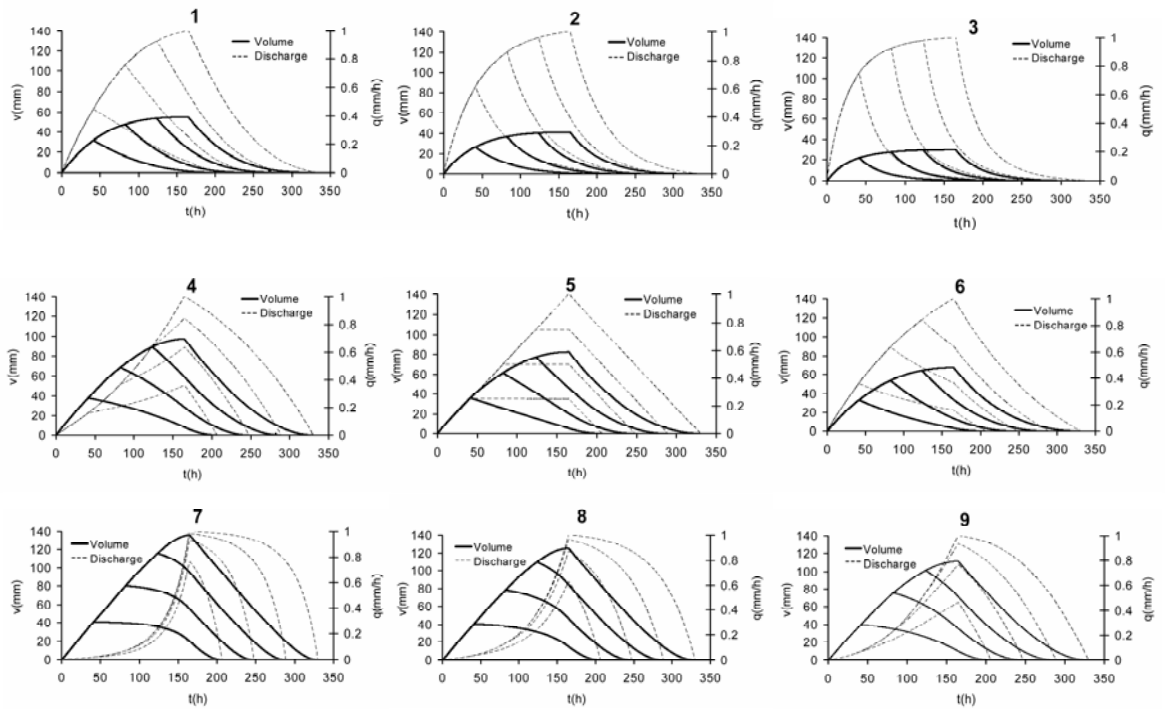

Figure 6-4. Time series of subsurface flow rates and hillslope saturated moisture content for the nine hillslopes

The hillslope saturated moisture content time series always display a pattern which approximates a first-order step response. This is very marked for diverging slopes and much less for converging slopes, with straight slopes exhibiting an intermediate behaviour. As a result, diverging slopes show an almost parallel pattern for outflow and saturated moisture content time series, both in the wetting and in the drying phase. This has a marked effect on both the maximum saturated moisture content and on the hysteretic behaviour, which decrease with increasing the degree of divergence. On the contrary, outflow and saturated moisture content exhibit a contrasting time pattern for converging slopes. Outflow increases very slowly (quickly) at the onset (end) of the recharge event, whereas moisture tend to follow a more steady increase throughout the recharge. The different patterns in volume and discharge time series translate in very distinct response trajectories in the storage-flux (V-Q) plot, with a marked hysteretic effect. This effect, as well as the maximum saturated moisture content, increases with increasing the degree of convergence.

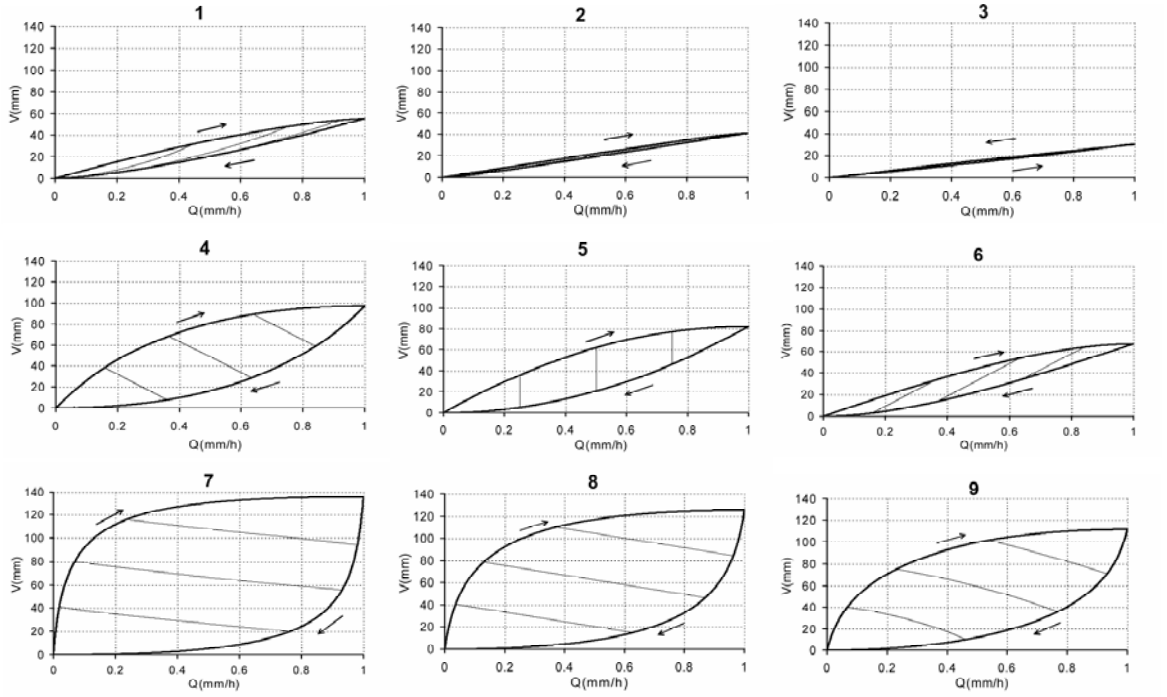

Figure 6-5. Storage-flux relationships for the nine hillslopes

In Figure 6-5 all slopes but case 3 exhibit clockwise hysteretic loop in the V-Q plot. It is interesting to note that the clockwise loop patterns are consistent with those reported by Ewen and Birkinshaw (2006 [12]) for storage-discharge plots based on runoff data from the Slapton Wood basin in UK. However, it should be noted that basin-scale hysteresis is controlled by the combination of hysteretic effects of hillslopes with different geometric configurations. Therefore, it is not easy to compare hysteretic effects observed at the basin scale with those emerging at the hillslope scale. Only slope 3, characterised by a combination of gradual divergence and convex profile curvature, shows a partly anticlockwise hysteretic loop.

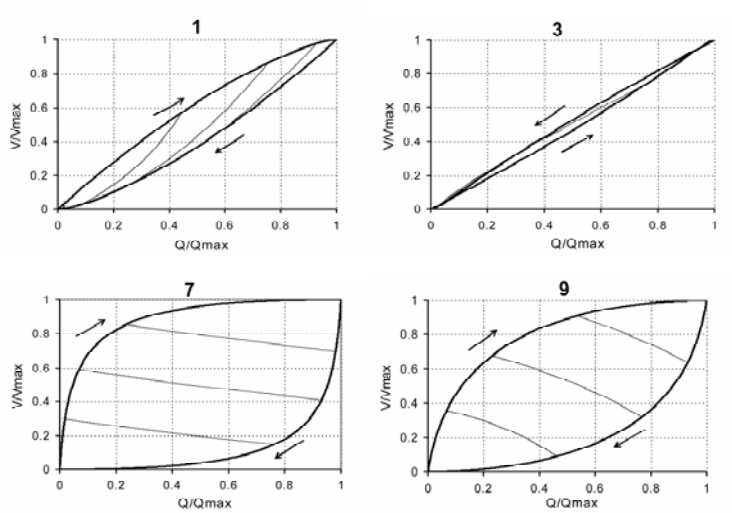

Figure 6-6. Normalised storage ($\sigma(t)=V(t)/V_{max}$) versus flux ($\varphi(t)=Q(L,t)/Q_{max}$) relationships for the hillslopes 1, 3, 7 and 9.

The hysteretic effect is controlled essentially by the different patterns of saturated soil moisture S(x,t) along the slope during the rising and falling limb. During the rising limb, saturated soil moisture increases downhill starting from the divide. During the falling limb, a drying wave propagates downhill starting from the divide, and the saturated profile slides down the bed. Owing to this reason, the patterns of S(x,t) will always be different during the rising and falling limb. Furthermore, for a given value of S(L), i.e., for a given value of discharge at the outlet, the mean value of the corresponding saturated soil moisture pattern will be generally less during the falling limb than during the rising limb, thus giving rise to the clockwise hysteretic effect reported in Figure 6-5.

Different trajectories are also associated to the response to recharge events with duration less than response time. As implied by Eq. (6.32), the relationship between discharge and volume is linear for cases 2, 4, 6 and 8, with a positive slope for cases 2 and 6, and a negative slope for cases 4 and 8. More generally, for hillslopes 1, 2, 3 and 6, the trajectory for the period comprised between the end of the recharge and the response time is associated to a decrease of both discharge and volume. For hillslope 5 the outflow stays constant during this period, as expected, while storage decreases. For remaining hillslopes 4, 7 8 and 9, this trajectory shows a decrease of storage and an increase of discharge.

The area of the loop in the dimensionless form of the hysteresis relationship (Figure 6-6) can be used to quantify the hysteretic behaviour. Following Hayden et al. (1986 [16]) and Mishra and Seth (1996 [21]), the area is expressed mathematically as:

$$\eta = \frac{1}{2}\int_0^2 \left(\varphi \frac{d\sigma}{d\tau} - \sigma \frac{d\varphi}{d\tau} \right) d\tau \tag{6.42}$$

The hysteresis η has been therefore computed for a range of values of α, ψ. This relationship is plotted in terms of α, ψ, (Figure 6-7). Figure 6-7 reports also the hysteresis for the hillslopes 1-9 discussed above.

The plot generalises the findings obtained above for the nine hillslope geometries. Slopes exhibit generally clockwise hysteretic loop in the V-Q plot. Hysteresis increases with decreasing α and ψ, i.e. with increasing convergence (for the shape) and concavity

(for the profile). The rate of change of hysteresis is relatively large at small values of α and ψ, then decreases with decreasing the values of the two dimensionless variable. Hysteresis approaches 1 as either α or ψ approaches negative infinity. This shows that by increasing convergence (for the shape) and concavity (for the profile) the hillslope response increases the exponential growth at later stages of the recharge, while saturated moisture content tends to increase linearly with time.

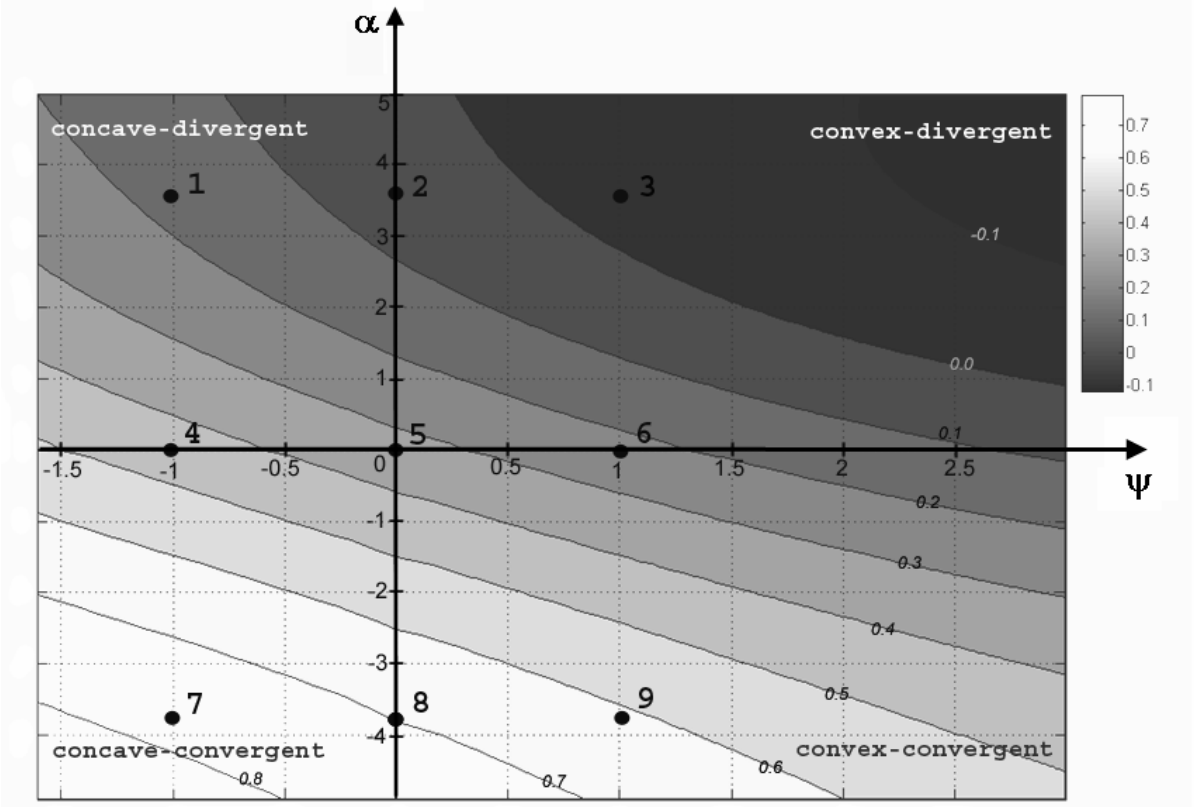

Figure 6-7. The α - ψ plot, with hysteresis η as function of the hillslope similarity parameters α and ψ.

For relatively large values of α and ψ the hysteresis may take negative values, i.e. the loop cycle may reverse his sign from clock-wise to anticlock-wise.

Note that the hysteresis in the α - ψ plan defines a symmetrical pattern relative to 45° axis. A characteristic point in the plot is that resulting for the planar and rectangular hillslope, i.e. for α= ψ=0. For this case, the hysteresis η amounts to $0.\overline{3}$.

6.4 Determination of the hillslope similarity parameters for three natural hillslopes

The hillslope similarity parameters were determined for three hillslopes located in the experimental mountainous Vauz basin in the Eastern Italian Alps (Figure 6-8; Figure 6-9). This is a very steep environment with altitude ranging between 1800 and 3100 m a.s.l. (Borga et al., 2002 [5]; Penna et al., 2007 [25]). Application of the theory to these hillslopes provides an opportunity to examine how natural topographies are represented by the two hillslope hydrological similarity parameters.

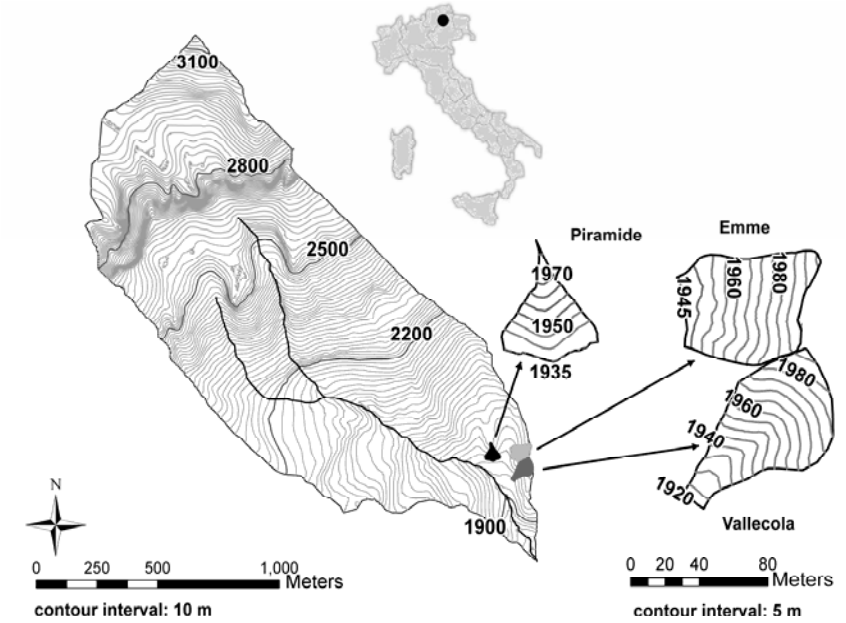

Figure 6-8. Rio Vauz basin and localization of the three natural hillslopes

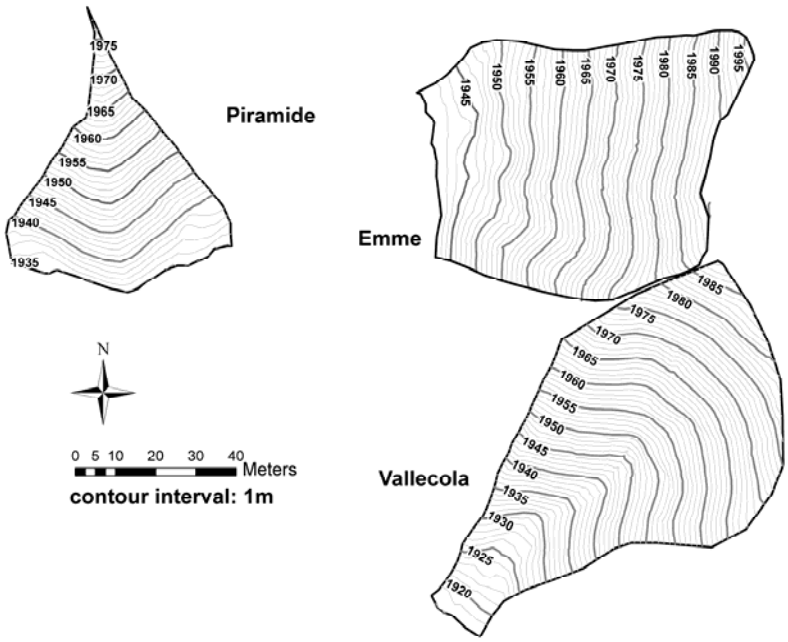

Figure 6-9. Topography of the three natural hillslopes

The hillslopes have been named “Piramide” (“Pyramid”), “Emme” and “Vallecola” (“Hollow”), after their main morphological feature, with area of 0.12, 0.37 and 0.36 ha, respectively. Topography is mainly convex (Piramide), planar (Emme) and concave (Vallecola) (Figure 6-9). Gradients range between around 1:5 to 1:1,1. A detailed digital elevation model (DEM) with a 1 m resolution is available for these hillslopes. We check the plausibility of using a second order polynomial function to describe the bedrock slope and an exponential function to describe the variation of the width of the hillslope as

function of distance downslope. The hillslope convergence rate *a* was determined from the area of each hillslope *A* and from the hillslope width at the divide *C* based on the relationship

$$A = \frac{C}{a}\left(\exp aL - 1\right) \tag{6.43}$$

This approach is preferable with respect to regression of hillslope width against downslope distance, since it ensures mass conservation. While regression of width against downslope distance minimizes the squared differences between observed and modelled widths, use of Eq. 6.43 identifies the function that, starting by the observed hillslope width at the divide (or at the base of the hillslope), has the area under the function equal to the observed one. The fit of these equations to measures of both hillslope elevation and hillslope width for the three hillslopes is described in Figure 6-10, with correlation always exceedings 0.99 for the second order polynomial and ranging from 0.75 to 0.95 for the exponential width function. This shows that the polynomial function describes adequately the hillslope elevations. Hillslope width is adequately described by the exponential function for Emme and Vallecola, while a lower accuracy is demonstrated for Piramide. In the case of Piramide, width measures close to the hillslope peak are rather small compared to DEM resolution. It is likely that errors in these measures contribute to the lower accuracy demonstrated in this case. The geometric parameters of the polynomial function and of the exponential function are reported in Table 6-2. In Table 6-2., the parameter C1 is the measured width at the hillslope base. Based on these geometric parameters, the hillslope similarity parameters were computed for the three hillslope (Table 6-3) and plotted in Figure 6-11. This figure shows how the two hillslope similarity parameters capture the essential geometric features of each hillslope. First of all, it can be seen that the three hillslopes fall within or close to the geometric space identified by the nine basic relief forms analysed in Section 6.3. Both similarity parameters are positive for Piramide, with the α divergency parameter larger than the ψ convexity parameter. This indicates that for this relief form divergency dominates over convexity. Emme is shown to be a relatively planar hillslope, with slightly negative values for both similarity parameters. Negative and relatively similar parameter values are reported for Vallecola, which is therefore identified as a convergent and concave hillslope, as expected. These findings show that the two hillslope similarity parameters can be effectively used to partition the landscape into converging and diverging hillsides, defining the hydrological similarity between hillslopes with respect to their characteristic response and hysteresis.

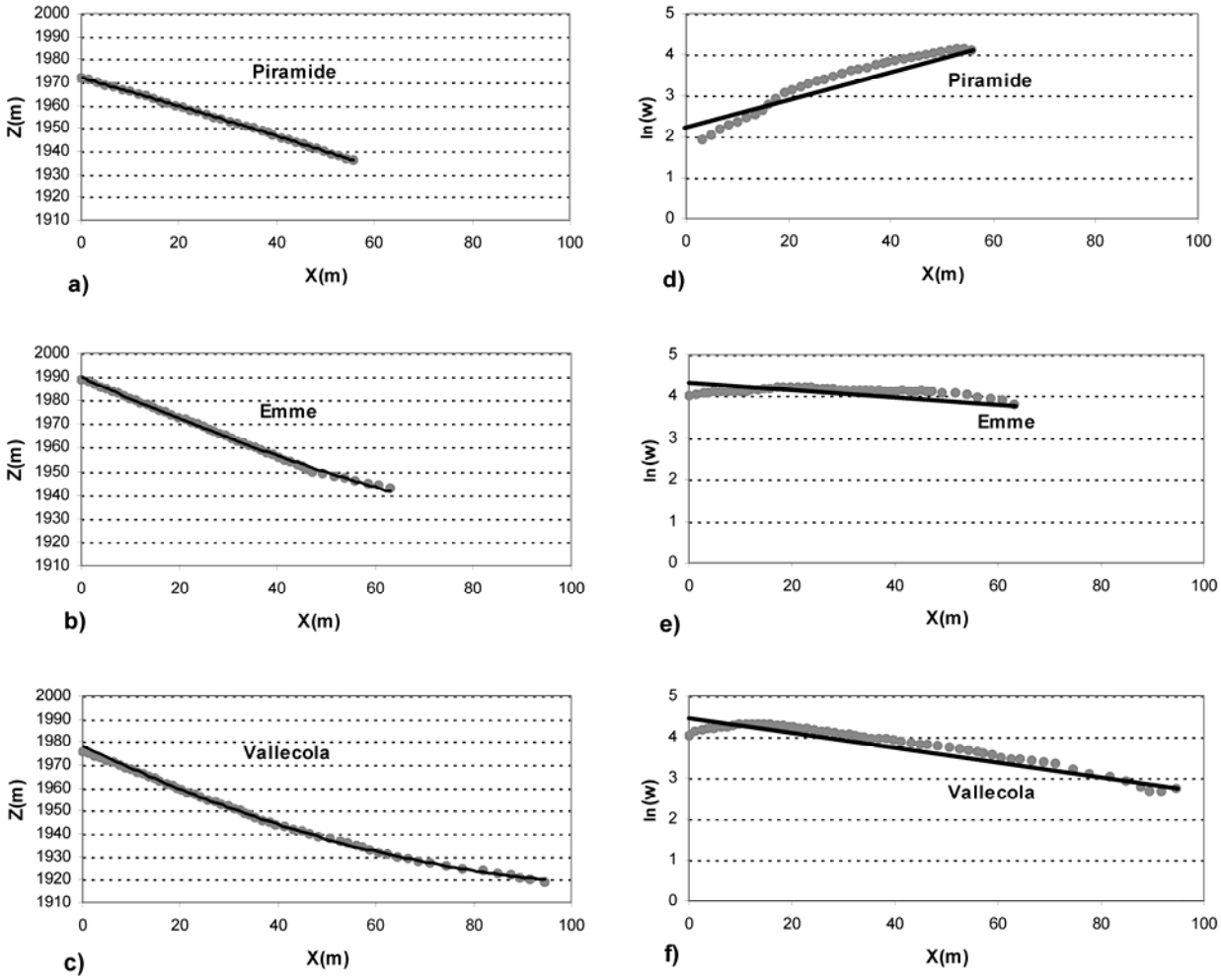

Figure 6-10. The centroid profiles (a,b,c) and the width of hillsopes (d,e,f) and their representation by means of the second order polynomial function (for profile) and the exponential function(for width).

Table 6-2. Geometrical parameters for the three natural slopes

Hillslope	A (m^2)	C_1 (m)	L (m)	a(m^{-1})	β(-)	γ(m^{-1})
Piramide	1565	60.52	55.8	0.032	-0.603	-0.0008
Emme	3756	55.94	63	-0.0021	-0.937	0.0026
Vallecola	3613	15.7	94.5	-0.0169	-0.965	0.0038

Table 6-3. Hillslope similarity parameters for the three natural hillsplopes

Hillslope	α(-)	ψ(-)
Piramide	1.786	0.138
Emme	-0.132	-0.430
Vallecola	-1.597	-1.363

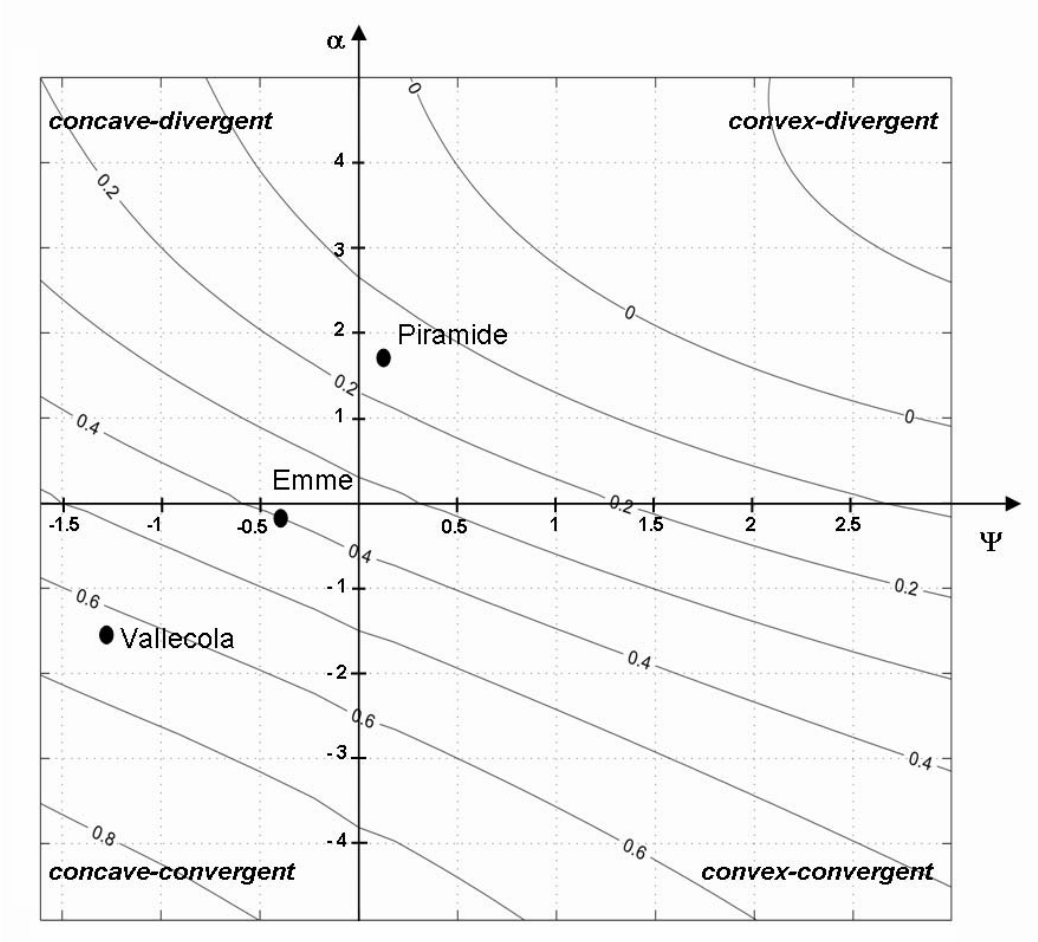

Figure 6-11. The hillslope similarity parameters α and ψ for the three natural hillsplopes.

6.5 Concluding remarks

In this chapter general analytical solutions to the hillslope-storage kinematic wave equation for subsurface flow have been presented. These solutions allow the computation of characteristic response functions for every type of hillslopes which can be described by using a second order polynomial function for the profile and an exponential equation for the width function. The hillslope-storage subsurface flow equation takes into account the topographic controls exerted on the flow processes by the plan shape and profile curvature. The found analytical solution provides a physical basis for deriving two geometric parameters α and ψ which define the hydrological similarity between hillslopes with respect to their characteristic response and hysteresis. Therefore, each hillslope may be represented in a α - ψ plot which allows to derive essential information on its response.

The hysteresis η, quantified by the area of the hysteretic dimensionless loop, has been therefore computed for a range of values of parameters α and ψ. Slopes exhibit generally clockwise hysteretic loop in the flux-storage plot. It has been found that hysteresis increases with decreasing α and ψ, i.e. with increasing convergence (for the shape) and concavity (for the profile), and viceversa. For relatively large values of α and ψ

the hysteresis may take a complex pattern, with combination of clock-wise to anticlock-wise loop cycles.

The analytical solutions like those provided here offer essential insights in the functioning of hillslopes and may form the basis of hillslope similarity analysis.

The validity of these results is restricted by: (1) the kinematic wave assumption of subsurface flow, (2) the assumption of specific functions for hillslope profile and width, (3) the assumption of spatially homogeneous hydraulic characteristics of the hillslopes, (4) the assumption that capillarity effects in the unsaturated zone above the phreatic layer can be neglected, (5) recharge is spatially uniform, and (6) the soil moisture capacity always exceeds the computed soil moisture. Because of the kinematic wave assumpion, the analysis presented here is limited to moderate to steep slopes. The lower limit of relevant slopes is defined by the ratio of gravity drainage versus diffusion drainage, as well as by water table gradients. Since the kinematic form of Darcy's law has been formulated under the assumption of horizontal flow lines, there exists also an upper limit to the relevant bedrock slopes (Childs, 1971 [7]).

Example applications have been described for three hillslopes in the eastern Italian Alps. These applications tested the suitability of the analytical functions to describe the plan and curvature shapes of natural hillslope and provided an opportunity to examine how natural topographies are represented by the two hillslope hydrological similarity parameters.

It is important to note that the type of hysteretic behaviour investigated here is limited to the saturated component of the hillslope response and does not include the unsaturated component. The contribution of unsaturated component will delay significantly the response (Beven, 1982 [3]) and as such it may modify significantly the hysteretic behaviour considered here.

It is likely that the strong hysteretic effect emerging for convergent-concave hillslopes will be limited by saturation effects when the soil moisture capacity is less than the computed soil moisture. As the water table swells, this increases the groundwater-surface water contact areas and results in enhanced outflow. This enhanced flow will reduce the hillslope storage, completing the negative feedback and bringing itself to the original state faster than otherwise (Eltahir and Yeh, 1999 [11]).

Further research is being carried out to extend the analytical framework to consider the unsaturated component of the hillslope response and to validate the hillslope geometrical similarity numbers defined here as hillslope subsurface flow similarity parameter by confrontation with experimental data. Further work on hysteresis is being conducted on deriving the relationship between saturated area and subsurface outflow. Finally, this analysis has been conducted at the hillslope scale and the scaling from hillslopes to basins deserves further investigation. This may take the form of analysis of hysteresis of a population of individual hillslopes, each defined with its geometrical parameters.

6.6 References

[1] Beven, K., 1977. Hillslope hydrograph by the finite element method. Earth Surf. Processes, 2, 13-28.

[2] Beven, K., 1981. Kinematic subsurface stormflow. Water Resour. Res., 17(5),1419–24.

[3] Beven, K.J., 1982. On subsurface stormflow: predictions with simple kinematic theory for saturated and unsaturated flows. Water Resour. Res., 18(6), 1627-1633.

[4] Beven, K., 2006. Searching for the Holy Grail of Scientific Hydrology: Qt=H(S, R)A as closure. Hydrol. Earth Syst. Sci. Discuss., 3, 769–792.

[5] Borga, M., Dalla Fontana, G., Gregoretti, C., Marchi, L., 2002. Assessment of shallow landsliding by using a physically based model of hillslope stability. Hydrological Processes, 16, 2833-2851.

[6] Chapman, T. G., Ong, G., 2006. A new equation for shallow groundwater flow over a curved impermeable boundary: Numerical solutions and laboratory tests. Water Resour. Res., 42, W03427, doi:10.1029/2005WR004437.

[7] Childs, E.C., 1971. Drainage of groundwater resting on a sloping bed. Water Resour. Res., 7(5), 1256–63.

[8] Chirico, G.B., 2001. Terrain-based distributed modeling for investigating scale issues in hydrology. PhD dissertation. Department of Hydrologic Engineering, Università Degli Studi di Napoli Federico II.

[9] Di Stefano, C., Ferro, V., Porto, P., Tusa,. G., 2000. Slope curvature influence on soil erosion and deposition. Water Resoir.Res., 36, 607-617.

[10] Dikau, R., 1989. The application of a digital relief model to landform analysis in geomorphology. In: Raper J, editor. Three dimensional applications in geographical information systems. London: Taylor and Francis; 1989, 51–77.

[11] Eltahir, E. A. B., Yeh, P. J. F., 1999. On the asymmetric response of aquifer water level to floods and droughts in Illinois. Water Resou. Res., 35(4): 1199-1217.

[12] Ewen, J. Birkinshaw, S.J., 2006. Lumped hysteretic model for subsurface stormflow developed using downward approach. Hydrological Processes, DOI: 10.1002/hyp.6344

[13] Fan, Y., Bras, R.L, 1998. Analytical solutions to hillslope subsurface storm flow and saturation overland flow. Water Resour. Res., 34(4):921-927.

[14] Flynn, D., McNamara, H., O'Kane, P., Pokrovskii, A., 2003. Application of the Preisach model in soil-moisture hysteresis, BCRI preprint 15. In: G. Bertotti and I.D. Mayergoyz (eds.), The Science of Hysteresis, Elsevier, London.

[15] Haynes, W.B., 1930. Studies in the physical properties of soil: V. The hysteresis effect in capillary properties, and the modes of moisture associated therewith, J. Agric. Sci. 20, 97-116.

[16] Hayden, H. W., Moffatt, W. G., Wulff, J., 1986. The structure and properties of materials: mechanical behaviour. Vol. III, Wiley Eastern Limited, New Delhi.

[17] Hilberts, A.G.J., van Loon, E.E., Troch, P.A., Paniconi, C., 2004. The hillslope-storage Boussinesq model for non-constant bedrock slope. Journal Hydrol., 291, 160–173.

[18] Horton, R. E., 1936. Maximum groundwater levels. Trans. Am. Geophys. Union. 17(2), 344–357.

[19] Kendall, K.A., Shanley, J.B., McDonnell, J.J., 1999. A hydrometric and geochemical approach to test the transmissivity feedback hypothesys during snowmelt. J. Hydrol., 219, 188-205.

[20] Myrabø, S., 1997. Temporal and spatial scale of response area and groundwater variation in till. Hydrol. Proces., 11(14), 1861-1880.

[21] Mishra, S. K., Seth, S. M., 1996. Use of hysteresis for defining the nature of flood wave propagation in natural channels. Hydrological Sci. J., 41(2), 153–170.

[22] Niedzialek, J.M., Ogden, F.L., 2004. Numerical investigation of saturated source area behavior at the small basin scale. Advances in Water Resources 27 (2004) 925–936.

[23] Norbiato, D., Borga, M., 2008b. Analysis of hysteretic behaviour of a hillsplope-storage kinemtaic wave model for subsurface flow, Adv Water Resour. 31, 118-131. doi:10.1016/j.advwatres.2007.07.001.

[24] O'Kane, J.P., Flynn, D., 2007. Thresholds, switches and hysteresis from the pedon to the basin scale: a non-linear system theory. Hydrol. Earth Syst. Sci., 11(1), 443-459.

[25] Penna, D., Borga, M., Norbiato, D., Dalla Fontana, G., 2007. Distribution of soil moisture over different depths in a small alpine basin. submitted.

[26] Richards, L. A., 1941. Uptake and retention of water by soil as determined by distance to a water table. Jour. Amer. Soc. Agron., 33:778-786.

[27] Schumann, S., Herrmann, A., 2002. Flood formation and modelling on a small basin scale from Integrative Basin Approach (ICA). ERB and Northern European FRIEND Project 5 Conference, Demänovská dolina, Slovakia, 2002.

[28] Troch P., van Loon, E., Hilberts, A., 2002. Analytical solutions to a hillslope-storage kinematic wave equations for subsurface flow. Advances in Water Resources, 25:637–49.

[29] Troch, P. A., van Loon, A. H., Hilberts, A. G. J., 2004. Analytical solution of the linearized hillslope-storage Boussinesq equation for exponential hillslope width functions. Water Resour. Res., 40, W08601, doi:10.1029/2003WR002850.

7 General conclusions

The objective of this thesis is to provide new insights into hydrological prediction in ungaged basins focusing manly on flash flood events. In this chapter I summarize the conlclusions and recommend avenues for future research.

Since flash-floods develop at space and time scales that conventional observation systems are not able to monitor for rainfall and river discharge, these events are generally characterised by a lack of experimental data and consequently the atmospheric and hydrological generatine mechanisms of flash-floods are poorly understood , leading to highly uncertain forecasts of these events. To improve the observability of these phenomena, an innovative flash flood observation methodology has been proposed in Chapter 2 and 3. The methodology couples analysis of radard rainfall estimates and post-flood surveys and affords the opportunity to derive unique observations concerning rainfall-runoff dynamics during flash flood events. Observations related to the case study of the August 29, 2003 flash flood on Fella river basin (North-eastern Italy) have been examined. The study has demonstrated that under the highly localized conditions and short duration of flash flood occurrence and development, hydrometeorological and geomorphological data can be obtained from rapid response survey teams. The hydrological analysis of the event point out the following consideration:

i) the flood response in the Fella basin suggests that the combination of high soil moisture storage capacity and low antecedent soil moisture conditions is an important factor determining landsurface response to extreme rainfall;
ii) non linearity has been observed also in the hydraulic basin response with a pattern whih reflects the systematic decrease of basin response with increasing the rainfall accumulation. Two major factors controlling this process are the expansion of stream network to unchanneled topographic elements during the flood and the increase of flow velocity with discharge.

Analysis of the storm severity for the August 29, 2003 flash flood on Fella river basin has been conducted in Chapter 3. Regional frequency analysis were conducted on Annual Maximum Precipitation data using the index variable method. The study area was the Eastern Italian Alps. AMP data were collected at 63 stations for durations of 1, 3, 6, 12 and 24 h. The region was analyzed as composed by three smaller subregions, namely, i) the southern plains, ii) the alpine foreland area and the upper Tagliamento basin closed upstream the junction with the Fella and iii) the region within and around the Fella basin. The last region was of particular interest because it includes the area hitted by the exceptional flash flood event. The subregions passed a regional homogeneity test and were treated as homogeneous. L-moments analysis suggests that either GEV or GLO may provide good fit to the data, depending on rainfall duration. For instance, in the case of the Fella-centered Subregion the GEV model may be a good choice for 1-h and 24-h, whereas the GLO model may be a better model for the 3-h, 6-h and 12-h data. This suggests that a

distribution intermediate between GEV and GLO may be more appropriate for analysis of all rainfall durations. The four-parameter Kappa distribution is such a distribution, and it was used together with GEV and GLO. The Kappa distribution was used to estimate growth curves for the Fella-centered region for the various rainfall durations, providing a framework to investigate the frequency characteristics of the 29 August 2003 flash-flood-generating storm for various rainfall durations. Rainfall maxima from the Pontebba station, which recorded the highest rainfall depths, were characterised by return periods in the range 200-500 years for 1-h and 24-h durations, and in the range 500-1000 years for 3-h, 6-h and 12-h durations.

Radar rainfall estimates, adjusted by using a physically-based methodology and data from a raingauge network, were used to characterise the return period of the storm rainfall amounts, highlighting the importance of considering its spatial dimension. Severity graphs were developed to visualise the return periods and their variability for different rainfall durations within the storm. The analysis shows that

i) attributing a single return period to a storm event is not realistic;
ii) the severity of this flash flood generating storm is poorly captured by using a conventional raingauge network, which is too sparse to provide adequate sampling;
iii) adjusted radar rainfall estimates may suffer for considerable uncertainty and that the uncertainty magnifies in the evaluation of the relevant return periods. Whereas this call for development of standard procedures for evaluation of uncertainties in radar rainfall estimation;
iv) the reported results show that these estimates may be useful to evaluate the severity of the storm for ungauged basins and to evaluate the spatial dimension of the frequency characterisation.

Both these features represent important basis for learning processes during ex-post evaluation of interventions in support of future development of strategies and strategic option in flood risk management in the study area.

In Chapter 4 a threshold-based flash flood warning approach has been developed and tested on a wide range of climatic and physiographic European conditions, and by focusing on ungauged basins. The system is derived from the Flash Flood Guidance approach. The FFG is the depth of rain of a given duration, taken as uniform in space and time on a certain basin, necessary to cause minor flooding at the outlet of the considered basin. This rainfall depth, which is computed based on a lumped hydrological model, is compared to either real time-observed or forecasted rainfall of the same duration and on the same basin. If the nowcasted or forecasted rainfall depth is greater than the FFG, then flooding in the basin is considered likely. The study provides an assessment of this technique based on operational quality data from eleven basins (six nested included in five larger parent basins) located in two European regions: north-eastern Italy and central France. The model used in this study is a semi-distributed conceptual rainfall-runoff model, following the structure of the PDM (Probability Distributed Moisture) model. System performances are evaluated by means of categorical statistics, such as the Critical Success Index (CSI).

Four questions were investigated to help understand the potential limitations and benefits of the FFG approach and guide further research and development. The experiments yielded the following answers:

i) *Which is the impact on FFG technique accuracy due to of time-uniform precipitation? (This issue was approached by comparing threshold-based results with those obtained by using the hydrological models with the observed precipitation input).*

Comparison of score statistics obtained by using the Flash Flood Guidance with those resulting from direct model application shows a slight degradation of system performance. Differences between FFG and direct model application are rather modest, and decrease with decreasing the accuracy of model application. The percent difference amounts to 18% for the parent basins, to 15% for interior basins with parameter transposition, and to 12% for interior basins with parameter and soil moisture status transposition. This is not unexpected, showing that the impact on system performances due to the use of time-uniform precipitations reduces when other sources of uncertainties, related to lack of calibration and biases in the soil moisture estimations, become more significant.

ii) *How simulation accuracy at ungauged interior points, simulated by using transposed parameters from parent basins, compare with results obtained for parent basins where calibration has been carried out?*

Results show that overall CSI is equal to 0.43 for the parent basins, where the hydrological model has been calibrated. CSI reduces to 0.28 for the interior basins, when model parameters are transposed from parent basins. This shows that the deterioration of performances following application of FFG to ungauged basins (with parameter transposition) is not negligible, and amounts to 35% (assuming that overall system performances on parent basins is comparable to the one that would have been attained on interior basins, in the case of model parameter calibration).

iii) *Which is the decrease in simulation accuracy associated to transposing both parameter and soil moisture from the larger scale parent basins?*

For interior basins, with parameters and soil moisture status transposed by parent basins, CSI reduces to 0.22 and shows a decrease of 21% with respect to the case of parameter transposition.

iv) *How technique performance degrades when a time-constant soil moisture status is used?*

Performance differences between FFG and use of constant depth-duration precipitation threshold are very high for the parent basins and decrease with decreasing the model accuracy. The percent difference amounts to 53% for the parent basins, to 25% for interior basins with parameter transposition, and to 19% for interior basins with parameter and soil moisture status transposition. This suggests that even a poor estimate of temporal variability of soil moisture, as the one derived from the parent basins, may improve markedly above the condition of no-information on antecedent soil moisture status.

These results show clearly that the performance of the FFG system hinges on the accurate representation of the initial soil moisture conditions. This shows that system improvements could be expected by additional work on real-time updating of model status. A natural choice would be to adjust the basin soil moisture state by making use of runoff data in a real time mode. Additional work should focus on the value of real-time updating for ungauged basins (by transposing updated soil moisture status to interior points) and at various spatial scales.

Chapter 5 examined the effect of climate, geology, land use, flood types and initial soil moisture conditions on the distribution functions of the event runoff coefficients for a set of 14 small-to-medium sized mountainous catchments located in the eastern Italian Alps. The principal observations that can be infered from the study are:

i) the large spatial variability in mean runoff coefficient, which ranges from 0.04 to 0.48, is relatively well explained by the mean annual precipitation. Runoff coefficients increase with mean annual precipitation. Variability and skewness of runoff coefficient distribution tend to reduce with increasing mean annual precipitation;

ii) geological characteristics (as indexed through the 'permeability index') are a dominant control on runoff coefficient, at least for mean annual precipitation less than 1200 mm, through their direct effect on hydrologic pathways and storage properties. Basins characterised by high permeability index have low values of mean runoff coefficient. Less permeable basins have larger runoff coefficients, as expected, but our data and the geological classification considered here cannot be used to isolate the individual effect of geology and climate in these cases, since basins with low permeability index have also high mean annual precipitation;

iii) land use, as indexed by the SCS curve number, influences runoff coefficient distribution to a lesser degree. This result seems to be related both to ambiguities in the SCS curve number-based indexing (particularly for rock outcrops) and to scale effects. Most of the basins considered here have areas exceeding 50 km2. Some of the land use and soil characteristics are likely to average out over this basin size;

iv) an analysis of the runoff coefficients by flood type indicates that runoff coefficients increase with event snowmelt, and are relatively low for rain floods. The effect of snow processes mainly seems to be in increasing antecedent soil moisture;

v) results show that it exists an optimum region of soil moisture capacity, as indexed by a flow duration curve-based index, which maximises the impact of initial soil moisture conditions on runoff coefficient. This means that the difference between runoff coefficients characterised by wet and dry initial conditions is negligible for basins with very larger groundwater capacity (given by largely karstified aquifer) and for basins with reduced groundwater capacity. For basins characterised by intermediate conditions, the difference (and hence the impact of the initial soil moisture conditions) is relatively large.

A logical extensions of the work it would be the use of the runoff coefficient data base obtained here for developing a model that is able to predict runoff coefficients for ungauged catchments in Norh-east Italian Alps and similar climates.

In Chapter 6 general analytical solutions to the hillslope-storage kinematic wave equation for subsurface flow were presented. These solutions allow the computation of characteristic response functions for every type of hillslopes which can be described by using a second order polynomial function for the profile and an exponential equation for the width function. The hillslope-storage subsurface flow equation takes into account the topographic controls exerted on the flow processes by the plan shape and profile curvature. Results of the application of this simplified model for subsurface flow processes show the existence of a hysteretic behaviour in the saturated storage - flux relationships at the hillslope scale. The analytical solutions like those provided here offer essential insights in the functioning of hillslopes and may form the basis of hillslope similarity analysis. The following considerations can be extracted from the work:

i) the found analytical solutions provide a physical basis for deriving two geometric parameters α and ψ which define the hydrological similarity between hillslopes with respect to their characteristic response and hysteresis. Therefore, each hillslope may be represented in a α - ψ plot which allows to derive essential information on its response.

ii) slopes exhibit generally clockwise hysteretic loop in the flux-storage plot. It has been found that hysteresis increases with decreasing α and ψ, i.e. with increasing convergence (for the shape) and concavity (for the profile), and viceversa. For relatively large values of α and ψ the hysteresis may take a complex pattern, with combination of clock-wise to anticlock-wise loop cycles;

iii) example applications have been described for three hillslopes in the Eastern Italian Alps. These applications tested the suitability of the analytical functions to describe the plan and curvature shapes of natural hillslope and provided an opportunity to examine how natural topographies are represented by the two hillslope hydrological similarity parameters.

It is important to note that the type of hysteretic behaviour investigated here is limited to the saturated component of the hillslope response and does not include the unsaturated component.

Further research is being carried out to extend the analytical framework to consider the unsaturated component of the hillslope response and to validate the hillslope geometrical similarity numbers defined here as hillslope subsurface flow similarity parameter by confrontation with experimental data. Further work on hysteresis is being conducted on deriving the relationship between saturated area and subsurface outflow. Finally, this analysis has been conducted at the hillslope scale and the scaling from hillslopes to basins deserves further investigation. This may take the form of analysis of hysteresis of a population of individual hillslopes, each defined with its geometrical parameters.

Curriculum Vitae

Daniele Norbiato

PERSONAL DETAILS

Name: Daniele Norbiato
Permanent address: via Corelli 17
35031 Abano Terme (PD), Italy
Date of Birth: 15th may 1979
Nationality: Italian

CONTACT INFORMATION

Department of Land and Agroforest Environments,
University of Padova, AGRIPOLIS, via dell'Università, 16
35131 Legnaro (PD), Italy,
Phone: +39-0498272681
E-mail: daniele.norbiato@unipd.it

JOB POSITION

01/2008 – present	Research assistant at Department of Land and Agroforest Environments, University of Padova.

EDUCATION

10/1998 – 07/2004	University of Padova, Italy. Master's Degree in Civil Hydraulic Engineering, Dissertation Topic: "Bidimensional modelling of a supercritical flow moving toward a circular pier"
01/2005 – 01/2008	University of Padova, Italy. Ph.D in Environmental Hydronomy, Dissertation Topic: "Regional analysis of flooding and flash flooding" Advisor: Prof. Marco Borga
09/2007 – 11/2007	Technische Universit¨at Wien, Austria. Institute for Hydraulic and Water Resources Engineering. Visiting student. Advisor: Prof. Günter Blöschl

LABORATORY EXPERIENCE

06-07/2005 and 06-07/2006	I took part in Field Hydrology Experiments in a small alpine catchment in the Dolomites (Rio Vauz, 1.9 km²). The instrumentation was composed by: an impedance probe (Theta Probe, Delta-T Devices Ltd, www.delta-t.co.uk) to monitor soil moisture at 0-6 cm depth; a TDR300 probe (Spectrum Technologies Inc., www.specmeters.com) to measure soil moisture up to 20 cm depth; a water content reflectometer (CS625, Campbell Scientific, www.campbellsci.com) to record continuously soil moisture data at 30 cm depth by means of four probes localized on a single experimental hillslope; a network of piezometers; raingauges and weirs.

ACADEMIC EXPERIENCE

10/2005 – 12/2005	Teacher assistant of "Hydraulic and Hydrology" course, prof. Marco Borga, Degree Course in 'Tutela e Riassetto del Territorio', University of Padova (15 hours)
10/2006	Teaching Intensive course "Hydrological Modelling with HEC-HMS"-base level. 23-24-25 October 2006, University of Padova (12 hours).
10/2006 – 12/2006	Teacher assistant of "Hydraulic and Hydrology" course, prof. Marco Borga, Degree Course in 'Tutela e Riassetto del Territorio', University of Padova (20 hours)
02/2007	Teaching Intensive course "Hydrological Modelling with HEC-HMS"-base level. 5-6-7 February 2007, University of Padova (24 hours).
06/2007	Teaching Intensive course "Hydraulic Modelling with HEC-RAS"-base level. 25-26-27 June 2007, University of Padova (8 hours).
06/2007	Teaching Intensive course "Hydrological Modelling with HEC-HMS"-advanced level. 20-21-22 June 2007, University of Padova (8 hours).

PROJECTS

2007 – present	HYDRATE Hydrometeorological data resources and technologies for effective flash flood forecasting. Working group member http://www.hydrate.tesaf.unipd.it/
2005 – present	FLOODSITE Integrated Flood Risk Analysis and Management Methodologies Working group member http://www.floodsite.net/

PUBBLICATIONS

INTERNATIONAL JOURNALS

Norbiato, D., Borga, M., 2008. Analysis of hysteretic behaviour of a hillsplope-storage kinemtaic wave model for subsurface flow, Adv Water Resour. 31, 118-131. doi:10.1016/j.advwatres.2007.07.001.

Norbiato, D., Borga, M.., Sangati, M., Zanon, F., 2007. Regional Frequency Analysis of Extreme Precipitation in the eastern Italian Alps and the August 29, 2003 Flash Flood, Journal of Hydrology. 345, 149-166. doi:10.1016/j.jhydrol.2007.07.009

Norbiato, D., Borga, M., Degli Esposti, S., Gaume, E., Anquetin, S., 2007. Flash flood warning based on rainfall depth-duration thresholds and soil moisture conditions: An assessment under European conditions, Journal of Hydrology. Submitted article.

Penna, D., Borga, M., Norbiato, D., Dalla Fontana, G., 2007. Distribution of soil moisture over different soil depths for an alpine basin: statistical analysis and assessment of temporal stability, Journal of Hydrology. Submitted article.

Borga M., Degli Esposti, S., Norbiato, D., 2006. Influence of errors in radar rainfall estimates on hydrological modeling prediction uncertainty, Water Resour. Res., 42, W08409, doi:10.1029/2005WR004559

ITALIAN JOURNALS

Norbiato, D., Borga, M., Sangati, M., 2006. Valutazione delle piogge estreme in Friuli Venezia Giulia ed analisi statistica dell'evento del 29 Agosto 2003 nel bacino del Fella. Quaderni di Idronomia Montana 26. 131-151.

Boscolo, P., Borga, M., Zanon, F., Sangati, M., Norbiato, D., 2006. Analisi idrologica di una piena improvvisa in ambiente alpino: l'evento del 29 agosto 2003 nel bacino del Fella. Quaderni di Idronomia Montana 26. 113-129.

Penna, D., Norbiato, D., Borga, M., Dalla Fontana, G., 2007. Analisi della stabilità temporale dell'umidità del suolo in un piccolo bacino montano. Quaderni di Idronomia Montana 27. 489-502.

CONFERENCE PROCEEDINGS

Borga, M., Gaume, E., Norbiato, D., 2007. Hydrological processes and flash flood generation, in Proceedings of the 32nd Congress of IAHR, July 1-6 2007, Venice, CD-ROM.

Degli Esposti, S., Norbiato, D., Dinale, R., Borga, M., 2005. Valutazione di alcune componenti del bilancio idrologico in bacini di tipo alpino. In D'Agostino V. & Carraro V. (eds) , Conoscere il sistema fiume in ambiente alpino, Pubblicazione del corso di cultura in Ecologia, Atti del 41.mo corso, Università di Padova: 64-74.

CONFERENCE PRESENTATIONS

Borga, M., Norbiato, D., Sangati, M., Zanon, F., 2007. Flash floods: innovative observation concepts for hydrometeorological process understanding and risk mitigation, 9th Plinius Conference on Mediterranean Storms, September 10-13 2007, Varenna, Italy.

Norbiato, D., Borga, D., 2007. HYDRATE: Development of an observation strategy to mitigate flash flood forecasting uncertainty, Geophysical Research Abstracts, Vol. 9, 09793, SRef-ID: 1607-7962/gra/EGU2007-A-09793

Norbiato, D., Borga, D., 2007. Flash Floods forecasts based on rainfall thresholds: application in an alpine region, Geophysical Research Abstracts, Vol. 9, 06264, SRef-ID: 1607-7962/gra/EGU2007-A-06264

COMPUTER SKILLS

- Applications: Arc GIS, MySQL database, ORACLE database, HEC RAS, HEC HMS, common Windows database spreadsheet, and presentation software.
- Languages: Fortran, Matlab
- Operating Systems: Windows.

Padova, 31 January 2008